UNIVERSITY OF OKLAHOMA

GRADUATE COLLEGE

MECHANISTIC AND STRUCTURAL STUDIES OF SACCHAROPINE DEHYDROGENASE FROM *SACCHAROMYCES CEREVISIAE*

A DISSERTATION

SUBMITTED TO THE GRADUATE FACULTY

in partial fulfillment of the requirements for the

Degree of

DOCTOR OF PHILOSOPHY

By

KOSTYANTYN DMYTROVYCH BOBYK

Norman, Oklahoma

2010

MECHANISTIC AND STRUCTURAL STUDIES OF SACCHAROPINE DEHYDROGENASE FROM *SACCHAROMYCES CEREVISIAE*

A DISSERTATION APPROVED FOR THE
DEPARTMENT OF CHEMISTRY AND BIOCHEMISTRY

BY

Dr. Paul F. Cook, Chair

Dr. Ann H. West

Dr. Phillip E. Klebba

Dr. Richard W. Taylor

Dr. Michael J. McInerney

Dedicated to my wife, my parents, and my sister

Acknowledgements

My sincere gratitude goes to my major advisor and mentor Dr. Paul F. Cook for taking me on-board of his research group and dedicating time and effort “to go down to level zero” and teach me the enzymology and kinetics tirelessly all the way up as much as I could possibly absorb. I appreciate his leadership by example on how to be a successful scientist and, perhaps more importantly, stay happy, laugh, and enjoy life at the same time. I am very glad I met Paul on my life path, since I became a better human being because of him.

I value the instruction and knowledge I received from Dr. Ann H. West on protein structure and crystallography through the special topics class and advising during the joint group research discussion meetings. I appreciate Dr. West’s diligence in attending all of my annual evaluation meetings, providing a constructive criticism of my research, and making sure I am staying on track towards fulfilling the degree requirements. This kept me in shape and I am glad to see I am arriving at the intended destination.

I would like to take this opportunity to thank my Advisory Committee members Dr. Phillip E. Klebba, Dr. Richard W. Taylor, and Dr. Michael J. McInerney for contributing to making a scientist out of me. I took advice and learnt from them about their scientific life passions through special topics classes, General Examination, and the annual evaluation meetings. Thank you for staying engaged and interested in my progress over all these years.

During my Ph.D. research I was standing on the shoulders of people who started the research project that I picked up where they left it, Dr. Hengyu Xu

(Carina) and Dr. Babak Andi. Their work was a standard I used to compare my work against to bring myself to the appropriate level. Special thanks go to Devi K. Ekanayake for freely exchanging the know-how on experimental techniques with me. A lot of knowledge flowed down to me from Dr. Babak Andi and Devi K. Ekanayake, which made it possible to complete my projects on time.

I appreciate the help, teaching, and the hands on training I received from Dr. Thomas M. Leonard, manager of the Macromolecular Crystallography Lab during execution of the structural studies part of my research project. Also, my thanks go to Dr. William E. Karsten, Dr. Lilian Chooback, and Dr. Xiaodong Zhao for providing advice on kinetics, molecular biology, and crystallization techniques, accordingly.

It has been a pleasure to work together with my scientific colleagues - postdocs and fellow graduate students, some by now turned into doctors themselves, Vidya Kumar, Chaonan Hsu, Lu Zhou, Dr. Rong Guan, Dr. Deniz F. Aktas, Dr. Ying Lin, Dr. Jinghua Qian (Edmond), Dr. Alla Kaserer, Hui Tian, Dr. Ashwani K. Vashishtha, Tierra Salvi, Joshua Trice, and Brittany Kitchens. These people were creating a stimulating atmosphere in the group(s) and I learnt something from each one of them, be it a scientific or a life lesson.

I thank administrative staff Jean Keil, Carol Jones, and Arlene Crawford for giving a helping hand with never-ending organizational chores and paperwork, and through this letting me have more time to spend on research.

I have been blessed to receive unconditional love and support of my parents, Dmytro Karpovych Bobyk and Lidiia Kostiantynivna Bobyk, throughout

all my life. It is not possible to replace some of the lost opportunities in the past and in the future to fulfill my son’s duties to you as my parents. Maybe, my modest successes will give you some joy that will provide at least a partial substitute, however unfit.

I highly cherish the moral support that my sister, Snizhana Dmytrivna Khalavka, has been providing me, perhaps at the expense of time which was supposed to be given to her own family, three wonderful children and a loving husband. Thank you for the joyful conversations we have on the weekends via the Skype.

To save the most important part for last, I am immensely grateful for the patience and endless support my beloved wife, Olga Kostiantynivna Magas, has been giving me over the years. Thank you for sharing my ups and downs, accepting my endeavor into the science, and, overall, standing shoulder to shoulder with me in all life situations. I could not have hoped for more understanding.

If you are reading these acknowledgements and thinking that you should have been mentioned here, you are absolutely correct! The contributions of many people maid my success possible, more people, in fact, than there is space on these pages to mention. I keep a part of my heart and a memory for you, and I thank all of you.

The work in this dissertation was supported by a grant (GM 071417) from the National Institutes of Health (to P.F.C. and A.H.W.), and the Grayce B. Kerr Endowment to the University of Oklahoma to support the research of P.F.C.

Strolling along the edge of the sea, a man catches sight of a young woman who appears to be engaged in a ritual dance. She stoops down, then straightens to her full height, casting her arm out in an arc. Drawing closer, he sees that the beach around her is littered with starfish, and she is throwing them one by one into the sea. He lightly mocks her: "There are stranded starfish as far as the eye can see, for miles up the beach. What difference can saving a few of them possibly make?" Smiling, she bends down and once more tosses a starfish out over the water, saying serenely, "It certainly makes a difference to this one." [1]

[1] Prologue to chapter four "Being a Contribution", Zander R.S., Zander B., (2002) *The art of Possibility*, 2nd ed., Penguin Books, New York, U.S.A., ISBN 0-87584-770-6

Table of Contents

List of Tables

List of Figures

Abstract

Lysine is an essential amino acid in mammals including humans. The α-aminoadipate (AAA) pathway for lysine biosynthesis is unique to fungal organisms and enzymes of this pathway are of interest as potential targets for anti-fungal drug design. Saccharopine dehydrogenase (SDH) [N^6-(glutaryl-2)-L-lysine:NAD-oxidoreductase (L-lysine-forming) (EC 1.5.1.7)] catalyzes the reversible NAD-dependent oxidative deamination of saccharopine to generate L-lysine and α-ketoglutarate. A disulfide bond between cysteines 205 and 249 is observed in structures of the apoenzyme and those with sulfate or oxalylglycine bound to the substrate-binding domain. However, in the structure with adenosine monophosphate bound in the dinucleotide-binding site, the disulfide bond is reduced.

In this dissertation, site-directed mutagenesis was used to generate the C205S mutant enzyme, which was characterized kinetically using a combination of steady state kinetics, pH-rate profiles, and isotope effects. The C205S mutant enzyme was also characterized crystallographically.

The kinetic and chemical mechanisms of the C205S mutant enzyme remained unchanged compared to those of the wild type enzyme. At pH 7, the first ($V/\mathbf{E_t}$) and second order ($V/K\mathbf{E_t}$) rate constants increased for the C205S mutant enzyme compared to wild type. Differences in the pH-rate profiles for V_1, V_1/K_{NAD}, V_2, and $V_2/K_{\alpha\text{-}Kg}$ compared to wild type indicated the increase in activity resulted from a decrease in the sensitivity of the C205S mutant enzyme to the protonation state of a group responsible for a pH-dependent conformational

change. The increased rate of the C205S mutant enzyme was also reflected in larger deuterium and solvent deuterium isotope effects on V_2 and V_2/K_{Lys}, with no significant change in the multiple isotope effect in which the solvent isotope effect was repeated with NADD. Thus, the rate of central complex interconversion contributes more to rate limitation, but the ratio of the rates of the hydride transfer step and imine hydrolysis is the same. Overall, data suggested the wild type enzyme is a mixture of disulfide- and dithiol-containing species, with the former dominating.

Structures of the C205S apoenzyme and one with NADH bound in the dinucleotide binding site have been solved. Structural data suggested the disulfide between the C205 and C249 in the wild type enzyme might prevent the dinucleotide binding. Movement of arginine 204, 130, and 131 side chains upon dinucleotide binding and the resulting positioning of arginine 131 into the correct location for the substrate binding has been proposed as a structural basis for the ordered kinetic mechanism proposed previously for SDH. Also, a role for the network of electrostatic interactions between K13, K77, H96, E16, and E78 has been proposed in positioning K77 and H96 for reaction and modulating the pK_as of these catalytic side chains close to neutrality, with K13 playing an essential part.

To probe the acid-base chemical mechanism of saccharopine dehydrogenase, K77M and H96Q, K77M/C205S and H96Q/C205S, and K77M/ H96Q/C205S single, double, and triple mutants, respectively, were prepared and characterized via initial velocity studies and isotope effects. A 100-fold

decrease in k_{cat} and a large $^{D}(V/K_{Lys})$ isotope effect suggest K77 is the base that accepts a proton from the secondary amine of saccharopine. A 4-fold decrease in k_{cat} and a large $^{D_2O}(V/K_{Lys})$ isotope effect suggest H96 is the base that catalyzes the imine hydrolysis via the activation of a water molecule.

Chapter 1

Introduction

C1.1 Lysine biosynthesis

L-Lysine (Lys) is the only known amino acid of the twenty common amino acids to have two distinct biosynthetic pathways: the diaminopimelate (DAP) pathway of the aspartic acid family of amino acid biosynthesis and α-aminoadipate pathway (AAA) of the glutamic acid family (*1, 2*). The DAP pathway is found in green plants, bacteria, and fungi of the genus *Phycomycetes* (*Hypochytriales*, *Saprolegniales*, and *Leptomytales*), while the AAA pathway is found only in lower eukaryotes, including some *Phycomycetes* (*Chytridiales*, *Blastocladiales*, and *Mucorales*), yeasts, other higher fungi (*Ascomycetes* and *Basidomycetes*), and Euglenoids (*3-10*). The dicotomous evolution of two Lys pathways is unique among the amino acid biosynthetic pathways since the AAA pathway is not present in prokaryotic organisms (*3*).

C1.1.1 Diaminopimelate pathway

Starting with aspartate semialdehyde and pyruvate, Lys is produced in seven steps in the DAP pathway, Scheme C1-1. While the DAP pathway is utilized to produce Lys for protein biosynthesis, some of the Lys produced together with diaminopimelate is incorporated into bacterial cell wall peptidoglycan. Therefore, enzymes of the DAP pathway are potential targets for the design of new antimycotic agents (*11-13*).

In the first step of the DAP pathway, aspartate is phosphorylated to produce the aspartyl-β-phosphate, followed by an NADPH-dependent reduction to give aspartate β-semialdehyde. Aldol condensation of aspartate β-semialdehyde with pyruvate yields 2,3-dihydrodipicolinate, which is then reduced by NADPH to Δ'-piperideine-2,6-dicarboxylate. Succinylation (or acetylation) and hydrolysis opens the ring to give *N*-succinyl (or acetyl) α-amino-ε-ketopimelate. After transamination, the N-acyl group is removed to yield L,L-DAP, which can be directly incorporated into peptidoglycan, or racemized to the *meso* form. The *meso* form of L,L-DAP is decarboxylated to give Lys (*14*).

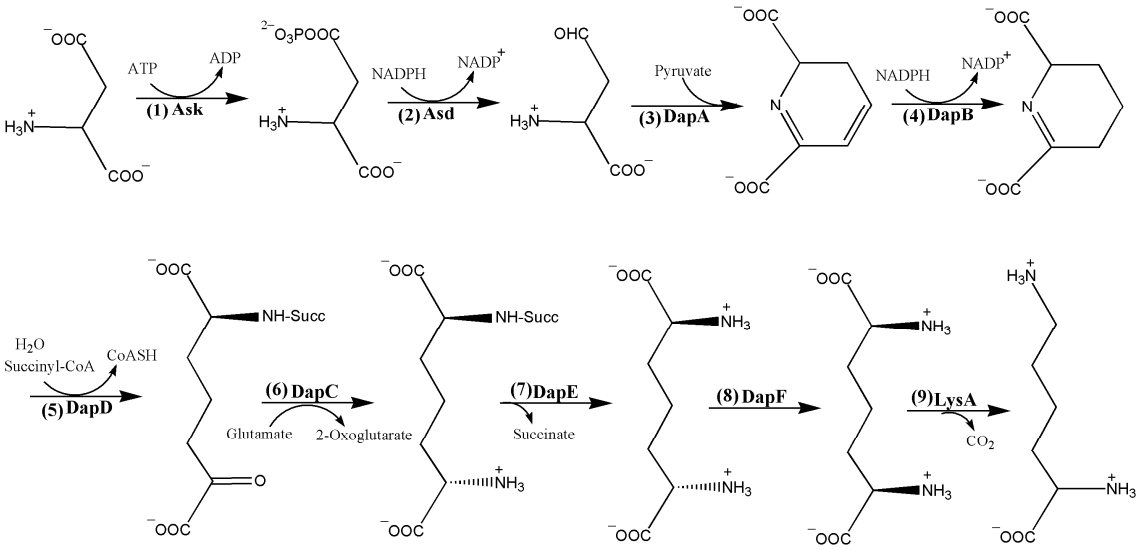

Scheme C1-1. The enzymes of the lysine DAP biosynthetic pathway: (1) Aspartate kinase (Ask, E.C. 2.7.2.4), (2) Aspartate semialdehyde dehydrogenase (Asd, E.C. 1.2.1.11), (3) Dihydrodipicolinate synthase (DapA, E.C. 4.2.1.52), (4) Dihydrodipicolinate reductase (DapB, E.C. 1.3.1.26), (5) Tetrahydrodipicolinate acyltransferase (DapD, E.C. 2.3.1.117), (6) N-succinyl-α-amino-ε-ketopimelate-glutamate aminotransaminase (DapC, E.C. 2.6.1.17), (7) N-acyldiaminopimelate deacylase (DapE, E.C. 3.5.1.18, E.C. 3.5.1.47), (8) DAP epimerase (DapF, E.C. 5.1.1.7), (9) DAP decarboxylase (LysA, E.C. 4.1.1.20).

C1.1.2 α-Aminoadipate pathway in fungi

Starting with acetyl CoA (AcCoA) and α-ketoglutarate (α-Kg), Lys is produced in eight steps, Scheme C1-2. Seven enzymes and more than twelve nonlinked genes contribute to the AAA pathway, Table C1-1. The AAA pathway is considered unique to fungi, thus, enzymes from this pathway are potential targets for the design of new antimycotic agents (*10*). Currently, however, only a few compounds exist, that target the AAA pathway, specifically, inhibitors of homocitrate synthase (*15*), and more recently, homoisocitrate dehydrogenase (*16*), which indicates a need for new agents.

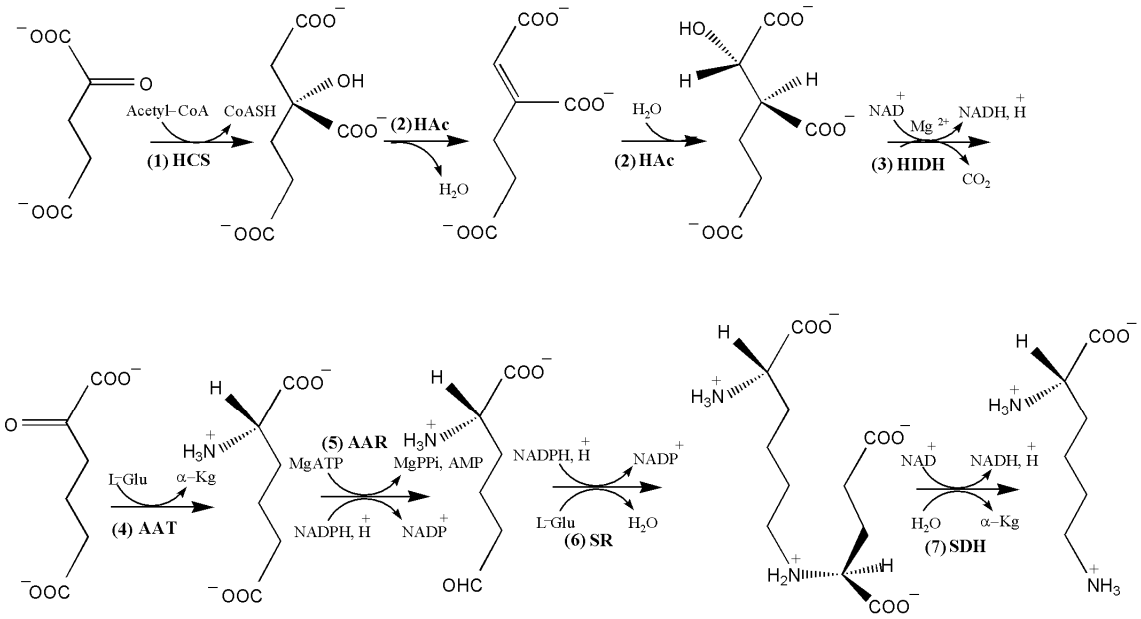

Scheme C1-2. The enzymes of the lysine AAA biosynthetic pathway: (1) Homocitrate synthase (HCS, E.C. 4.1.3.21), (2) Homoaconitase (HAc, E.C. 4.2.1.36), (3) Homoisocitrate dehydrogenase (HIDH, E.C. 1.1.1.87), (4) α-aminoadipate aminotransferase (AAT, E.C. 2.6.1.39), (5) α-aminoadipate reductase (AAR, E.C. 1.2.1.31), (6) Saccharopine reductase (SR, E.C. 1.5.1.10), (7) Saccharopine dehydrogenase (SDH, E.C. 1.5.1.7).

In the first step of the AAA pathway, acetyl CoA (AcCoA) and α-Kg are condensed to produce homocitric acid, which undergoes a dehydration to *cis*-homoaconitic acid, which in turn is converted to homoisocitric acid. Oxidation of homoisocitric acid results in the transient formation of oxaloglutarate followed by loss of carbon dioxide to produce α-ketoadipate. Transamination of α-ketoadipate with L-glutamate as an amino donor produces L- α-aminoadipate. Although this first half of the pathway takes place in the mitochondrion, the second half takes place in the cytoplasm (*17*). The aminotransferase, which catalyzes the transamination reaction, has two isozymes, one mitochondrial and one cytoplasmic, with only cytoplasmic form thought to contribute to the AAA pathway (*18, 19*).

Table C1-1: The genes of the AAA pathway in *S. cerevisiae*

Enzyme	**Gene**
Homocitrate synthase	*LYS20* (cytosol), *LYS21* (mitochondria)
Homoaconitase	*LYS4* (*LYS7*)
Homoisocitrate dehydrogenase	*LYS12*
α-Aminoadipate aminotransferase	-
α-Aminoadipate reductase	*LYS2*
(Phospopantetheinyl transferase)	*(LYS5)*
Saccharopine reductase	*LYS9* (regulated by *LYS14*)
Saccharopine dehydrogenase	*LYS1*

In the cytoplasm, the side chain carboxylate group of L-α-aminoadipate is reduced to give α-aminoadipate δ-semialdehyde, which is a MgATP and NADPH-dependent process. Then, α-aminoadipate δ-semialdehyde is condensed with L-glutamate and the resulting imine is reduced to generate L-saccharopine (Sacc). The last step is the cleavage of the carbon-nitrogen bond within the glutamate moiety of Sacc to produce Lys and α-Kg (*10, 14*).

C1.1.2.1 Enzymes of the AAA pathway

Homocitrate synthase (HCS) (3-hydroxy-3-carboxyadipate-2-oxoglutarate-lyase [CoA-acetylating]; EC 2.3.3.14) catalyzes a Claisen condensation of AcCoA and α-ketoglutarate to give homocitrate and CoA. A Claisen condensation is a base-catalyzed condensation of a carbon α to an ester carbonyl and another carbonyl-containing compound, like an aldehyde or ketone (*20*).

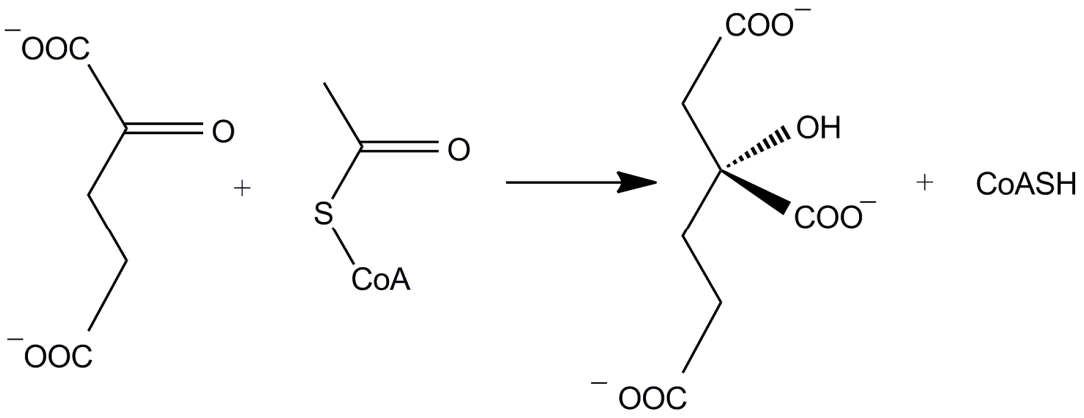

α-ketoglutarate AcCoA homocitric acid

A sequential ordered kinetic mechanism has been reported for HCS with α-ketoglutarate binding before AcCoA and CoA released before homocitrate. However, fluorescence titration data showed finite binding of CoA and AcCoA to

free enzyme, suggesting the mechanism may be random with a high degree of synergism of binding between the reactants (*21*). The activity of HCS is highly regulated. HCS is feedback-inhibited by lysine, the end product of the pathway. Also, the Na^+ binds to the free enzyme and affects the activity of HCS in a concentration-dependent manner. Na^+ is an activator at a low concentration, when the concentration of AcCoA is high and α-ketoglutarate is low, but it is an inhibitor at high concentration; these effects occur as a result of the monovalent ion binding to two different sites in the free enzyme (*22*). Additionally, the product of the HCS reaction, CoASH, can inactivate the enzyme from *S. cerevisiae*, preventable by Lys and α-Kg. Once inactivated the enzyme could not be reactivated by addition of AcCoA (*23*). The HCS was found to be a Zn-containing metalloenzyme using inductively coupled plasma mass spectroscopy. A chemical mechanism has been proposed for HCS in which α-Kg first binds to the active site Zn via its α-carboxylate and α-oxo groups, followed by acetyl-CoA. A general base then accepts a proton from the methyl of acetyl-CoA, and a general acid protonates the carbonyl of α-Kg in the formation of homocitryl-CoA. The general acid then acts as a base in deprotonating $Zn\text{-}OH_2$ in the hydrolysis of homocitryl-CoA to give homocitrate and CoA. Probing the proposed chemical mechanism using site-directed mutagenesis followed by kinetic characterization and constant pH molecular dynamics simulation studies, suggested that a catalytic dyad comprised of E155 and H309 acts to deprotonate the methyl group of AcCoA, while Y320 may aid

in orienting the reactant and/or the catalytic dyad, but is likely not directly involved in catalysis (*24, 25*).

Homoaconitase (HAc, E.C. 4.2.1.36), also known as homoaconitate hydratase, inter-converts homocitrate and homoisocitrate via the intermediacy of *cis*-homoaconitate.

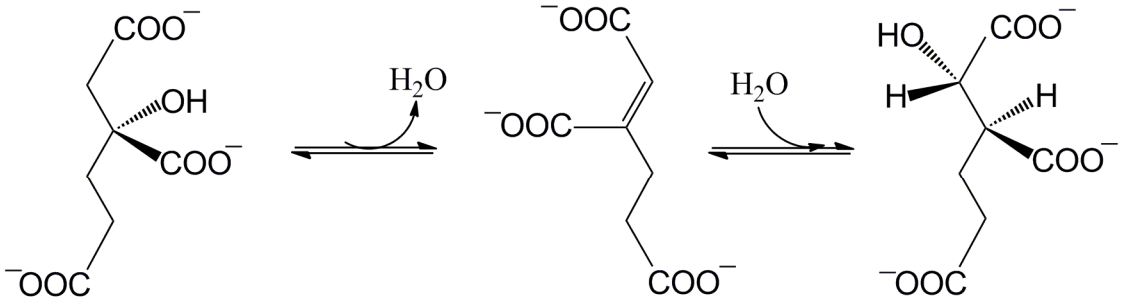

homocitrate *cis*-homoaconitate homoisocitrate

HAc is a mitochondrial enzyme which contains an FeS cluster (*10*). It is repressed by both Lys and glucose (*26*). Little is known of the mechanism of the HAc from *S. cerevisiae*. However, the enzyme is a member of aconitase superfamily and its mechanism is likely similar to that of aconitase (*27*).

Homoisocitrate dehydrogenase (HIDH, E.C. 1.1.1.87) (3-carboxy-2-hydroxyadipate dehydrogenase; EC 1.1.1.87) catalyzes the conversion of homoisocitrate to α-ketoadipate, using NAD^+ as an oxidizing agent. A kinetic mechanism has been determined from initial velocity studies in the absence and presence of product and dead-end inhibitors. The mechanism is steady-state with random addition of MgHIc and NAD, but with preferred ordered release of CO_2, α-ketoadipate and NADH (*28*).

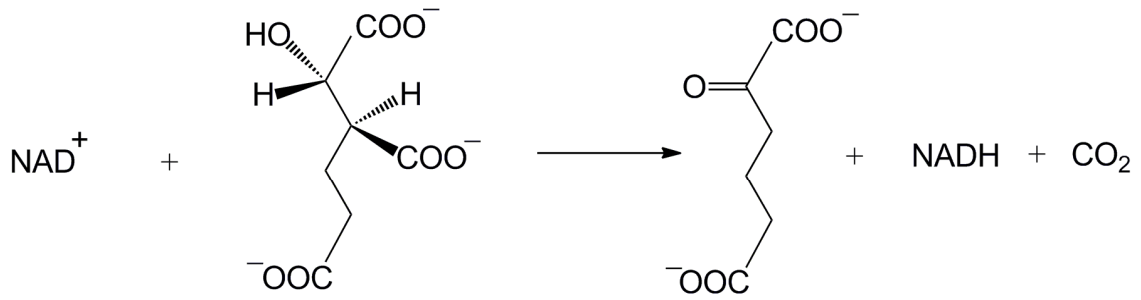

homoisocitrate α-ketoadipic acid

A chemical mechanism of HIDH has been proposed on the basis of the pH dependence of kinetic parameters, dissociation constants for competitive inhibitors, and isotope effects. Two enzyme groups act as acid-base catalysts in the reaction. A group with a pK_a of about 6.5-7.0 acts as a general base accepting a proton as the β-hydroxy acid is oxidized to the β-keto acid. This residue participates in all three of the chemical steps, shuttling a proton between the C2 hydroxyl and itself. The second group acts as a general acid with a pK_a of 9.5 and likely catalyzes the tautomerization of the enol of α-ketoadipate to the ketone by donating a proton to the enol (*29*). K^+ is an activator of the reaction catalyzed by HIcDH with either the natural substrate, homoisocitrate, or the slow substrate isocitrate. There is a group with a pK_a of about 5.5−6 seen in the pH profiles that has to be protonated for optimal activity. When this group is unprotonated in the absence of K^+, more than 10-fold decrease in the affinity of enzyme for NAD is observed. However, the affinity for NAD is relatively constant at high pH in the presence of 200 mM KCl. The enzyme residue may be a neutral acid, aspartate or glutamate. Data suggest that K^+ replaces the proton, and likely bridges the enzyme residue and

the carboxamide side chain of NAD^+, similarly to the mechanism of K^+ activation proposed for tartrate dehydrogenase, another member of the family, with 36% sequence identity to HIDH (*30-32*). Probing the chemical mechanism using site-directed mutagenesis followed by the kinetic studies suggest K206 is acting as a general base in the hydride transfer step of the WT enzyme but as a general acid in the Y150F enzyme, replacing Y150 in the tautomerization reaction. In addition, Y150 acts as a general acid in the tautomerization reaction of the WT enzyme and replaces K206 as the general base in the hydride transfer step of the K206M enzyme (*33*).

α-aminoadipate aminotransferase (AAT, E.C. 2.6.1.39) is a PLP-dependent enzyme that converts α-ketoadipate to AAA using L-glutamate as the amino donor and generating α-ketoglutarate as the second product (*18, 19*).

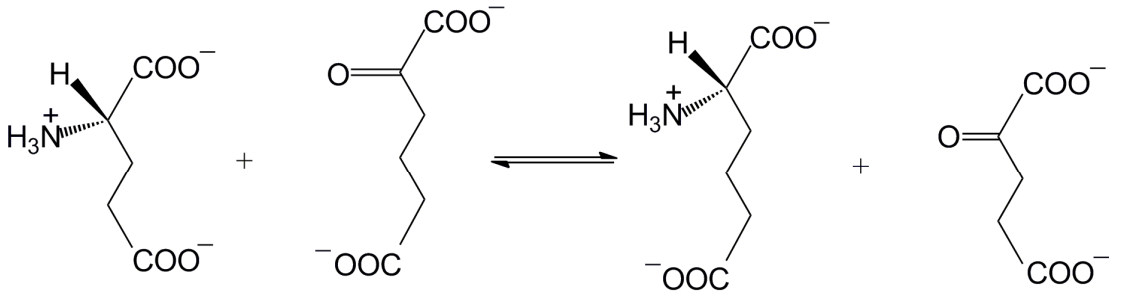

In *S. cerevisiae*, two isozymes of AAT have been isolated with different preferences for amino donors and sensitivity to α-Kg inhibition. Isozyme II is located in the cytosol and is thought to be specific for the AAA pathway. It has a strict requirement for L-glutamate as the amino donor, and is not inhibited by α-Kg, though its expression is slightly repressed by glucose (*18, 19*). On the basis

of many examples from other aminotransferases, the mechanism of AAT is expected to be ping pong (*34, 35*).

α-aminoadipate reductase (AAR, E.C. 1.2.1.31) also known as L-α-aminoadipate-δ-semialdehyde (AAS) dehydrogenase, catalyzes the reduction of L-α-aminoadipate (AAA) to AAA-δ-semialdehyde in the cytoplasm (*36-38*).

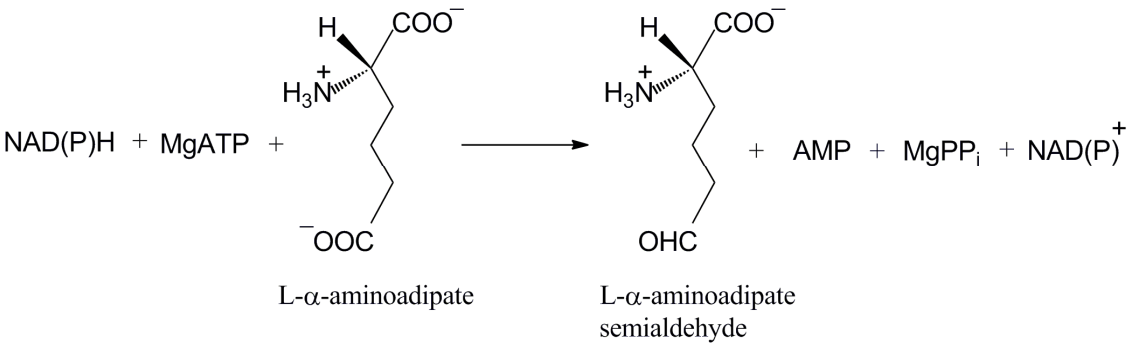

A mechanism has been proposed in which phosphopantetheinylated reductase catalyzes the adenylation of the δ-carboxylate of AAA via the adenylation (A) domain, followed by acyl transfer of the aminoadipoyl moiety to the thiol of the phosphopantetheine to generate the thioester of the phosphopantetheinyl cleavage protein domain. This covalent thioester intermediate is reduced by NADPH to produce the final semialdehyde product and regenerate the reduced phosphopantetheine (*39*).

Pyridine nucleotide-linked oxidative deaminations

Saccharopine Reductase (SR) and Saccharopine Dehydrogenase (SDH) catalyze similar reactions and both belong to the class of pyridine nucleotide-linked amino acid oxidoreductases. Enzymes in this class include L-alanine (AlaDH), L-phenylalanine (PheDH), L-leucine (LeuDH), and L-glutamate

(GluDH) amino acid dehydrogenases. These enzymes catalyze the reversible oxidative deamination of an amino acid to its keto acid and ammonia using $NAD(P)^+$ as an oxidizing agent (*40*).

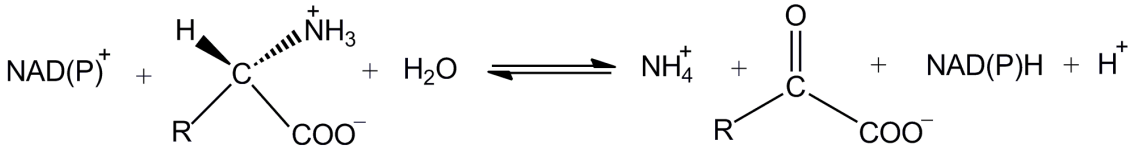

However, in the reactions catalyzed by the SDH and SR the amino group of the amino acid is substituted to produce a secondary amine.

The kinetic mechanism reported for most amino acid dehydrogenases is ordered with a respective dinucleotide bound to the enzyme first and released last. A generalized chemical mechanism for amino acid dehydrogenases is shown in Scheme C1-3, and is based on that for GluDH and AlaDH, two of the most extensively studied enzymes. The bound amino acid is first oxidized by $NAD(P)^+$ to an imine. In the next step, the water activated by a general base, usually an ε-amine of lysine (GluDH) or imidazole of histidine (AlaDH) side chain, attacks the imine to form a carbinolamine intermediate. At last, ammonia is expelled and the keto acid product is formed.

Crystal structures have been solved for Glu (*41*), Ala (*42*), Leu (*43*), Phe (*44*), and meso-DAP (*45*) dehydrogenases. All of the structures have similar structural and functional features, and in most cases the amino acid residues involved in catalysis and binding are conserved with differences often attributed to different substrate specificities. A subunit is composed of large N- and C-terminal domains that are separated by a deep cleft, where the active site is

located. The Rossmann fold is found usually in the C-terminal domain and provides a binding site for the dinucleotide. The amino acid binding site is located in the other domain. A conformational transition from an open to a closed form exists in the enzyme and is thought to be triggered by binding of substrates or inhibitors in the amino acid binding site (*41, 43, 45*).

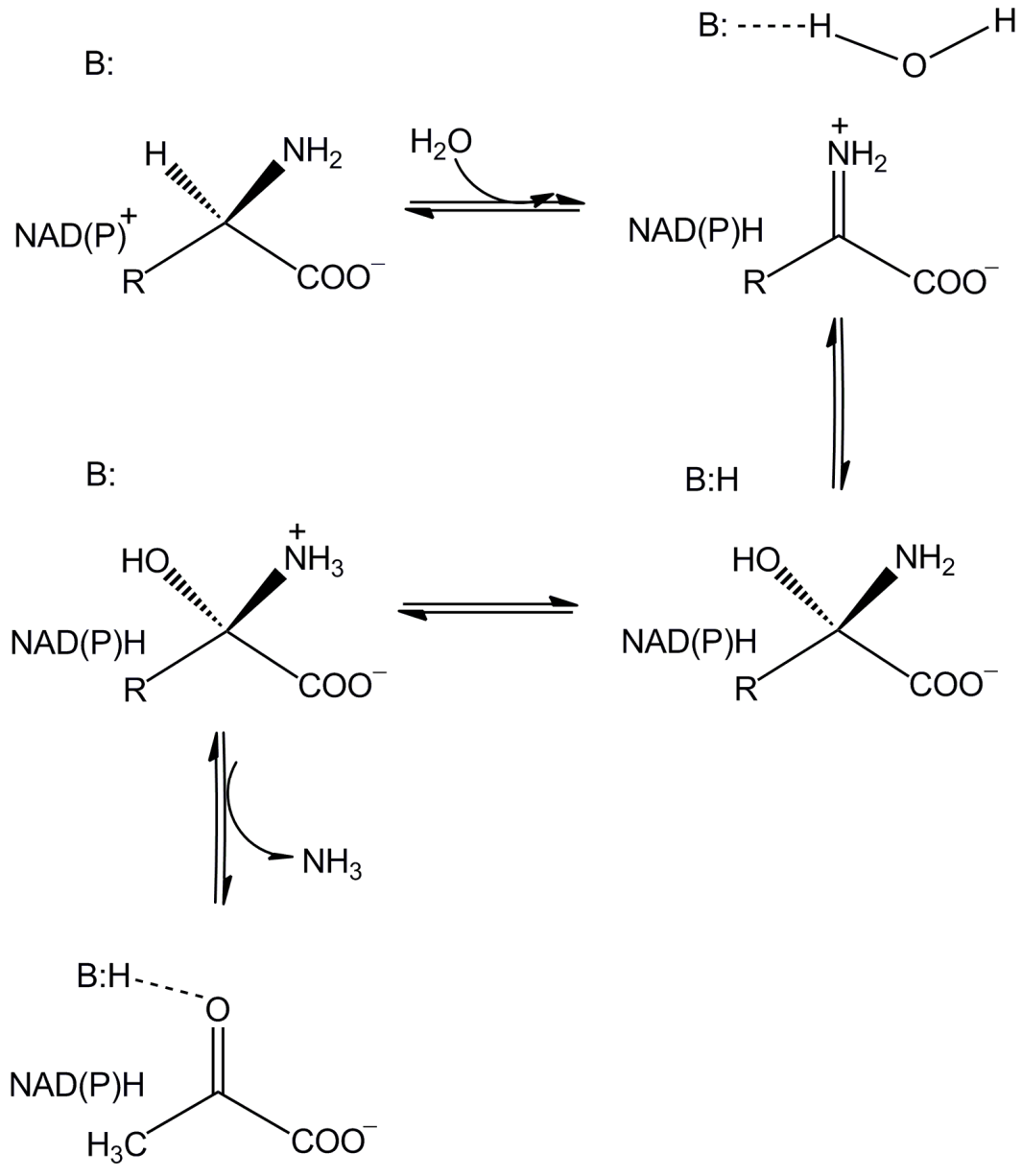

Scheme C1-3. Proposed general chemical mechanism for amino acid dehydrogenases

Prokaryotic L-AlaDH and SDH have a common ancestor (*46*). L-AlaDH, catalyzes the reversible reductive amination of pyruvate to L-alanine with NADH as the reductant. The sequence alignment of L-AlaDH and SDH shows the active site residues of AlaDH, such as Arg15, His95, and Lys74, are also conserved in SDH (*14*).

Saccharopine reductase (SR, E.C. 1.5.1.10), also known as aminoadipate semialdehyde-glutamate reductase or saccharopine dehydrogenase [N6-(L-1,3-dicarboxypropyl)-L-lysine:$NADP^+$ oxidoreductase (L-glutamate-forming)] catalyzes the synthesis of saccharopine via the condensation of L-α-aminoadipate-δ-semialdehyde with L-glutamate with NADPH as the reducing agent (*3, 47, 48*).

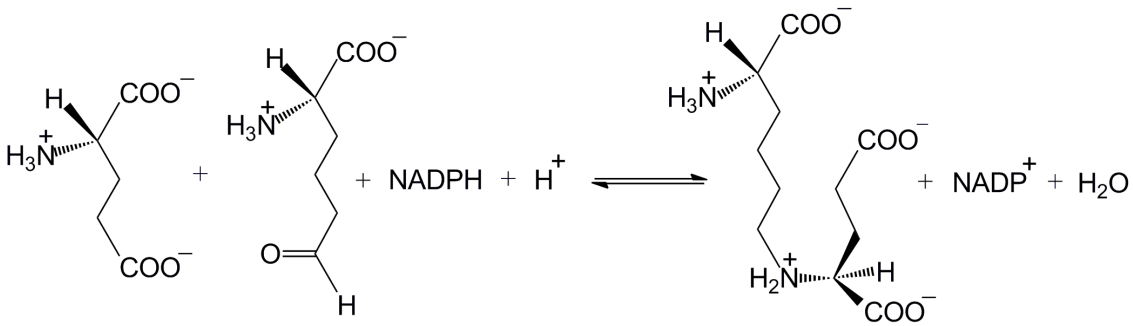

The kinetic mechanism is sequential with ordered addition of NADPH to the free enzyme followed by AAS, which adds in rapid equilibrium prior to L-glutamate in the forward reaction direction. In the reverse reaction direction, NADP adds to the enzyme followed by saccharopine (*49*). A chemical mechanism has been proposed for SR. Briefly, two groups are involved in the acid−base catalysis. The first group, with a pK_a of 8.0, catalyzes the steps involved in forming the

imine between the α-amine of glutamate and the aldehyde of AAS. The second group, with the pK_a of 5.6, accepts a proton from the α-amine of glutamate so that it can act as a nucleophile in forming a carbinolamine upon attack of the carbonyl of AAS (*50*). In general, the chemical mechanism of SR is the same as that of SDH and will be discussed in detail together with SDH.

Saccharopine dehydrogenase [N^6-(glutaryl-2)-L-lysine:nicotinamide adenine dinucleotide (NAD^+) oxidoreductase (L-lysine-forming) (EC 1.5.1.7)] is the last enzyme of the AAA pathway for lysine biosynthesis in *S.cerevisiae* (*14*). Its mechanism is the focus of this dissertation and is discussed in a separate section below.

C1.2 Saccharopine Dehydrogenase: last enzyme of α-Aminoadipate pathway from *Saccharomyces cerevisiae*

SDH from *S. cerevisiae* is a monomer of 373 amino acids, with a pI of 10.1, a calculated molecular weight of 41,464 Da and one binding site for reactants per molecule of enzyme (*51-54*). The enzyme is encoded by the *LYS1* gene, which also has the systematic name YIR034C in the *Saccharomyces* Genome Database, located in chromosome IX of *S. cerevisiae* (*55*).

C1.2.1 SDH: catalyzed reaction and kinetic mechanism, functional and structural aspects

SDH catalyzes the reversible pyridine nucleotide-dependent oxidative deamination of Sacc to generate Lys and α-Kg with NAD as the oxidizing agent (*14*). Previously, an ordered kinetic mechanism was proposed for SDH, on the basis of studies with α-Kg as the keto acid substrate (*56, 57*). However, when an alternative slow keto acid substrate, pyruvate, was used, inconsistencies in the order of product release emerged (*58*). Also, noncompetitive inhibition patterns were observed with OAA, pyruvate, α-ketobutyrate, α-ketovalerate, and α-ketocaproate independent of the substrate, NADH, α-Kg, or Lys varied (*57, 59*).

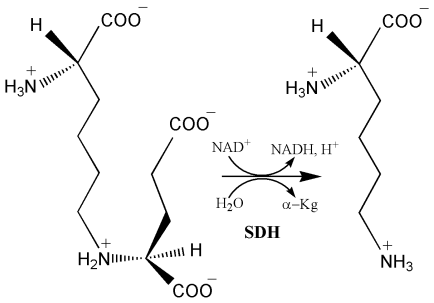

Recently, the kinetic mechanism of SDH was revisited and an overall kinetic mechanism of SDH was proposed as shown below in the Scheme C1-4. The mechanism is steady state random, but with ordered addition of NAD before Sacc, and random release of α-Kg and Lys followed by NADH in the direction of Lys formation. The order is reversed in the Sacc formation reaction direction, where NADH binds first followed by random addition of α-Kg and Lys and a release of Sacc before NAD (*60*). This kinetic mechanism was corroborated by initial velocity studies in the absence and presence of product and dead-end inhibitors and is in agreement with the previously published data. Estimated rate constants are as follows: $V_1/\mathbf{E_t}$ = (1.1±0.1) s^{-1}, $V_2/\mathbf{E_t}$ = (20±1.2) s^{-1}; and $V_1/K_{NAD}\mathbf{E_t}$=(1.2±0.2)×10^3 $M^{-1}s^{-1}$, $V_1/K_{Sacc}\mathbf{E_t}$=(1.6±0.4)×10^2 $M^{-1}s^{-1}$,

$V_2/K_{NADH}\mathbf{E_t}$ = (1.05±0.1)×10^6 $M^{-1}s^{-1}$, $V_2/K_{\alpha\text{-}Kg}\mathbf{E_t}$=(1.8±0.4)×$10^5$ $M^{-1}s^{-1}$, $V_2/K_{Lys}\mathbf{E_t}$= (1.8±0.3)×10^4 $M^{-1}s^{-1}$ (*60*).

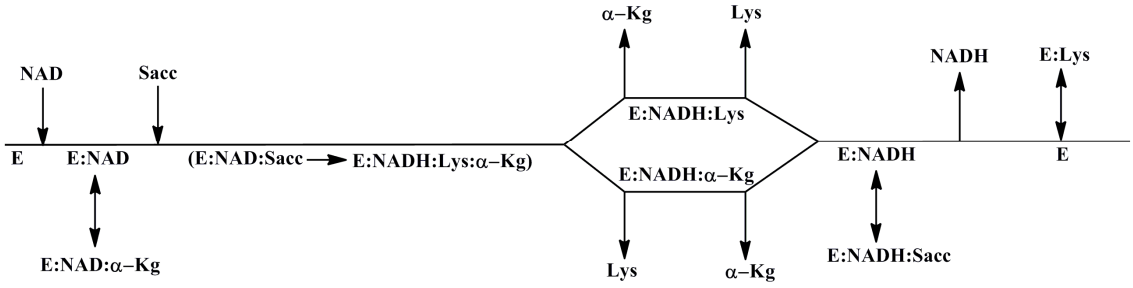

Scheme C1-4. Proposed Kinetic Mechanism for SDH.

Initial velocity studies of SDH in the presence of product and dead-end inhibitors provided additional data in support of the proposed kinetic mechanism. Discussing all the details of these studies is beyond the scope of this introduction, but discussion of some aspects is worthwhile, since they shed light on structure-function relationships in SDH. For example, substrate inhibition by α-Kg is uncompetitive against NADH at saturating Lys. Data suggest α-Kg binds E•NAD product complex, and this was corroborated by a double-inhibition experiment measuring the initial rate at fixed low NADH and Lys and varying NAD at different inhibitory levels of α-Kg. Interestingly, a synergism of binding between NAD and α-Kg was observed based on enhancement of inhibition. The affinity of enzyme for α-Kg increased 8-fold in the presence of NAD (*60*). Data support the “induced fit” model of substrate binding in SDH and the “plasticity” of structural elements in the substrate-binding pockets of enzyme. Also, uncompetitive inhibition by Sacc against NADH was observed which can be explained by the binding of Sacc to

E•NADH in a dead-end fashion. The noncompetitive patterns observed for Sacc against Lys and α-Kg provided additional evidence for the binding of Sacc to both, E•NADH and E•NAD complexes (*60*). Data speak to the structural similarity of the bound conformations of NAD and NADH, as well as the similarity of the enzyme conformations generated upon binding of NAD or NADH. Additionally, a couple of interesting observations were made in the dead-end inhibition studies. OAA is a dead-end analogue of α-Kg, however it was competitive against Lys, suggesting it binds to the same enzyme form(s) to which Lys binds. Also, it was noncompetitive against both α-Kg and NADH, suggesting that it binds to E as well as the E•NADH and E•NADH•α-Kg enzyme forms. Glutarate as a dead-end inhibitor is noncompetitive against α-Kg and competitive against Lys as is OAA. However, it exhibited S-parabolic noncompetitive inhibition against NADH, which means it binds to E twice to give E•$(glutarate)_2$ in addition to E•NADH. The E•$(glutarate)_2$ complex likely results from occupying both lysine- and α-Kg-binding sites in the active site. Data for glutarate inhibition indicated the first molecule of glutarate bound has a very low affinity, while the second molecule of glutarate binds with increased affinity, trapping the first molecule on enzyme. As a result of the studies above, SDH was proposed to have a flexible and large substrate-binding pocket for Sacc, Lys and α-Kg, with three likely subsites for the interaction of the three carboxylates of Sacc. Subsites I and III would accommodate two carboxylates of Sacc from its glutamyl moiety (α-Kg portion), and subsite II would accommodate one carboxylate from the lysyl moiety (Lys portion). Also, based

on the difference in the substrate inhibition constant and K_m (steady-state dissociation constant) for Lys, NADH binding was suggested to cause a conformational change, increasing the affinity of the E for Lys and α-Kg (*60*).

Thus, initial velocity studies of SDH in the absence and presence of product and dead-end inhibitors not only confirmed the kinetic mechanism, but also generated clues on the structure of the SDH active site.

C1.2.2 SDH: chemical mechanism, binding and catalytic groups

On the basis of chemical modification studies, a number of amino acid residues were identified as important for binding and/or catalysis in SDH. Modification of SDH by *p*-chloromercuribenzoate and iodoacetate suggested the presence of essential cysteine residue(s) (*54*). Inactivation of SDH by diethylpyrocarbonate suggested the presence of essential histidine residue(s) (*61*). A reversible inactivation by pyridoxal and pyridoxal-5'-phosphate suggested the presence of essential lysine residue(s) (*62*). Inactivation of SDH by 2,3-butanedione suggested the presence of essential arginine residue(s) (*63*).

Two general acid-base catalytic groups, base 1 (B_1) and base 2 (B_2), complete all necessary acid-base chemistry steps in the proposed proton shuttle chemical mechanism of SDH, Scheme C1-5 (*64*). Upon formation of the E•NAD•Sacc central complex and active site closure, the first base (pK_a = 6.2) accepts a proton from the Sacc secondary amine as a hydride is transferred to the 4-R position of the nicotinamide ring of NAD. The second base (pK_a = 7.2)

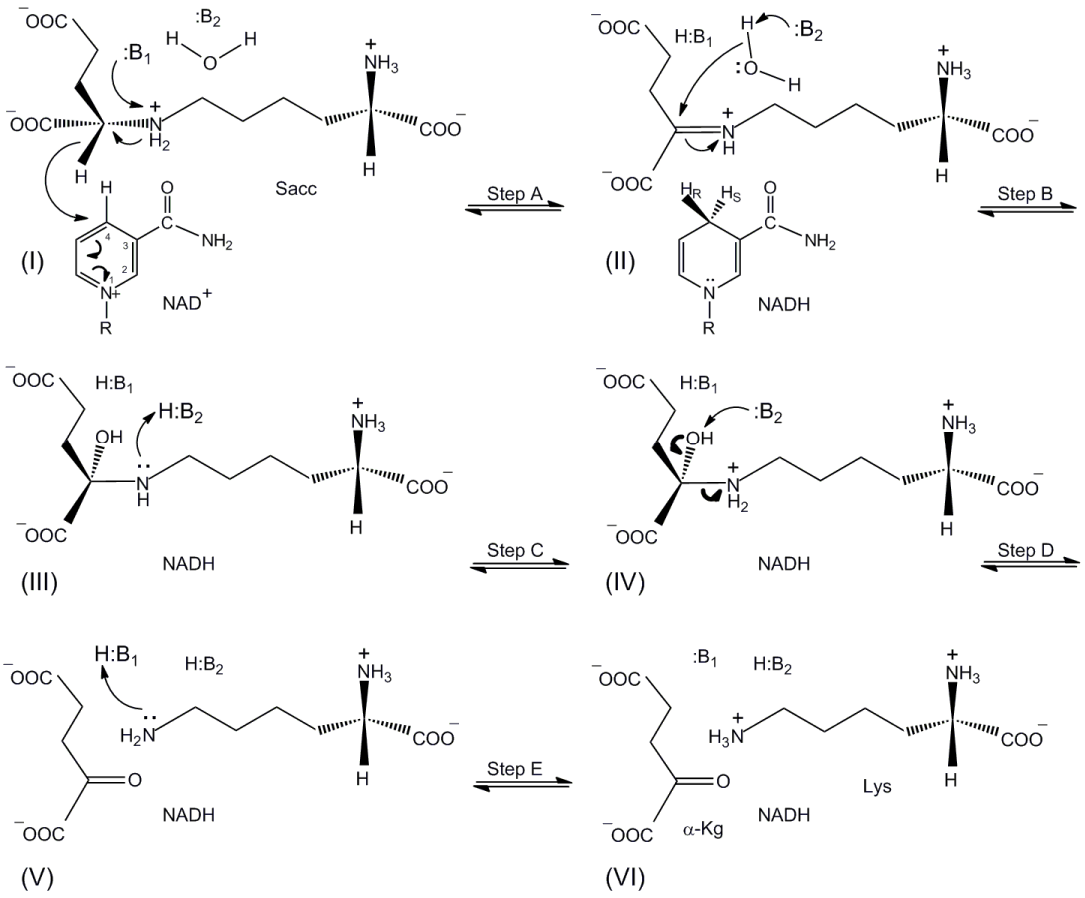

Scheme C1-5. Proposed proton shuttle chemical mechanism for SDH **I** central complex E•NAD^+•saccharopine upon NAD^+ and saccharopine binding; **II** Schiff base (imine) intermediate; **III** carbinolamine intermediate; **IV** protonated carbinolamine; **V** central complex E•NADH•α-Kg•Lys; **VI** protonated lysine

activates water to hydrolyze the imine and then shuttles a proton between itself and the carbinolamine intermediates, which collapse to give α-Kg and Lys with a neutral ε-amine. The ε-amine of Lys is then protonated by the conjugate acid of the base with pK_a of 6.2.

On the basis of the pH dependence of kinetic parameters in the direction of Lys formation, two groups were identified, one with the pK_a of about 6.2 and the second one with a pK_a of about 7.2. Both groups have to be unprotonated for optimal activity. The group with the pK_a of 6.2 is observed only in the

V_1/K_{Sacc} pH profile. It was proposed this group is B_1, and it contributes to catalysis and Sacc binding. The second group is observed in the V_1/K_{Sacc} (pK_a = 7.2), V_1/K_{NAD} (pK_a = 7.4), and V_1 (pK_a = 7.3) pH-rate profiles. It was proposed that this group with an average pK_a of 7.2 is the same one in all three pH-rate profiles, and that it contributes to binding and catalysis as B_2. The group seen in the V_1/K_{NAD} profile with the pK_a of 7.4 was not seen in the V_2/K_{NADH} profile. NADH binding is not sensitive to the protonation state of this group, likely due to the absence of the + charge on the nicotinamide ring. It was proposed this group is a cationic acid, Lys or His residue, located in the vicinity of the + charged nicotinamide ring of NAD (*64*).

In the direction of Sacc formation, two groups were identified in the V_2/K_{Lys} pH profile, with an average pK_a of 7.2. However, one has to be unprotonated and one protonated for optimal activity. The group that must be unprotonated is B_1 (pK_a = 6.2 in the direction of Lys formation), while B_2 must be protonated. Both of these groups were proposed to contribute to catalysis and binding of Lys. A group with the pK_a of 9.6 that must be protonated for dinucleotide binding was observed in the V_2/K_{NADH} profile. This group likely interacts with the negatively charged phosphoryl oxygens of NADH via an ionic interaction, and is likely a Lys or Arg. Two groups were observed in the V_2 pH profile. The first group with the pK_a of 5.8 had to be unprotonated for optimal activity and was proposed to be important for activity, while titration of the second group exhibited a partial change at high pH (pK_a = 8.4), and was thus not essential for activity. A decrease in the primary deuterium isotope effect

from 1.6 at pH 6.1 to 1.2 at pH 5.6 is observed, suggesting a step other than the hydride transfer (e.g. a conformational change) becomes rate-limiting at low pH. A group with the pK_a of 8.9 was observed in the $V_2/K_{\alpha\text{-Kg}}$ pH profile, which had to be protonated for optimal activity, and it was suggested this is the same group as that with pK_a of 8.4 seen in the V_2 profile, and is a kinetic pK_a responsible for a change in kinetic mechanism at pH >8.5. The pathway with α-Kg binding before Lys is a slower pathway (*64*).

The above-described studies provided a complete proposed chemical mechanism for SDH and suggested identities and approximate locations of catalytic and binding amino acid residues in the active site of the enzyme. However, data do not allow assignment of specific amino acid side chains to a given function.

C1.2.3 SDH: rate-limiting steps in the reaction

SDH catalyzes the *pro*-R specific transfer of a hydride from the Sacc secondary amine (C2 of the Sacc glutaryl moiety) to the C4 position of the nicotinamide ring of NAD (*65, 66*), concomitant with proton transfer from the secondary amine to base 1. If hydride transfer contributes to rate limitation a deuterium isotope effect will be observed upon deuteration of NADH in the *pro*-R position at C-4 of the dihydronicotinamide ring (*67, 68*). A finite isotope effect was observed, indicating hydride transfer contributes to rate limitation. Interestingly, the isotope effect was pH dependent, with the maximum effect observed at low pH, which decreased as the pH increased above the pK_a of 7.2, observed in the V_2/K_{Lys} pH profile; at a high pH the isotope effect tends to unity.

Data suggested that pH- and isotope-dependent steps were not the same in the direction of Sacc formation (*69*).

In addition to primary substrate deuterium kinetic isotope effects, solvent deuterium kinetic isotope effects were measured. Isotope effects, obtained as a ratio of the pH(D)-independent values of the kinetic parameters, were significant, suggesting proton transfer step(s) contribute to rate limitation of the overall reaction (*64*).

Multiple solvent deuterium/substrate deuterium kinetic isotope effects may potentially define the interrelationship between two isotope sensitive steps (*70*). When NADD was fixed and the multiple isotope effects were measured in D_2O and H_2O, the $^{D2O}(V/K)_D$ was smaller as compared to $^{D2O}(V/K)_H$, while when D_2O was fixed and the multiple isotope effects were measured with NADD and NADH as the substrate, the $^{D}(V/K)_{D2O}$ was equal to $^{D}(V/K)_{H2O}$. Data suggested a concerted proton and hydride transfer that is rate-limiting for the overall reaction, and also that hydride transfer cannot be the only rate-limiting step. To reconcile the data, a proton transfer was suggested in the hydride transfer step and some other step (likely the imine hydrolysis). The one in hydride transfer step causes the primary deuterium isotope effect to increase. The one in some other step causes it to decrease. The net result is no change in isotope effect (*64*).

To sum up, on the basis of isotope effects, hydride transfer and hydrolysis of the imine contribute to rate limitation along the reaction pathway in SDH. In addition, at low pH an isotope-independent step contributes to rate

limitation. This step is likely a conformational change in the free enzyme, which needs to occur prior to binding of the first substrate.

C1.2.4 SDH: active site mapping and substrate specificity, functional and structural aspects

In order to define the substrate specificity of SDH and to map the active site, a study of NADH, α-Kg, and Lys analogues was undertaken (*71*). Data formed the basis of the proposed hydrophobic/hydrophilic nature of the binding interactions in the SDH substrate-binding pockets and the potential identity of functional groups on all substrates important for binding (*71*).

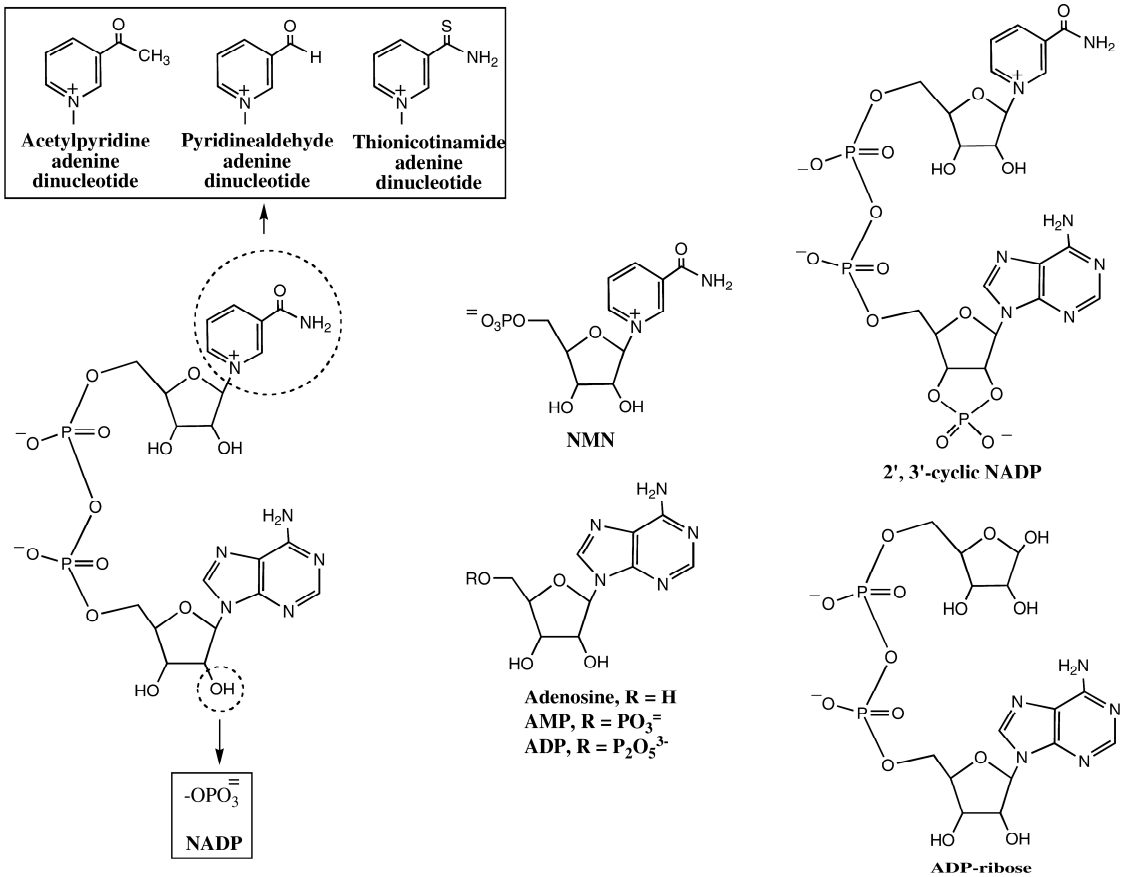

Figure C1-1. Substrate and inhibitory analogues of NAD. Reproduced with permission. Structures given in boxes exhibit substrate activity when they are used in place of NAD, while the other analogues are inhibitory.

NADP, 3-acetylpyridine adenine dinucleotide (3-APAD), 3-pyridine-aldehyde adenine dinucleotide (3-PAAD), and thionicotinamide adenine dinucleotide (thio-NAD) are slow substrates for SDH, Figure C1-1. Since 3-PAAD and thio-NAD bind to free enzyme with approximately the same affinity as NAD, it is likely the amide NH_2 group of the nicotinamide ring does not contribute much to dinucleotide binding. However, the affinity for 3-APAD was decreased 10-fold in comparison to NAD, suggesting SDH cannot accommodate the hydrophobic methyl group of 3-APAD, indicating a hydrophilic binding pocket for the nicotinamide ring of NAD. On the basis of inhibition experiments, NAD, NADP, and 2',3'-cyclic NADP all had comparable K_i values with NAD(P)H as the varied substrate, suggesting little or no effect of 2'- or 3'-phosphate. NADH binds 86-fold tighter to free enzyme than NAD, indicative of the preference for binding the reduced nicotinamide ring. AMP binds about 30-fold tighter than NAD and has only 3-fold lower affinity compared to NADH, while adenosine binds with an 8-fold lower affinity than AMP, indicative of the importance of the α-phosphate. ADP gives a 3-fold increase in affinity compared to ADP-ribose, but it is still about 5- and 2-fold lower than that of NADH and AMP, respectively. NMN binds poorly to the dinucletotide-binding site, with a 5-fold lower affinity than NAD. On the basis of these data, it was proposed that (a) the binding pocket of the nicotinamide ring of NAD is relatively hydrophilic, (b) most of the NAD-binding energy comes from the AMP moiety of NAD, and (c) since NAD binds with an approximately 2 orders of magnitude lower affinity than NADH, the oxidized and reduced

dinucleotides produce distinctly different conformations upon binding. Also, two distinctly different conformations were proposed to exist upon binding of NADH or NADPH. NADH binds about 2-fold tighter than NADPH (K_{iNADPH} value increased about 2-fold), and the presence of the 2'phosphate groups resulted in about 1 order of magnitude increase in Michaelis constants of all substrates. In agreement, K_{iLeu} also increased by a factor of 10 with NADPH vs. NADH (*71*).

Glyoxylate, pyruvate, α-ketobutyrate, α-ketovalerate, α-ketomalonate, and α-ketoadipate acted as substrates that can substitute for α-Kg in the SDH reaction. A number of analogues of α-Kg are inhibitory, including aliphatic (from oxalate to α-ketopimelate) and aromatic (from pyridine-2,4-dicarboxylate to pipecolic acid), Figure C1-2. Initial velocity and inhibition studies using these analogues of α-Kg suggested that (a) the keto acid binding pocket of SDH is relatively large and flexible, on the basis of the bulky aromatic ring of a pyridine dicarboxylic acid, as well as a negative charge at C3 but not C4 of α-Kg being accommodated, (b) a side chain with three carbon atoms (from the α-keto group up to and including the side chain carboxy group) is optimal for binding of α-keto acids, (c) the distance between the C1−C2 unit and the C5 carboxylate of the α-keto acid is also important for binding (two carbons is optimal), and (d) the α-oxo group contributes a factor of 10 to affinity (*71*).

In order to define the amino acid substrate binding pocket, Lys substrate analogues were tested for their effectiveness to inhibit the reaction. Several aliphatic amino acids acted as competitive inhibitors of Lys, Figure C1-3. The

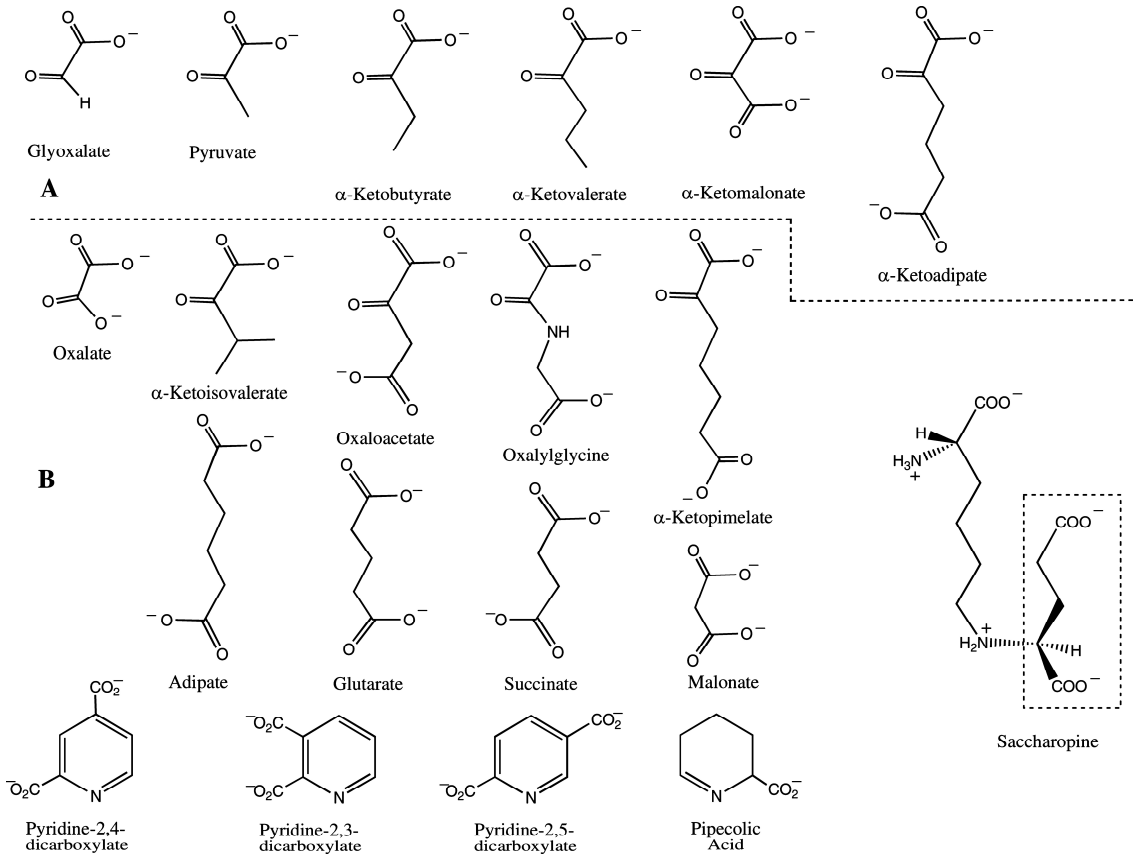

Figure C1-2. Substrate and inhibitory analogues of α-ketoglutarate or the glutamyl portion of saccharopine. Reproduced with permission. **(A)** substrate analogues and **(B)** competitive inhibitors. The portion of Sacc in the dotted box is mimicked by the inhibitors.

measured inhibition constants indicated that hydrophobic amino acids with a linear three- or four-carbon side chain were good inhibitors. It was proposed by the authors that (a) the amino acid substrate binding pocket is hydrophobic, (b) the optimal length of the hydrophobic portion of the amino acid side carbon chain is three or four carbons, and (c) the amino acid binding pocket can accommodate a branch at the γ-carbon, but not at the β-carbon (*71*).

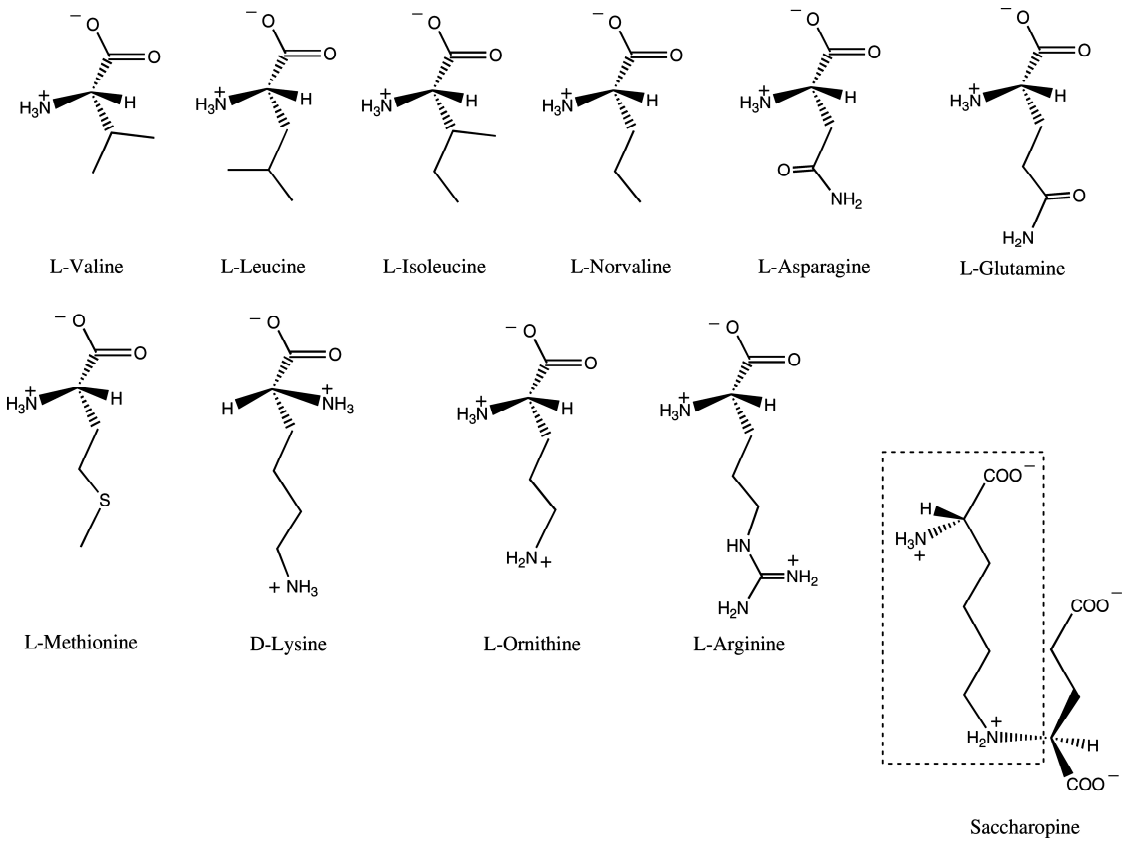

Figure C1-3. Inhibitory analogues of L-lysine or the lysyl portion of saccharopine. Reproduced with permission. The portion of Sacc in the dotted box is mimicked by the inhibitors.

C1.2.5 SDH WT apoenzyme structure

The 1.64 Å apoenzyme structure of SDH was solved (*52*). SDH is composed of two domains, Figure C1-4. The N-terminal domain, which also contains the C-terminus of the molecule (residues 2-134, 326-373), and C-terminal domain (residues 135-325) form a narrow cleft between them, and this is where the active site is located. Both domains consist of central parallel β-sheet flanked by mostly helical structure on one side of the β- sheet, and an extended polypeptide chain with some α-helical segments on the other side of the β-sheet (*52*).

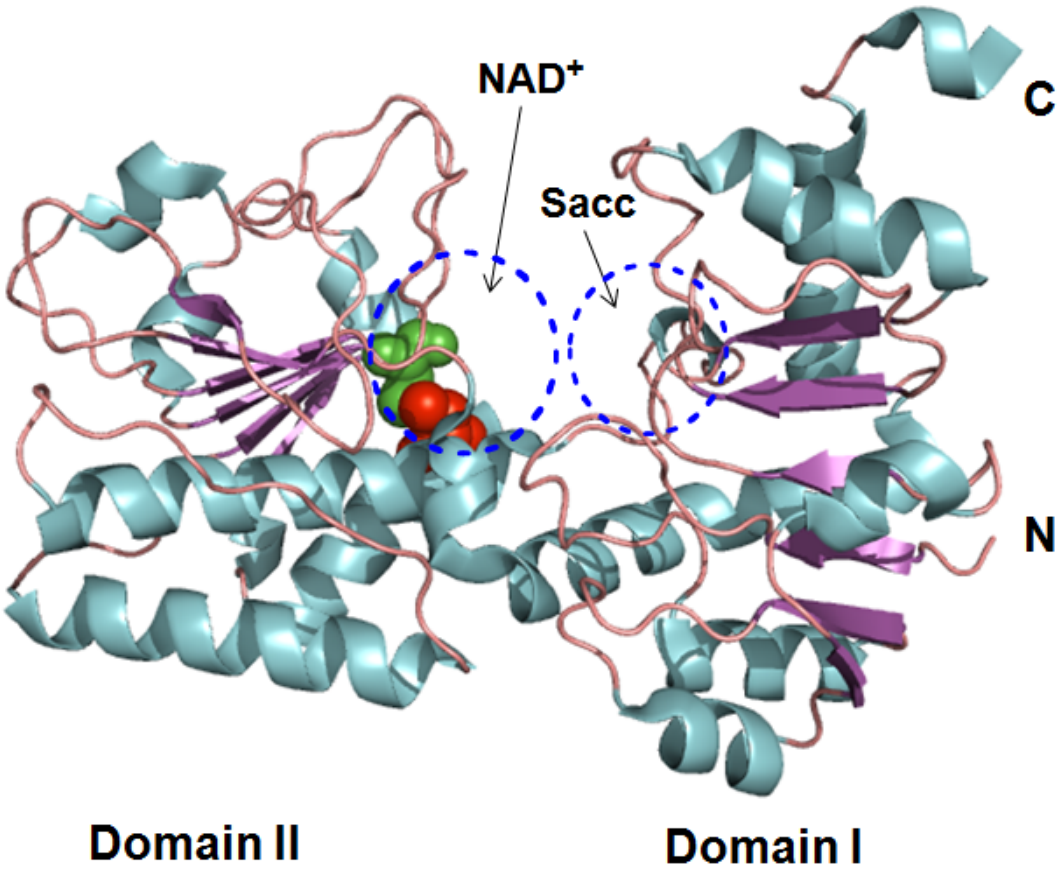

Figure C1-4. Apoenzyme SDH WT structure: two domains embrace the active site inside the cleft. Secondary structural elements, α-helix (cyan), β-sheet (purple), and loop (salmon) are color-coded. N-terminal Domain I, which also includes the C terminus of SDH, provides a substrate-binding surface. C-terminal Domain II contains a Rossmann fold motif and provides a dinucleotide binding surface. Proposed substrate binding sites, estimated via modeling, are circled in blue dotted lines to show their approximate location. Cys 205 (red) and 249 (green), shown in spheres, are forming the disulfide bond. The cartoon representation of SDH in this figure was generated using the PyMOL and the pdb coordinates of the SDH apoenzyme PDB ID: 2Q99 (*52*).

Domain II contains the dinucleotide binding motif, or the Rossmann fold (*72*) and Domain I is of a similar α/β fold topology and contains the substrate-binding domain, Figure C1-4. Also, the structure reveals a disulfide bond between conserved C205 and C249 residues. No conformational strain or perturbation of the Rossmann fold was observed. Data suggested the C205-C249 disulfide bond may be physiologically relevant (*52*).

A model of the E•NAD•Sacc ternary complex was proposed based on the substrate-bound structures of a homologous alanine dehydrogenase from the cyanobacteria *Phormidium lapideum*, PDB IDs: 1PJC and 1SAY (*42*). Residues K77, E122, and H96 were identified as potentially important for substrate binding and/or catalysis, while R18 and R131 were implicated in the interaction with two carboxylates of Sacc. Also, a conformational change was suggested to be required for catalysis with K99 and D281 potentially mediating this conformational change (*52*).

C1.2.6 Crystal structures of SDH WT with ligands bound

Three structures of SDH WT have been determined in the presence of sulfate, adenosine monophosphate (AMP), and oxalylglycine (OxGly). On the basis of the superposition of these structures, and modeling parts for which no data were available (Lys moiety of Sacc and NMN^+ moiety of NAD^+) a semiempirical model of E•NAD•Sacc ternary complex was generated (*51*).

C1.2.6.1 Structural analysis of the adenosine monophosphate bound SDH structure

As suggested above, AMP contributes the majority of the binding energy of NAD (*71*). Efforts to co-crystallize WT SDH in the presence of NMN^+ or NAD^+ failed, likely due to inappropriate crystallization conditions, or their weak binding. In addition, NADH which has higher affinity also failed to co-crystallize (*51*).

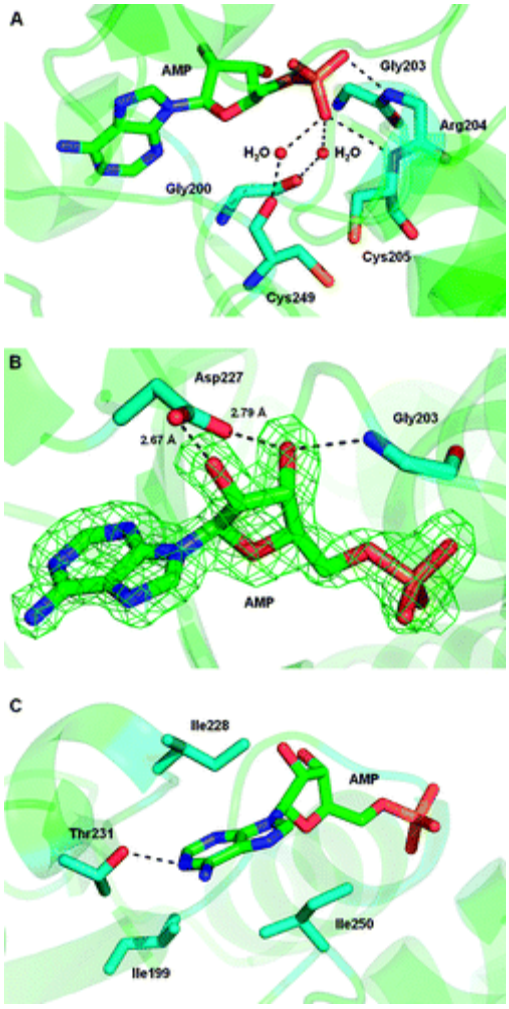

Figure C1-5. Interaction of the AMP molecule with SDH. Reproduced with permission. **(A)** The phosphate moiety of the AMP interacts solely with the main chain of the enzyme. It interacts directly with N atoms of Arg204 and Cys205 and indirectly through water molecules with O atoms of Gly200 and Cys249. **(B)** The ribose moiety interacts directly with Asp227 and the main chain N atom of Gly203. The surrounding $F_o - F_c$ electron density for AMP is also shown. **(C)** Adenine interaction is mainly hydrophobic via Ile199, Ile228, and Ile250. However, Thr231 makes one hydrogen bond to N^1 of adenine (*51*).

Consistent with tight binding of AMP, three hydrophobic residues and eight hydrogen bonds are involved in AMP binding to SDH, Figure C1-5. The ribose moiety of AMP is involved in hydrogen bonding with D227. The Rossmann fold of SDH shows the characteristics of a classical $NAD(P)^+$ binding domain, since D227 is located 20 residues C-terminal to the

conserved GXXGXXG motif (*73, 74*). It was previously suggested on the basis of the pH dependence of the K_i for AMP that two groups on the enzyme are important for AMP binding, one protonated and one unprotonated (*71*). Crystal structure of the AMP-bound SDH suggests the unprotonated group is Asp227 (*51*).

C1.2.6.2 Cysteines 205 and 249 are involved in disulfide bond formation

A disulfide bond between C205 and C249 is observed in apo-SDH and the sulfate-bound SDH structures with distances between the sulfur atoms of 2.04 and 2.10 Å, respectively. Interestingly, no disulfide bond was observed in the AMP-bound SDH molecule with a distance between the sulfur atoms of 3.64 Å, Figure C1-6.

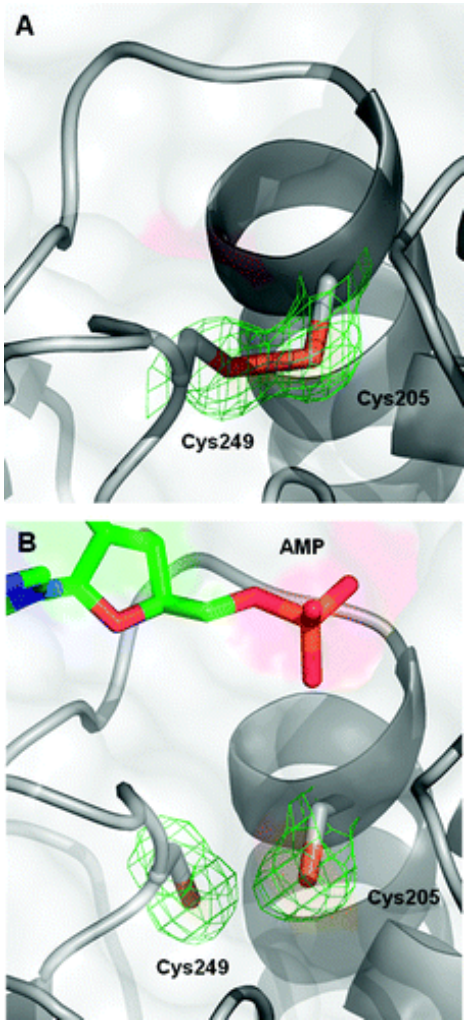

Figure C1-6. Close-up view of Cys205 and Cys249, which are involved in disulfide bond formation. Reproduced with permission.

(A) Disulfide bond in the sulfate-bound SDH molecule and surrounding $2F_o - F_c$ density. The apo-SDH (*52*) also contained a disulfide bond in a conformation similar to that shown in (A).

(B) Reduced cysteines and their surrounding $2F_o - F_c$ density in the AMP-bound structure (*51*).

C1.2.6.3 Structural analysis of the Oxalylglycine-bound SDH

It was previously determined that for binding of α-keto acids, a substrate containing up to six carbons can be accommodated, with three carbons being optimal, and that the α-oxo group contributes a factor of 10 to affinity. Among the surveyed α-Kg analogues, OxGly binds to SDH most tightly (*71*). Co-crystallization with natural substrates failed but a crystal structure of the OxGly-bound SDH was obtained. The α- and γ-carboxylates of OxGly interact with R18 and R131 respectively, Figure C1-7, and the optimum number of carbon atoms that can be accommodated is five, in agreement with kinetic data (*51, 71*).The α-keto (α-oxo) group of OxGly accepts hydrogen bonds from K77 (2.81 Å) and H96 (3.03 Å), which were proposed as candidates for the role of general acid-base catalysis in the chemical mechanism of SDH (*64*).

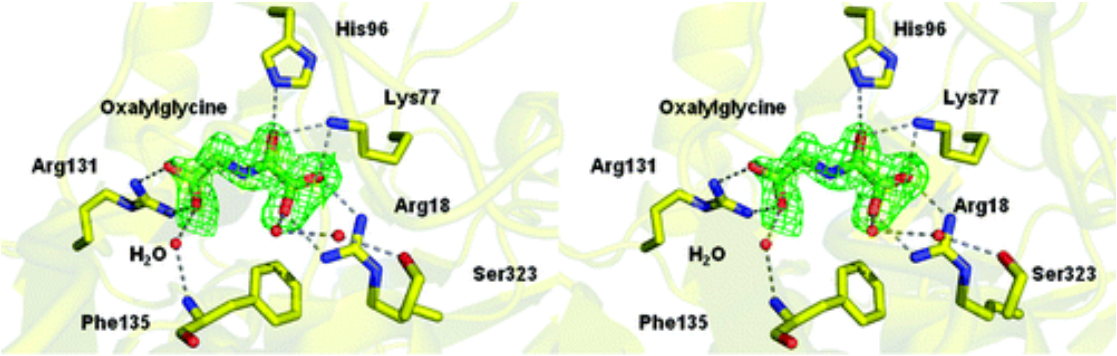

Figure C1-7. Stereoview of the binding of OxGly in the SDH active site. Reproduced with permission. R18 and R131 coordinate binding of OxGly via two carboxylates. K77 and H96 interact with the α-keto group, and K77 also interacts with α-carboxylate. F135 and S323 interact indirectly through a water network (*51*).

C1.2.6.4 Semiempirical model of substrate binding and chemical mechanism

Superposition of the AMP and OxGly structures and modeling the lysyl moiety of Sacc and the NMN^+ moiety of NAD^+ produced a semiempirical model of the E•NAD•Sacc ternary complex. The model is compatible with kinetic studies, but does not take into account any conformational changes upon substrate binding and possible synergistic interactions for binding of substrates (*51*). Several important observations can be made from the model, Figure C1-8. A number of ionizable residues are in close proximity to the secondary amine of Sacc. On the basis of pH studies and location of side chains in the ternary complex model, E78 or E122 were proposed to be candidates for the role of the catalytic base B_1, and K77 or H96 for the role of B_2 (*51, 64*).

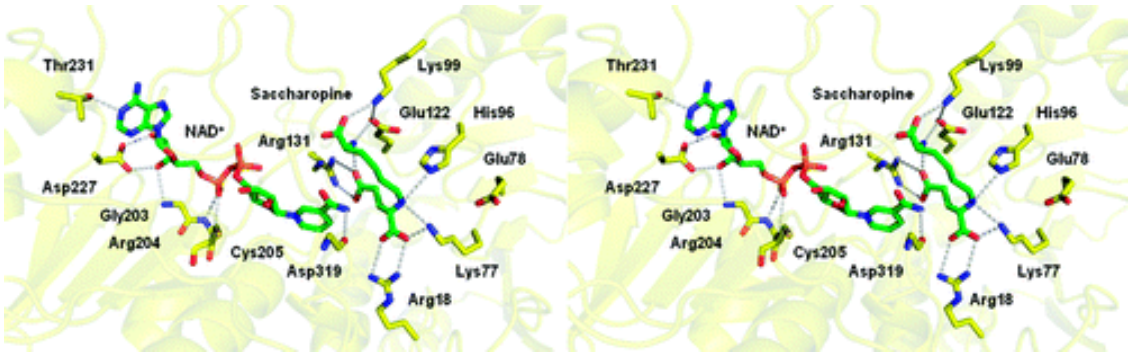

Figure C1-8. Semiempirical model for the SDH•NAD^+•saccharopine ternary complex, stereoview. Reproduced with permission. All of the interactions between enzyme residues and saccharopine are shown in gray dotted lines (average distance is 2.96 ± 0.18 Å). In the model, Sacc may form an intramolecular electrostatic bond, which folds the Sacc onto itself to accommodate the substrate in the highly hydrophilic SDH active site and to minimize the binding energy by intramolecular hydrophobic interaction between the aliphatic segments of lysine and the glutamate moiety of the Sacc.

The nicotinamide ring of NAD^+ is located in the appropriate position for the *pro-R* hydride transfer. However, while the optimum distance for hydride transfer is of 2.6−3 Å, the distance between C4 of nicotinamide and C8 of Sacc is 4.7 Å. These data suggest a need for active site closure before the catalytically competent enzyme conformation is generated. R18 and R131 coordinate binding of Sacc via the electrostatic and hydrogen-bonding interactions with the carboxylates of the glutamate moiety of Sacc. K77 and H96 directly interact with the secondary amine of Sacc. K99, E122, and the Sacc lysyl moiety make a network of electrostatic and hydrogen bond interactions (*51*).

C1.3 Research carried out in this dissertation, experimental design

The overall goal of the investigation described in this dissertation is to elucidate the details of the previously proposed chemical mechanism of saccharopine dehydrogenase from *Saccharomyces cerevisiae*.

The specific aims are to

(1) study the role of the disulfide formed between C205 and C249 in the dinucleotide-binding site of SDH;

(2) generate a model of the dinucleotide-bound SDH structure; and

(3) identify B_1 and B_2, the catalytic groups in the active site of SDH.

We chose to address the specific aims with mechanistic and structural approaches. The C205S mutant enzyme was characterized with initial velocity, pH profiles and isotope effect studies. Apo- and NADH-bound C205S crystal

structures were solved. To probe the acid-base chemical mechanism of SDH, kinetic parameters at pH 7.0 were obtained for K77M and H96Q single mutant enzymes via the initial velocity studies. Additionally, the isotope effects were measured for K77M/C205S and H96Q/C205S double mutant enzymes. Currently, the complete kinetic characterization of the K77M/C205S and H96Q/C205S double mutant enzymes is under way, including initial velocity, pH-rate profiles, and pH-dependence of the isotope effects studies.

C1.4 Significance of the project

Lysine is an essential amino acid in mammals including humans. It cannot be synthesized *de novo* and must be supplied from the diet (*75*). However, plants, bacteria, and fungi are able to synthesize lysine using two distinct biosynthetic pathways, the DAP and AAA pathways (*1, 3, 10, 14*). Among examples of organisms with the AAA pathway are human pathogenic fungi *Candida albicans*, *Cryptococcus neoformans,* and *Aspergillus fumigatus*, and the plant pathogen *Magnaporthe grisea*, but also nonpathogenic yeasts and molds, including *Saccharomyces cerevisiae* (*76, 77*), *Yarrowia lipolytica* (*78*)*, Schizosaccharomyces pombe* (*79*)*, Rhodotorula glutinis* (*80*)*, Candida maltosa* (*81*) *, Neurospora crassa* (*47*)*,* and *Penicillium chrysogenum* (*82*).

The AAA pathway is unique to fungal organisms, therefore, enzymes of this pathway are of a particular interest as potential targets for anti-fungal drug design (*10*). The enzymes of the AAA pathway from *S. cerevisiae* display a high degree of identity at the level of amino acid sequence to their homologues from pathogenic fungi, as seen in multiple sequence alignments. For example, the

identity of saccharopine dehydrogenase (SDH) from *S. cerevisiae* is 81%, 69%, 61%, 58%, 56%, and 54% to its homologues from *Candida glabrata*, *Candida albicans*, *Magnaporthe grisea*, *Cryptococcus neoformans*, *Aspergillus fumigatus*, and Emericella nidulans, respectively. Even more crucial is the conservation of the active site residues at the level of three-dimensional structure in SDH from these organisms (*52*). Therefore, the knowledge of enzyme mechanisms obtained with enzymes *S. cerevisiae* can be useful when designing inhibitors of enzymes from pathogenic fungi.

Among the enzymes of the AAA pathway, homocitrate synthase (*15*) and more recently homoisocitrate dehydrogenase (*16*) have been targeted in drug design efforts. No drug candidates have been reported to date, that would target saccharopine dehydrogenase. Interestingly, two of seven Lys auxotrophs obtained with gene disruption experiments of *Candida albicans* did not have a detectable SDH activity. A plasmid containing the *LYS1* gene, encoding SDH, complemented *lys1* mutants in both *S. cerevisiae* and *C. albicans* (*83*). Data suggest an inhibited SDH would effectively prevent the growth of fungi. Having a complete understanding of the chemical mechanism of SDH will help determine its conduciveness to drug design.

In a broader sense, this investigation contributed to the basic field of mechanistic enzymology, i.e., the body of knowledge about how enzymes work. While knowledge of the general mechanism of amino acid dehydrogenases is now textbook, the details of the chemical mechanism of SDH from *S. cerevisiae* may find future applications.

Chapter 2

Role of the C205-C249 Disulfide Bond in the Dinucleotide-Binding Site of Saccharopine Dehydrogenase from *Saccharomyces cerevisiae*

C2.1 Introduction

Immunocompromised patients, those suffering from cancer, AIDS, or post-transplantation conditions, are susceptible to infection by opportunistic pathogenic fungi. Fungi resistant to the present arsenal of antifungal agents have been found, indicating a need for more effective agents (*84*). Enzymes of the α-aminoadipate pathway (AAA) for L-lysine biosynthesis are unique to fungi and have been proposed as targets for antifungal drug design (*10, 83*). Saccharopine dehydrogenase (SDH) [N^6-(glutaryl-2)-L-lysine:NAD-oxidoreductase (L-lysine-forming) (EC 1.5.1.7)] catalyzes the final step of the AAA pathway, the reversible NAD-dependent oxidative deamination of saccharopine to generate L-lysine and α-ketoglutarate (eq.1).

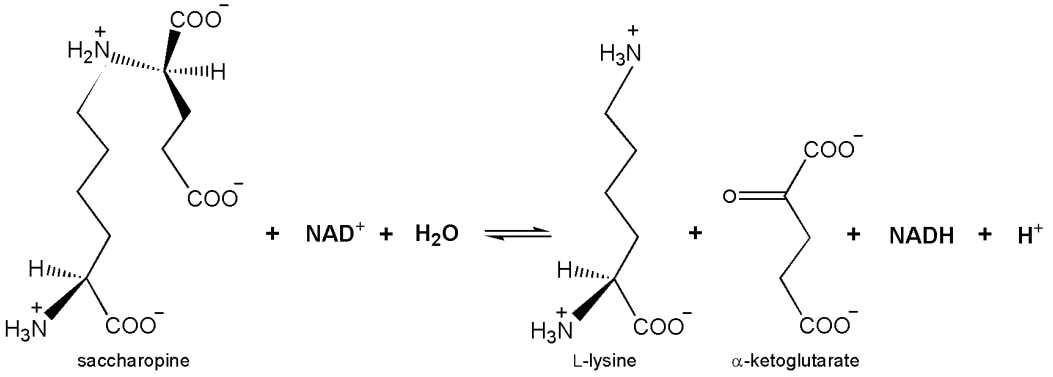

(1)

A multiple sequence alignment of the amino acid sequence of SDH from *Saccharomyces cerevisiae* against the database of all organisms reveals a high degree of conservation with the sequences of human pathogenic fungi. The sequences of SDH from *Emericella nidulans*, *Aspergillus fumigatus*, *Cryptococcus neoformans*, *Candida albicans*, and *Candida glabrata* have identities of 54%, 56%, 58%, 69%, and 81%, respectively, to the sequence of SDH from *S. cerevisiae*. Alignment of the SDH sequences of *E*. *nidulans*, *C*. *albicans*, and *C*. *glabrata* to that of *S. cerevisiae*, taking into account the three dimensional structure, indicated that similarities were highest in the core regions including the active site. In addition, all of the active site residues are completely conserved, and thus information obtained for the *S. cerevisiae* SDH should generally apply to the enzyme from pathogenic fungi (*52*).

The *S. cerevisiae* SDH is a monomer of 373 amino acids, with a calculated molecular mass of 41,464 Da and one binding site for reactants per molecule of enzyme (*51-54*). Chemical modification of SDH by *p*-chloromercuribenzoate and iodoacetate resulted in alkylation of the same cysteine residue. Alkylation was prevented in the presence of NADH, and protection was enhanced by the addition of the substrates α-Kg and Lys. Data suggested a cysteine might be essential for coenzyme binding (*54*). In the crystal structure of the apoenzyme form of SDH, two of four available cysteine residues (C205 and C249) are located near one another in the center of the Rossmann fold of domain II and can form a disulfide bond (S-S distance: 2.04Å), Figure C2-1. The two cysteines, C205 and C249, are conserved in all

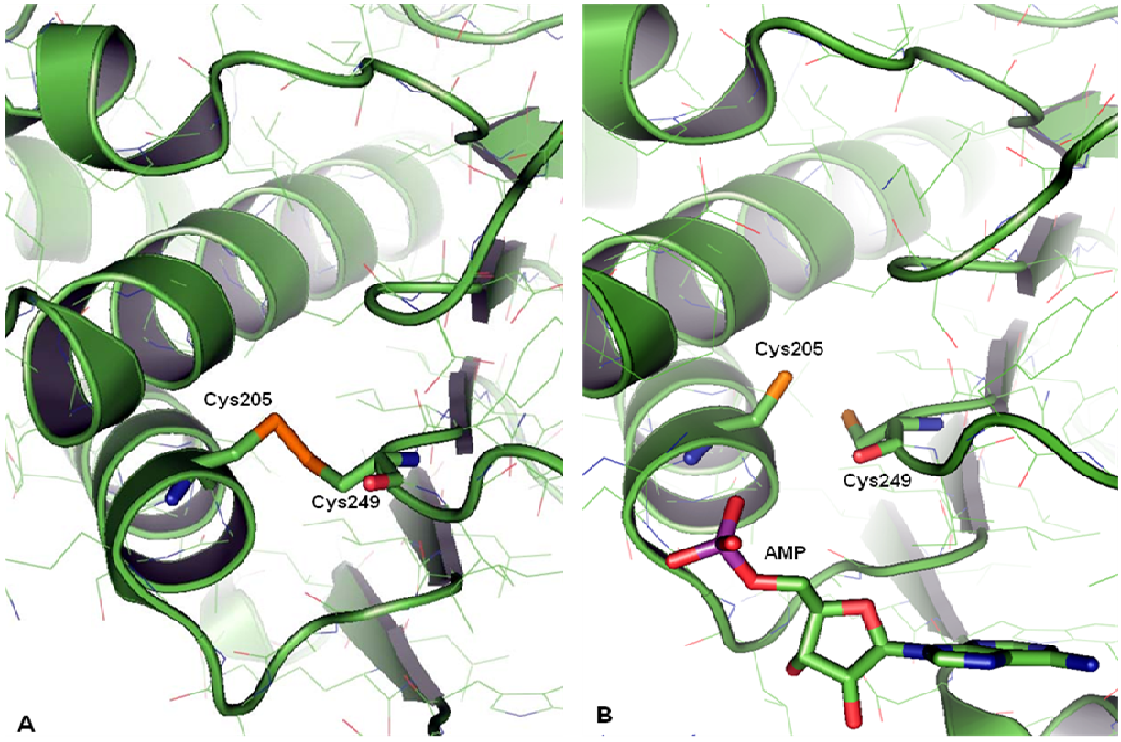

Figure C2-1: **Close-up View of the Disulfide Formed From Two Thiols, C205 and C249, Near the Dinucleotide-binding Site. (A)** Disulfide between C205 and C249 in the WT SDH (S-S distance is 2.04 Å). **(B)** Reduced cysteines in the AMP-bound WT SDH (S-S distance is 3.64 Å). Cartoon representation was made using the SDH apo-enzyme structure, PDB ID: 2Q99 (*52*), AMP-bound structure, PDB ID: 2QRK (*51*), and PyMol program version 0.95.

fungal SDH sequences available, and may be physiologically relevant (*52*). A disulfide bond is observed in structures of the apoenzyme and those with ligands bound to the substrate-binding domain. However, a structure was solved with AMP bound in the dinucleotide binding site with a dithiol present (S-S distance: 3.64Å) (*51*). Both cysteines are conserved in eukaryotic organisms, and C249 is conserved in bacteria, but C205 is replaced by either valine (e.g. in *Silicibacter lacuscaerulensis*, *Rhodobacteraceae bacterium*, and *Rhodobacter sphaeroides*) or serine (e.g. in *Photobacterium profundum*). Taken together, data are consistent with the physiological importance of the disulfide bond between C205 and C249.

The kinetic mechanism of SDH from *S. cerevisiae* is steady state random, but with dinucleotide reactants binding to free enzyme, and with random addition of α-Kg and Lys (*60*). A chemical mechanism has been proposed for SDH that makes use of two acid-base catalytic groups, Scheme C2-1 (*64*). Once the E•NAD•Sacc central complex is formed, a base (pK_a 6.2) accepts a proton from the Sacc secondary amine as a hydride is transferred to the 4-R position of the nicotinamide ring of NAD. A second base (pK_a 7.2) activates water to hydrolyze the imine and then shuttles protons between itself and carbinolamine intermediates to give α-Kg and Lys with a neutral ε-amine. The ε-amine of Lys is then protonated by the conjugate acid of the base with a pK_a of 6.2. On the basis of isotope effects, hydride transfer and hydrolysis of the imine contribute to rate limitation along the reaction pathway (*64*).

In this manuscript, we used site-directed mutagenesis to change C205 to V or S to probe the role of the disulfide in the mechanism of SDH. The C205S mutant enzyme was completely characterized using a combination of steady state kinetics, pH-rate profiles, and isotope effects. Findings are discussed in terms of the overall mechanism of SDH.

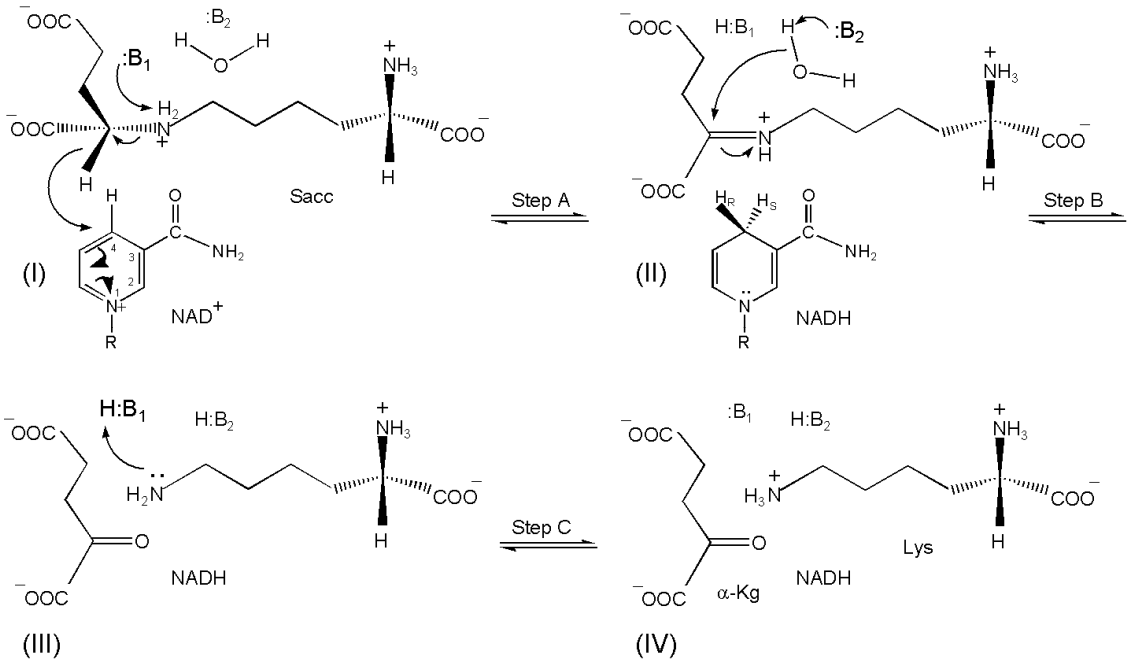

Scheme C2-1: Chemical Mechanism Proposed for Saccharopine Dehydrogenase.

I, the ternary central complex E•NAD•Sacc; **II**, imine (Schiff base) intermediate. NADH is shown with the C-4 *pro*-R position indicated; **III**, central product vcomplex E•NADH•α-Kg•Lys with a neutral lysine ε-amine; **IV**, the central product complex E•NADH•α-Kg•Lys with a protonated ε-amine of lysine. With the exception of saccharopine, no stereochemistry is implied.

Step A, contains the concerted proton and hydride transfer, acid-base chemistry is catalyzed by B_1; **Step B**, imine hydrolysis, contains the formation of carbinolamine and protonated carbinolamine intermediates, all acid-base chemistry is catalyzed by B_2; **Step C**, protonation of the ε-amine of lysine, acid-base chemistry is catalyzed by B_1.

C2.2 Materials and Methods

Chemicals. L-saccharopine, chloramphenicol, phenylmethylsulfonyl fluoride (PMSF), baker's yeast alcohol and aldehyde dehydrogenases, Sephadex G-10, acrylamide, β-mercaptoethanol (β-ME), ethylenediaminetetraacetic acid (EDTA), lysozyme, and lithium chloride were obtained from Sigma-Aldrich. L-lysine, α-ketoglutarate, β-NADH and β-NAD, imidazole, ampicillin (Amp), Luria-Bertani (LB) broth, and LB agar were purchased from USB. Mes, Hepes, Taps, and Ches, were from Research Organics. AG MP-1 resin was from Bio-Rad. Deuterium oxide (D_2O) (99 atom % D), ethanol-d_6 (99 atom % D), deuterium chloride (DCl) (99.5 atom % D), and sodium deuteroxide (NaOD) (99 atom % D) were purchased from Cambridge Isotope Laboratories. Sodium chloride, potassium chloride, and nickel sulfate were from Mallinckrodt Baker. The nickel-nitrilotriacetic acid (Ni-NTA) agarose resin, isopropyl-β-D-1-thiogalactopyranoside (IPTG), and the QuikChange site-directed mutagenesis kit were purchased from Qiagen, Gold Biotechnology, and Stratagene, respectively. All other chemicals and reagents were obtained from commercial sources, were reagent grade, and were used without further purification.

***Synthesis of A-side NADD*.** SDH catalyzes the transfer of a hydride from the *pro*-R position of C-4 of the nicotinamide ring of NADH to the C-2 position of the glutaryl moiety of saccharopine (*65, 66*). A-side NADD was synthesized according to Viola et al. (*85*) with minor modifications. Baker's yeast alcohol dehydrogenase was used instead of horse liver alcohol

dehydrogenase, and at the stage of the AG MP-1 anion exchange chromatography NADD was eluted with 0.4 M LiCl, pH 10.0, instead of 0.2 M LiCl. Finally, a 0.7 × 50 cm Sephadex G-10 column was used for gel filtration at the desalting stage instead of the 1.6 × 60 cm Bio-Gel P-2 column.

***Site-Directed Mutagenesis*.** Two site-directed mutants of SDH, C205V and C205S, were prepared using the QuikChange site-directed mutagenesis kit. A pET-16b derivative plasmid pSDHHX1 containing the *LYS1* gene from *Saccharomyces cerevisiae* inserted into the *Nde*I/*Bam*HI restriction sites was used as a template (*60*). Whole gene sequencing was performed at the Sequencing Core facility of the Oklahoma Medical Research Foundation. To confirm the mutations, the resulting sequence was compared to that of the wild type using ClustalW and/or BLAST. To make the C205V mutant enzyme, the forward and reverse primers were 5'-GGT GCG CTA GGA AGA **GTT** GGT TCC GGT GCC-3' and 5'-GGC ACC GGA ACC **AAC** TCT TCC TAG CGC ACC-3', respectively, and for the C205S mutant enzyme, the forward and reverse primers were 5'-GGT GCG CTA GGA AGA **TCT** GGT TCC GGT GCC-3' and 5'-GGC ACC GGA ACC **AGA** TCT TCC TAG CGC ACC-3', respectively. The mutated codons are shown in bold letters.

Enzyme Expression and Purification. The C205V and C205S mutant enzymes were expressed in BL21 (DE3)-RIL *Escherichia coli* cells and purified following the procedure reported previously (*60*) with some modifications. Briefly, induction of protein expression at 37°C was carried out by addition of 0.2 mM IPTG, once cell growth exhibited an OD_{600nm} of 0.3−0.4 and the cell

growth was then continued at 37°C for an additional 3-4 h before harvesting. Cells were harvested by centrifugation, resuspended in 100 mM Hepes pH 7.0, 100 mM NaCl, 5 mM imidazole, 1 mM PMSF, 100 µg/mL lysozyme, and 0.5 mM EDTA, and maintained at -20°C until needed. The cells were thawed and sonicated on ice for twelve minutes with a 10/50 seconds on/off cycle, using a MISONIX Sonicator XL. After centrifugation to remove the cell debris, the supernatant was applied to a Ni−NTA affinity column, and the chromatogram was developed by a step imidazole gradient from 30 to 300 mM in the sonication buffer. The concentration of NaCl was increased to 300 mM in all elution buffers, and the 150 -300 mM imidazole elution buffers did not contain 1 mM PMSF. Fractions of 150-300 mM imidazole were pooled and the purity of the SDH was assessed using Coomassie Blue stained SDS gels; the purity of the enzymes was >95%. Enzyme was dialyzed against 10 mM Hepes pH 7.0, 300 mM NaCl for pH studies. Otherwise, the storage conditions were 100 mM Hepes pH 7.0 and 300 mM NaCl at 4°C.

WT SDH was purified in the presence of 15 mM β-ME before and during the Ni-NTA column chromatography, adjusting the β-ME concentration to 50 mM at all later stages. After purification, the sample was split into two parts and one part was dialyzed to remove β-ME. Initial velocity assays were done for dialyzed and undialyzed SDH over a period of two months. No significant difference in the activity of the two samples was observed (data not shown).

Enzyme Assays. Initial velocities were measured using a Beckman DU 640 UV-visible spectrophotometer. All assays were performed at a temperature

of 25℃. Enzyme activity was measured by monitoring the increase (forward reaction direction) or decrease (reverse reaction direction) in absorbance at 340 nm (ε_{340} = 6220 M^{-1} cm^{-1}) as NAD is reduced or NADH is oxidized. When NADH had to be maintained at high concentrations the reaction was monitored at 366 nm (ε_{366} = 3110 M^{-1} cm^{-1}). Reactions were initiated by addition of 10 µL of an appropriately diluted enzyme solution to quartz cuvettes with a path length of 1 cm containing 100 mM Hepes, pH 7.0 and all other reaction components in a final volume of 0.3 mL (forward reaction direction) or 1 mL (reverse reaction direction). In the forward reaction direction, the initial velocity was measured as a function of NAD (0.5-5 K_m) at fixed saccharopine (0.5-5 K_m). In the reverse reaction direction, the initial velocity was measured as a function of two substrates, while maintaining the third at saturation in a pairwise analysis. Also, a systematic analysis was carried out, first measuring the initial rate as a function of NADH (0.5-5 K_m) at different fixed α-Kg concentrations (0.5-5 K_m) and a fixed Lys concentration, and then repeating the experiment at different fixed Lys (0.5-5 K_m). The C205V and C205S mutant enzymes were stable even in dilute solution.

pH Studies. Initial rates were measured in the direction of Lys formation and Sacc formation, varying one reactant at saturating levels of all others for the C205S mutant enzyme as a function of pH at a temperature of 25℃. The kinetic parameters *V* and *V/K* were estimated and the data were plotted as log($V/\mathbf{E_t}$) or log($V/K\mathbf{E_t}$) vs. pH. The pH was maintained using the following buffers: Mes 5.5-6.8; Hepes 6.8-8.2; Taps 8.2-9.0; and Ches 9.0-10.0. To

minimize pH fluctuations, 10 μL of the appropriately diluted enzyme in 10 mM stock buffer was added to a 1 mL reaction mixture buffered at the desired pH with 100 mM buffer. When buffers were changed, data were collected with the new buffer at a pH overlapping the old buffer to test for inhibitory effects of the buffers; no buffer effects were observed. For reactions measured at the pH extremes, below 5.5 and above 10.0, Mes pH 5.5 was titrated with concentrated HCl and Ches pH 10.0 was titrated with concentrated NaOH to keep the buffer stock at about the same concentration. The pH was measured before and after the reaction with observed changes limited to ≤ 0.1 pH unit. The C205S mutant enzyme is stable when incubated for 20 min or longer over the pH range 4.5-10.5.

***Primary Substrate Deuterium Kinetic Isotope Effects*.** Primary substrate deuterium kinetic isotope effects were measured by direct comparison of initial rates obtained with NADH(D) as the labeled substrate. $^{D}V_2$ and $^{D}(V_2/K_{Lys})$ were obtained by measuring the initial velocity as a function of Lys concentration at saturating levels of NADH(D) and α-Kg in the high and low pH-independent regions of the V_2 pH-rate profile, pH 5.5 and 9.0.

Notation for isotope effects used in this manuscript is that of Northrop (*86*), as modified by Cook and Cleland (*87*). An isotope effect on a kinetic parameter is indicated by a leading superscript. A primary deuterium kinetic isotope effect on V and V/K is written ^{D}V and $^{D}(V/K)$, while a solvent deuterium kinetic isotope effect is written ^{D2O}V, and $^{D2O}(V/K)$. A multiple isotope effect is written with a leading superscript to indicate the isotope varied and a following

subscript to indicate the fixed isotope. For example, an isotope effect on *V/K* measured in H_2O and D_2O with NADD fixed would be written as $^{D2O}(V/K)_D$.

***Solvent Deuterium Kinetic Isotope Effects*.** Isotope effects were obtained by direct comparison of initial rates in H_2O and D_2O at pH(D) 7.3. A value of 0.4 was added to pH meter readings to calculate pD (*88*). For rates measured in D_2O, substrates (α-Kg and Lys) and buffers were first dissolved in a small amount of D_2O and then lyophilized to replace exchangeable protons. The lyophilized powders were then redissolved in D_2O to give the desired concentrations, and pD was adjusted using either DCl or NaOD. NADH was dissolved in D_2O directly. Data were obtained as a function of Lys concentration at fixed saturating levels of NADH and α-Kg. Reactions were initiated by adding 6 µL of enzyme in H_2O to a total of 300 µL reaction mixture in D_2O; the final % D_2O is ca. 98.

***Multiple Solvent Deuterium/Substrate Deuterium Kinetic Isotope Effects*.** Multiple solvent deuterium/substrate deuterium kinetic isotope effects were obtained by direct comparison of initial rates in H_2O and D_2O with Lys varied and NADD and α-Kg fixed at 10 K_m. Rates were measured at pH(D) 7.3.

Data Processing and Analysis. Double reciprocal plots of initial rate vs. substrate concentration, secondary and tertiary replots were initially analyzed graphically to determine data quality and determine the correct rate equation for data fitting. Data were fitted to appropriate rate equations (*89*) using the Marquardt-Levenberg algorithm (*90*) supplied with the EnzFitter program by BIOSOFT, Cambridge, U. K. and the Fortran programs of Cleland (*91, 92*).

Kinetic parameters and their corresponding standard errors were estimated using a simple weighting method.

Data for substrate saturation curves were fitted using eq. 2. Data from the initial velocity patterns in the forward and reverse reaction directions were fitted to eq. 3. Data obtained from a systematic analysis, in which all reactant concentrations were varied, were fitted to eq. 4, while data for *V* and *V/K* deuterium isotope effects were fitted using eq. 5. The SE of a product or dividend was estimated using eq. 6.

$$v = \frac{V\mathbf{A}}{K_{\mathrm{a}} + \mathbf{A}} \tag{2}$$

$$v = \frac{V\mathbf{AB}}{K_{\mathrm{ia}}K_{\mathrm{b}} + K_{\mathrm{a}}\mathbf{B} + K_{\mathrm{b}}\mathbf{A} + \mathbf{AB}} \tag{3}$$

$$v = \frac{V\mathbf{ABC}}{\mathrm{constant} + (\mathrm{coefA})\mathbf{A} + K_{\mathrm{a}}\mathbf{BC} + K_{\mathrm{b}}\mathbf{AC} + K_{\mathrm{c}}\mathbf{AB} + \mathbf{ABC}} \tag{4}$$

$$v = \frac{V\mathbf{A}}{(K_{\mathrm{a}} + \mathbf{A})(1 + F_i E_V)} \tag{5}$$

$$\mathrm{SE}\,\frac{x}{y} = \frac{x}{y}\left[\left(\frac{\mathrm{SE}\,x}{x}\right)^2 + \left(\frac{\mathrm{SE}\,y}{y}\right)^2\right]^{1/2} \tag{6}$$

In eqs. 2-5, *v* and *V* are initial and maximum velocities, respectively, **A**, **B**, and **C** are substrate concentrations, K_{a}, K_{b}, and K_{c} are Michaelis constants for substrates A, B, and C, respectively, and K_{ia} is the dissociation constant of A from the EA complex. In eq. 4, the constant and coef terms are products of kinetic constants that depend on mechanism. In eq. 5, F_i is the fraction of D_2O in the solvent or deuterium label in the substrate, and E_V and $E_{V/K}$ are the

isotope effects minus 1 on *V* and *V/K*, respectively. In eq. 6, SE *x*, and SE *y* are computer generated standard errors of values for kinetic parameters *x* and *y*.

Data for pH-rate profiles that decreased with a slope of 1 at low pH and a slope of −1 at high pH were fitted to eq. 7. Data for pH-rate profiles with a slope of −1 at high pH were fitted to eq. 8. Data for pH-rate profiles with constant values at low and high pH were fitted to eqs. 9 and 10. Data for pH-rate profile that decreased with a slope of 2 at low pH were fitted to eq. 11. Data for the $V_2/K_{\alpha\text{-Kg}}$ pH-rate profile, which exhibited two pH dependent terms as the pH was increased, were fitted to eq. 7 from pH 4.8 to 6.9 and eq. 10 from pH 6.6 to 8.9, and the curves were normalized to one another; the curve from pH 8.9 to 9.8 is a hand-drawn line.

$$\log y = \log\left[C / \left(1 + \frac{\mathbf{H}}{K_1} + \frac{K_2}{\mathbf{H}} \right) \right] \tag{7}$$

$$\log y = \log\left[C / \left(1 + \frac{K_2}{\mathbf{H}} \right) \right] \tag{8}$$

$$\log y = \log\left[Y_{\mathrm{L}} + Y_{\mathrm{H}} \left(\frac{\mathbf{H}}{K_1} \right) / \left(1 + \frac{\mathbf{H}}{K_1} \right) \right] \tag{9}$$

$$\log y = \log\left[Y_{\mathrm{L}} + Y_{\mathrm{H}} \left(\frac{K_1}{\mathbf{H}} \right) / \left(1 + \frac{K_1}{\mathbf{H}} \right) \right] \tag{10}$$

$$\log y = \log\left[C / \left(1 + \frac{\mathbf{H}}{K_1} + \frac{\mathbf{H}^2}{K_1 K_2} \right) \right] \tag{11}$$

In eqs. 7-11, *y* is the observed value of *V* or *V/K* at any pH, *C* is the pH-independent value of *y*, **H** is the hydrogen ion concentration, K_1 and K_2 are the acid dissociation constants of functional groups required in a given protonation

state on enzyme or substrate for optimal binding and/or catalysis, and Y_L and Y_H are pH-independent constant values of *y* at low and high pH, respectively.

***Molecular Graphics*.** The three dimensional structure figure was prepared using PyMol version 0.95, DeLano, W. L. (2004) The PyMOL molecular graphics system, DeLano Scientific, San Carlos, CA, www.pymol.org.

C2.3 Results

Kinetic Parameters of the Mutant Enzymes. Initial velocity patterns for the C205V and C205S mutants were obtained at pH 7.0 by measuring the initial rate as a function of substrate concentrations as discussed in Material and Methods. Kinetic parameters are summarized in Table C2-1, and compared to those obtained for WT. Replacing C205 with S or V resulted in 2- and 3-fold increases, respectively, in $V_1/\mathbf{E_t}$, and 5- and 7-fold increases, respectively, in $V_2/\mathbf{E_t}$. Changes in the K_m values for reactants are minimal with the exception of K_{Sacc}, which decreased by 5- and more than 30-fold, respectively, for the C205V and C205S mutant enzymes; as a result, $V_1/K_{Sacc}\mathbf{E_t}$ is increased by a factor of 15- and 70-fold, respectively. In all other cases the increase in *V/K* reflects the increase in *V*. The remaining studies focused on the C205S mutant enzyme, since it has the most conservative substitution.

***pH Dependence of Kinetic Parameters*.** Over the entire pH-range studied the kinetic mechanism for WT SDH is sequential ordered, with NAD binding prior to saccharopine in the physiologic reaction direction (*64*). In the direction of saccharopine formation, the kinetic mechanism is steady state random, with NADH binding to free enzyme, but with random addition of α-Kg

and Lys. At the extremes of pH (≤ 5.0 and ≥ 8.5) the mechanism changes to an ordered one with NADH binding first followed by rapid equilibrium addition of α-Kg before Lys (*64*). There were no changes observed in the kinetic mechanism of the C205S mutant enzyme compared to WT SDH (data not shown).

The pH dependence of kinetic parameters obtained previously for the WT enzyme are reproduced in Figures C2-2 and C2-3 for comparison to those of the C205S mutant enzyme. pK_a values and pH-independent values of the parameters are summarized in Table C2-2 (*64*).

In the direction of Lys formation, the reaction of the C205S mutant enzyme is pH-dependent. $V_1/\mathbf{E_t}$ decreases from a constant value of about 1.3 s^{-1} at high pH to a constant value of about 0.7 s^{-1} at low pH; a pK_a value of about 7.5-7.7 was estimated for this partial change, Figure C2-2D. A partial change is also observed for $V_1/K_{NAD}\mathbf{E_t}$, which decreases from a constant value of $(5.3 \pm 0.2) \times 10^3$ $M^{-1}s^{-1}$at high pH to a constant value of $(2.4 \pm 0.1) \times 10^2$ $M^{-1}s^{-1}$at low pH; a pK_a value of about 7.1 is estimated for the change, Figure C2-2E. $V_1/K_{Sacc}\mathbf{E_t}$ decreases at low pH with a limiting slope of +2, giving pK_a values of about 5.7 and 6.5, Figure C2-2F.

In the direction of saccharopine formation, the reaction of the C205S mutant enzyme is also pH-dependent. $V_2/\mathbf{E_t}$ decreases from a constant value of $(9.3 \pm 0.8) \times 10^1$ s^{-1} at low pH to a new constant value of $(1.10 \pm 0.08) \times 10^1$ s^{-1}at high pH; a pK_a value of about 7.5 is estimated from the data, Figure C2-3E. $V_2/K_{NADH}\mathbf{E_t}$ decreases at high pH with a limiting slope of -1 giving a pK_a of about 9.5, Figure C2-3F. $V_2/K_{\alpha\text{-}Kg}\mathbf{E_t}$ decreases at low pH below a pK_a of about 5.7,

while at high pH, a partial change is observed, with a pK_a of about 7.4, Figure C2-3G. A bell-shaped pH-rate profile with limiting slopes of +1 and -1 was obtained for $V_2/K_{Lys}\mathbf{E_t}$; pK_a values of about 7.0 and 8.1 are estimated from the data, Figure C2-3H.

***Primary Deuterium Kinetic Isotope Effects*.** Finite primary substrate deuterium kinetic isotope effects were measured for the C205S mutant enzyme in the low and high pH-independent regions of the V_2 pH-rate profile, and at pH 7.3. Values of $^{D}(V_2/K_{Lys})$ and $^{D}(V_2)$ are somewhat higher for C205S than WT at all three pH values. Data, in comparison to those of WT, are summarized in Table C2-3 (*64*).

***Solvent Deuterium Kinetic Isotope Effects*.** Finite solvent deuterium kinetic isotope effects were measured at the neutral pH, and values of $^{D2O}(V_2/K_{Lys})$ and $^{D2O}(V_2)$ are, on average, slightly larger for C205S than WT, repeating the trend observed in the primary substrate deuterium kinetic isotope effects. Data, in comparison to those of WT, are summarized in Table C2-3 (*64*).

***Multiple Solvent Deuterium/Substrate Deuterium Kinetic Isotope Effects*.** Finite multiple solvent deuterium/substrate deuterium kinetic isotope effects were also measured at neutral pH, and values are comparable to those of WT within error. Data are summarized in Table C2-3 (*64*).

Table C2-1: Kinetic Parameters for SDH WT and Mutant Enzymes at pH 7.0

Parameter	WT[a]	C205V	C205S
forward reaction			
$V_1/\mathbf{E_t}$ (s^{-1})	1.1 ± 0.1[b]	3.20 ± 0.02	2.1 ± 0.2
Fold change	–	+(3 ± 0.3)[c]	+(2 ± 0.3)
$V_1/K_{NAD}\mathbf{E_t}$ ($M^{-1}s^{-1}$)	(1.2 ± 0.2)×10^3	(2.70 ± 0.03)×10^3	(1.2 ± 0.3)×10^3
Fold change	–	+(2.0 ± 0.4)	–
$V_1/K_{Sacc}\mathbf{E_t}$ ($M^{-1}s^{-1}$)	(1.6 ± 0.4)×10^2	(2.30 ± 0.04)×10^3	(1.1 ± 0.2)×10^4
Fold change	–	+(14.0 ± 3.6)	+(69± 21)
K_{NAD} (mM)	0.9 ± 0.1	1.20 ± 0.01	1.8 ± 0.4
Fold change	–	–	+(2.0 ± 0.5)
$K_{i\ NAD}$ (mM)	1.1 ± 0.3	1.50 ± 0.04	1.4 ± 0.5
Fold change	–	–	–
K_{Sacc} (mM)	6.7 ± 1.4	1.40 ± 0.03	0.20 ± 0.04
Fold change	–	-(5.0 ± 1.0)	-(34 ± 10)
reverse reaction			
$V_2/\mathbf{E_t}$ (s^{-1})	20 ± 1.2	(1.4 ± 0.1)×10^2	(1.06± 0.02)×10^2
Fold change	–	+(7.0 ±0.7)	+(5.0 ± 0.3)
$V_2/K_{NADH}\mathbf{E_t}$ ($M^{-1}s^{-1}$)	(1.05± 0.1)×10^6	(3.0 ± 0.5)×10^6	(1.1 ± 0.2)×10^7
Fold change	–	+(3.0 ± 0.5)	+(11 ± 2)
$V_2/K_{\alpha\text{-}Kg}\mathbf{E_t}$ ($M^{-1}s^{-1}$)	(1.8 ± 0.4)×10^5	(3.8 ± 1.0)×10^5	(9.7 ± 0.6)×10^5
Fold change	–	+(2.0 ± 0.7)	+(5 ± 1)
$V_2/K_{Lys}\mathbf{E_t}$ ($M^{-1}s^{-1}$)	(1.8 ± 0.3)×10^4	(4.7 ± 1.2)×10^4	(1.2 ± 0.1)×10^5
Fold change	–	+(2.6 ± 0.8)	+(7 ± 1)
K_{NADH} (mM)	0.019 ± 0.002	0.05 ± 0.01	0.010 ± 0.002
Fold change	–	+(2.6 ± 0.5)	-(2.0 ± 0.4)
$K_{\alpha\text{-}Kg}$ (mM)	0.11 ± 0.03	0.38 ± 0.10	0.11 ± 0.01
Fold change	–	+(3.5 ± 1.0)	–
K_{Lys} (mM)	1.1 ± 0.2	3.0 ± 0.7	0.89 ± 0.10
Fold change	–	+(2.7 ± 0.8)	–

[a]Values are from Xu et al. (*60*). [b]Values are ± SE. [c]The symbols, + and -, represent increase and decrease, respectively.

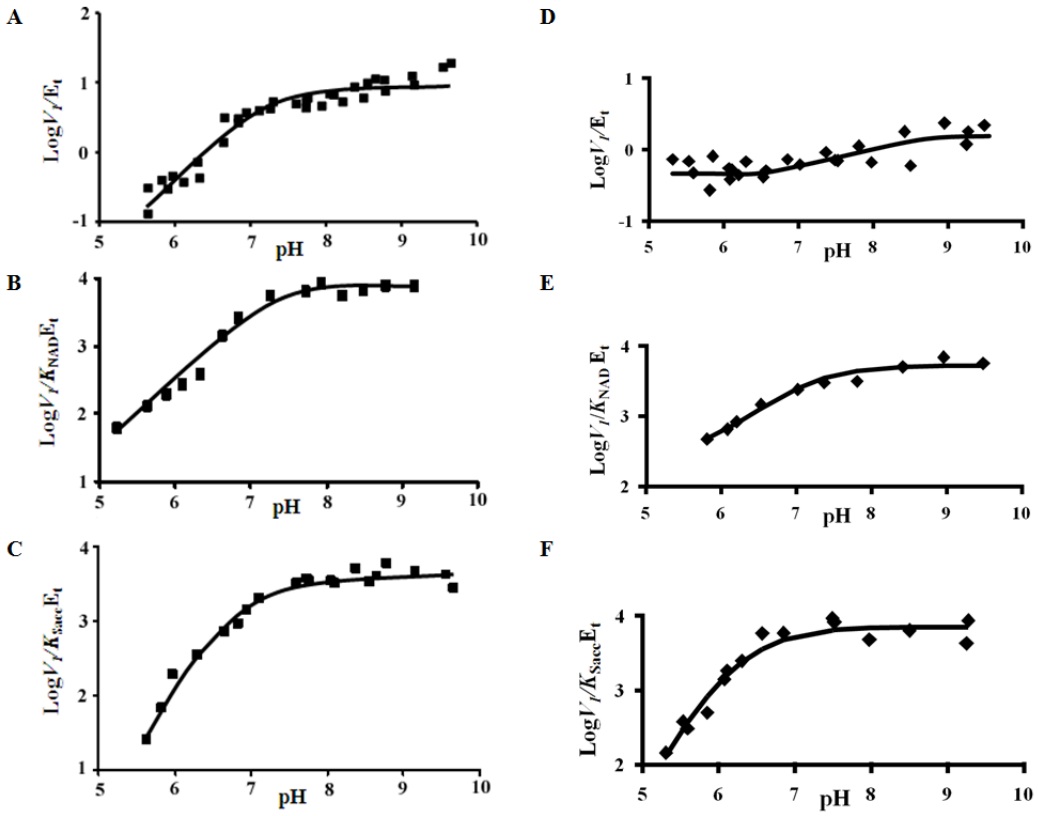

Figure C2-2: pH Dependence of Kinetic Parameters for SDH WT and C205S Mutant Enzyme, in the Direction of Lysine Formation. Data for WT (A-C) are from ref. (*64*), and are reproduced with permission, while (D-F) are for the C205S mutant enzyme. Units for V/E_t and $V/K E_t$ are s^{-1} and M^{-1} s^{-1}, respectively. Points are the experimentally determined values. With the exception of panel D, the curves are theoretical and based on fits to eq. 9 for panel E and eq. 11 for panel F. In panel D, V_1/E_t profile, the curve is the hand-drawn best-fit line.

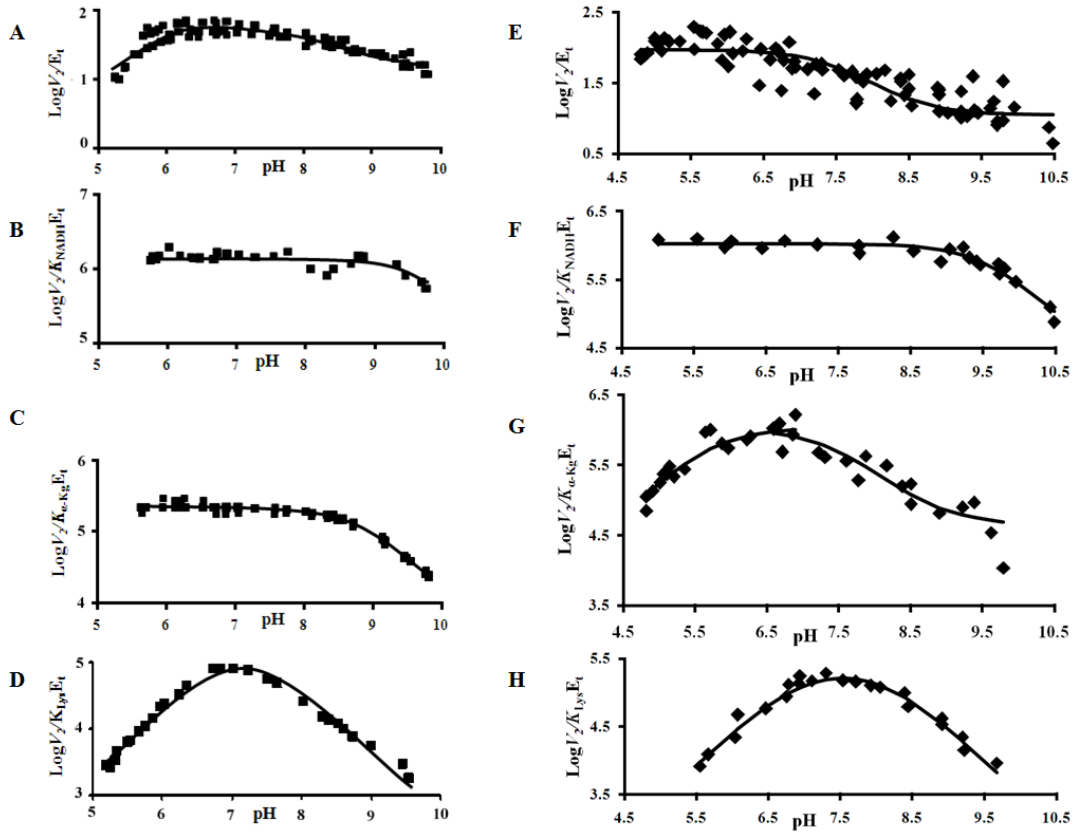

Figure C2-3: pH Dependence of Kinetic Parameters for SDH WT and C205S Mutant Enzyme, in the Direction of Saccharopine Formation. Data for WT (A-D) are from ref. (*64*), and are reproduced with permission, while (E-H) are data for the C205S mutant enzyme. Units for V/E_t and V/KE_t are s^{-1} and M^{-1} s^{-1}, respectively. Points are the experimentally determined values. The curves are theoretical and based on fits to eq. 10 for panel E, eq. 8 for panel F, and eq. 7 for panel H. The curve in panel G is based on a combination of fits to eq. 7 (pH 4.8 to 6.9), and eq. 10 (pH 6.6 to 8.9) as discussed under Materials and Methods.

Table C2-2: pH Dependence of Kinetic Parameters for SDH WT and C205S Mutant Enzyme

parameter[a]	pK_a	C[b]	pK_a	C
	_____ WT[c] _____		_____C205S_____	
V_1 (s^{-1})	7.3 ± 0.2[d]	9.5 ± 0.9	7.5-7.7[e]	0.7[e] (Y_L)[f] 1.3[e] (Y_H)
V_1/K_{NAD} ($M^{-1}s^{-1}$)	7.4 ± 0.2	(9 ± 2)×10^3	7.1 ± 0.1	(2.4 ± 0.1)×10^2 (Y_L) (5.3 ± 0.2)×10^3 (Y_H)
V_1/K_{Sacc} ($M^{-1}s^{-1}$)	6.2 ± 0.3 7.2 ± 0.2	(4.4 ± 0.4)×10^3	5.7 ± 0.3 6.5 ± 0.2	(7.1 ± 1.1)×10^3
V_2 (s^{-1})	5.8 ± 0.2 8.4 ± 0.5	(5.8 ± 0.3)×10^1	7.5 ± 0.1	(9.3 ± 0.8)×10^1 (Y_L) (1.10 ± 0.08)×10^1 (Y_H)
V_2/K_{NADH} ($M^{-1}s^{-1}$)	9.6 ± 0.2	(1.40 ± 0.06)×10^6	9.5 ± 0.1	(1.1 ± 0.1)×10^6
$V_2/K_{\alpha\text{-Kg}}$ ($M^{-1}s^{-1}$)	8.9 ± 0.1	(2.20 ± 0.08)×10^5	5.7 ± 0.2 7.4 ± 0.3	(1.1 ± 0.3)×10^6 (Y_L) (4.5 ± 3.4)×10^4 (Y_H)
V_2/K_{Lys} ($M^{-1}s^{-1}$)	7.2 ± 0.5[g]	(1.40 ± 0.07)×10^5	7.0 ± 0.1 8.1 ± 0.1	(2.5 ± 0.1)×10^5

[a]All parameters are divided by $\mathbf{E_t}$. [b]C is the pH-independent value of the parameter. [c]From Xu et al. (*64*). [d]Values are ± SE. [e]Value estimated from a curve drawn by hand. [f]Y_L and Y_H are pH-independent constant values of the parameter at low and high pH. [g]Average value.

Table C2-3: Summary of the Kinetic Isotope Effects for SDH WT and C205S Mutant Enzyme

Enzyme	$^{D}(V_2/K_{Lys})$	$^{D}(V_2)$	$^{D_2O}(V_2/K_{Lys})$	$^{D_2O}(V_2)$	$^{D_2O}(V_2/K_{Lys})_D$	$^{D_2O}(V_2)_D$
	PKIE[a]		SKIE		MKIE	
WT[b]						
pH 5.6	1.66 ± 0.12[c]	1.20 ± 0.07	ND[d]	ND	ND	ND
pH 7.1	1.56 ± 0.05	1.45 ± 0.07	1.9 ± 0.1	2.2 ± 0.1	1.86 ± 0.08	1.76 ± 0.08
pH 8.4	1.03 ± 0.04	1.16 ± 0.03	ND	ND	ND	ND
C205S[e]						
pH 5.4	1.9 ± 0.3	1.9 ± 0.3	ND	ND	ND	ND
pH 7.3	2.15 ± 0.07	2.15 ± 0.07	2.6 ± 0.4	2.6 ± 0.4	1.8 ± 0.1	1.8 ± 0.1
pH 9.0	1.3 ± 0.2	1.3 ± 0.2	ND	ND	ND	ND

[a]PKIE, primary substrate deuterium kinetic isotope effect; SKIE, solvent deuterium kinetic isotope effect; MKIE, multiple solvent deuterium/substrate deuterium kinetic isotope effect. [b]From Xu et al. (*64*). [c]Values are ± SE. [d]ND, no data available. [e]Data obtained from the fit to eq. 5, where $V=V/K$.

C2.4 Discussion

A disulfide linkage was observed in the dinucleotide binding site of the WT enzyme in the apo form or with sulfate or OxGly bound to the substrate binding site. As AMP binds, however, it appears to select enzyme with the disulfide reduced to the dithiol. Data led to the hypothesis that the SDH enzyme exists in two forms, disulfide and dithiol, and the dithiol form is more active and binds the dinucleotide substrate with greater affinity. Data obtained in this manuscript support the hypothesis and suggest the redox state of the disulfide also affects the conformation of the enzyme at low pH. Attempts to reduce the disulfide with dithiothreitol were unsuccessful. The redox potential of dithiothreitol is -0.332 V at pH 7.0 and -0.366 V at pH 8.1, and thus the redox potential of the disulfide must be much lower than -0.366 V (*93*). Below, data are discussed in terms of the difference between WT and the mutant enzyme as well as in terms of the hypothesis described above and the mechanism of SDH.

Initial Velocity Studies at pH 7.0. As shown in Table C2-1, with the exception of $V_1/K_{NAD}\mathbf{E_t}$, all first and second order rate constants are increased in the C205S and C205V mutant enzymes. The C205 mutant enzymes are unable to form the disulfide observed in structures of SDH (*51, 52*). Data are thus consistent with two forms of SDH, a less active disulfide form and a more active dithiol form. On the basis of the maximum rate of WT in the direction of Sacc formation, the fraction of enzyme in the active form as isolated is about 20% ($V_2/\mathbf{E_t}$ for WT is 20 s^{-1}, while $V_2/\mathbf{E_t}$ for C205S is 106 s^{-1}), with the remaining

80% in the disulfide form. It is the 20% active enzyme that is observed for WT enzyme at low pH, Figure C2-2A. There is likely an equilibrium established in the cell between the disulfide and dithiol enzyme forms. However, the identity of the electron donor and acceptor in the equilibrium is at present unknown. Of interest, attempts to reduce the disulfide have not been successful, and isolation of enzyme with reducing agent present during the entire purification procedure did not alter the amount of disulfide-containing enzyme.

Interpretation of Isotope Effects. The kinetic mechanism of the C205S mutant at pH 7.0 is qualitatively identical to that of WT. A chemical mechanism has been proposed for WT SDH (*64*). There are at least two isotope sensitive steps in the mechanism, Scheme C2-1. The substrate deuterium sensitive step, hydride transfer, contained in Step A, exhibits an isotope effect upon deuteration of NADH at the C-4 *pro*-R hydrogen of the dihydronicotinamide ring (*64*). All of the chemical steps involve proton transfer, Steps A, B, and C in Scheme C2-1, and may contribute to a solvent deuterium isotope effect. Among possible rate-limiting proton transfer steps, the proton transfer concerted with hydride transfer, and the imine hydrolysis step contribute to the observed solvent kinetic deuterium isotope effect (*64*).

Primary substrate deuterium kinetic isotope effects $^{D}(V_2/K_{Lys})$ and $^{D}(V_2)$, for the C205S mutant enzyme are generally similar to those of WT, albeit slightly larger. Thus, hydride transfer contributes to rate limitation in C205S slightly more than in WT. In addition, the solvent deuterium kinetic isotope effects observed for C205S are slightly greater than those of WT at pH 7.0.

The multiple isotope effects $^{D2O}(V_2/K_{Lys})_D$ and $^{D2O}(V_2)_D$ observed for C205S are identical within error to those of WT. As discussed below, the pH dependence of V_2 at low pH differs for C205S and WT. V_2 for the C205S mutant enzyme is pH dependent, but does not exhibit the pK_a of 5.8 observed for WT, Figure C2-3. The pK_a of 5.8 observed for WT was attributed to a pH dependent conformational change that contributes to rate limitation. The loss of the pH dependent change in the C205S mutant enzyme would increase the contribution of hydride transfer and imine hydrolysis to rate limitation, consistent with the larger deuterium and solvent deuterium isotope effects observed on V_2 and V_2/K_{Lys}. Of the two isotope effects, the substrate deuterium kinetic isotope effect increases by a greater amount than the solvent effect for C205S compared to WT. As a result, a larger contribution from the proton transfer in the hydride transfer step to the measured solvent isotope effect is predicted. The multiple isotope effect [$^{D2O}(V_2)_D$ = $^{D2O}(V_2/K_{Lys})_D$] exhibits a bigger decrease compared to the solvent deuterium effect, likely a result of isolating the solvent isotope effect on the hydride transfer step, i.e. [$^{D2O}(V_2)_D$ = $^{D2O}(k_{hydride\ transfer})$].

Interpretation of the pH Dependence of Kinetic Parameters. The V_1/K_{Sacc} profile for the C205S mutant enzyme is qualitatively similar to that of WT, Figure C2-2C, F, although there may be a slight perturbation of the pK_a values from 7.2 and 6.5 in WT to 6.2 and 5.7 in C205S, Table C2-2. (Given the errors on the pK_as, and the fact that the estimates are from a pH-rate profile that decreases with an eventual slope of 2, the perturbation is not substantial.) The groups with observed pK_as have the same function as those assigned in the WT

enzyme, i.e., the base catalytic groups that 1) accept a proton from the secondary amine of Sacc (pK_a = 6.2), and 2) accept a proton from water in the imine hydrolysis steps (pK_a = 7.2).

The difference in the pH-rate profiles resides in the V_1 and V_1/K_{NAD} pH-rate profiles. In the WT enzyme, these two pH-rate profiles decreased at low pH giving a pK_a within error identical to one of the pK_as (7.2) observed in the V_1/K_{Sacc}. Thus, the V_1 and V_1/K_{NAD} pH-rate profiles of WT gave pK_a values of 7.3 and 7.4, respectively, Table C2-2. Data were interpreted in terms of the catalytic group (pK_a of 7.2 in V_1/K_{Sacc}) affecting V_1 and the binding of NAD (*64*). It is clear from the C205S pH-rate profiles that this is not correct. Although the group observed in the V_1 and V_1/K_{NAD} pH-rate profiles is likely the same, it is not the same as that observed in the V_1/K_{Sacc} pH-rate profile, and is not involved in catalysis. The V_1 pH-rate profile obtained for C205S indicates the mutant enzyme, which does not allow disulfide formation, has only a slight partial change in which the rate decreases by about 2-fold from high pH to low pH. This can be compared to the apparent all-or-none change observed for WT with the rate decreasing more than 100-fold over the same pH range. The same phenomenon is seen to a somewhat lesser extent for V_1/K_{NAD}, which decreases by more than two orders of magnitude over the same pH range as $V_1/\mathbf{E_t}$ for WT, but only by a factor of about 20 for C205S, Table C2-2. Data suggest a group on enzyme with a pK_a in the neutral pH range must be unprotonated to generate the active conformation of the enzyme. This same group affects the binding of NAD. The effect on NAD binding is obtained from the ratio of the

changes in *V* and *V/K*, i.e., 10-fold. As suggested previously, the group is either a cationic acid or causes a positively charged group to come into proximity to the nicotinamide ring of NAD, since the effect is not observed in the V_2/K_{NADH} pH-rate profile (*64*).

The pH-dependent conformational change observed in the V_1 and V_1/K_{NAD} pH-rate profiles likely reflects an isomerization in free enzyme, prior to binding of NAD (since NAD binds to free enzyme), and perhaps also in central complexes, although this is not necessary. A slow conformational change in E would be observed at saturating substrate. The dramatic attenuation of the pH dependent conformational change in the C205S mutant enzyme indicates the formation of the active site disulfide somehow stabilizes the less active conformer.

In the direction of Sacc formation, the V_2/K_{NADH} pH-rate profile obtained for the C205S mutant enzyme is identical to that of WT (*64*). The V_2/K_{Lys} pH-rate profile for C205S is qualitatively similar to WT, but the pK_a of one of the bases is perturbed from about 7 to 8, suggesting a change in the environment around this base in the E•NADH•α-Kg enzyme form. The change must reflect a change in conformation of the enzyme active site in the reduced disulfide form of the enzyme, consistent with the increased activity of the mutant enzyme.

Differences are observed in the V_2 and $V_2/K_{\alpha\text{-}Kg}$ pH-rate profiles of the C205S mutant enzyme compared to WT (*64*). V_2 is pH independent at low pH and decreases to a new pH independent value at high pH. The WT V_2 pH-rate profile also exhibits the partial change observed at high pH, but additionally

exhibits a pK_a of 5.8 for a group that must be unprotonated for optimum activity, and this is not observed for C205S. In addition, the pK_a of the group responsible for the partial change is lower in C205S (pK_a = 7.5) than in WT (pK_a = 8.4). The change in pK_a may again be a result of a change in environment as discussed for V_2/K_{Lys}. The V_2 pH-rate profile of WT is the only pH profile that exhibited the pK_a of 5.8, and it was attributed to a conformational change that resulted in a change in the kinetic mechanism from steady state random addition of Lys and α-Kg to equilibrium ordered addition of α-Kg before Lys (*64*). Elimination of the possibility of disulfide formation eliminates the pH dependence.

The $V_2/K_{\alpha\text{-}Kg}$ pH-rate profile of the C205S mutant enzyme also exhibits a partial change with the same pK_a as that observed in the V_2 pH-rate profile. The ratio of the pH independent values observed in the $V_2/K_{\alpha\text{-}Kg}$ and V_2 pH-rate profiles are about the same, 20 and 9, respectively, with both rate constants greater at low pH. The $V_2/K_{\alpha\text{-}Kg}$ and V_2 pH-rate profiles for the WT enzyme exhibit the same pH dependencies, but with a pK_a about a pH unit higher than that observed for C205S. In addition, a second pK_a of 5.7 is observed at low pH, as observed for the V_2 pH-rate profile of WT. A change in kinetic mechanism is observed for the WT enzyme from steady state random with either Lys and α-Kg adding to E•NADH to equilibrium ordered with Lys adding last to the E•NADH• α-Kg ternary complex. This change in mechanism occurs at pH 8.5, and coincides with the partial change in the V_2 pH-rate profile and the pK_a of 8.9 observed in the $V_2/K_{\alpha\text{-}Kg}$ pH-rate profile, and the pK_a of 5.8 observed

in the V_2 pH-rate profile (*64*). It is likely the same is true in the C205S mutant enzyme, with the conformation of enzyme at low and high pH disfavoring binding of lysine to E•NADH. Inspection of the pH range covered for WT and C205S provides an explanation for the lack of the pK_a of 5.7 in the WT $V_2/K_{\alpha\text{-}Kg}$ pH profile. Data were only measured to pH 5.7 for the WT enzyme, while data were measured to pH 4.6 for C205S, and thus the pK_a of 5.7 would likely be observed if data were collected for WT. However, the K_m for Sacc increases and V_2 decreases at low pH making it very difficult to obtain these data.

Overall, the group seen in the V_2 profile with a pK_a of 7.5 is likely the same as the group seen in the V_1 profile, with a pK_a of 7.5-7.7. In the direction of Lys formation unprotonated enzyme is more active, while in the Sacc formation reaction direction, the protonated enzyme is more active. The absence of the pH dependence of V_2 at low pH likely reflects the change in affinity of the enzyme for the product NAD, as shown in the V_1 and V_1/K_{NAD} pH-rate profiles. At pH 7, the WT enzyme exhibits uncompetitive substrate inhibition by α-Kg binding to E•NAD, consistent with a contribution to rate limitation by release of NAD (*60*). The K_m for NAD of WT enzyme does not change at low pH, since V_1 and V_1/K_{NAD} exhibit the same pK_a. However, the C205S mutant enzyme, as discussed under the pH dependence of kinetic parameters in the direction of Lys formation, exhibits about a 10-fold increase in K_{NAD}. Thus, the rate of release of NAD increases as the pH is decreased for C205S, but not WT.

Mechanism of SDH. On the basis of data for WT SDH, a chemical mechanism has been proposed, Scheme C2-1, and is modified on the basis of the C205S mutant enzyme data discussed here. A group (B_1) on the enzyme with the pK_a of 5.7-6.2 in the V_1/K_{Sacc} pH-rate profile, and about 7.0 in the V_2/K_{Lys} pH-rate profile, Figures C2-2C, F and C2-3D, H, deprotonates the secondary amine of Sacc as it is oxidized to the imine (Step A in Scheme C2-1). This same group donates a proton to the ε-amine of Lys as it is released as a product. A second group (B_2) on enzyme with a pK_a of 6.5-7.2 in the V_1/K_{Sacc} pH-rate profile, and 7-8 in the V_2/K_{Lys} pH-rate profile, Figures C2-2C, F and C2-3D, H, activates water in the imine hydrolysis step and then shuttles protons between itself and reaction intermediates, finally forming the Lys and α-Kg products (*64*). The pH dependence of V_1 and V_1/K_{NAD}, as discussed above, reflects a pH dependent conformational change. The inability to form the disulfide bond in C205S greatly diminishes the effect of the conformational change at low pH.

It appears there may be an equilibrium established between the oxidized and reduced enzyme in the cell, but the electron donor/acceptor is at this point unknown, and will require additional studies. The C205-C249 disulfide may be a redox sensor that regulates Lys synthesis under conditions of oxidative or other cellular stress. As suggested above, the redox potential of disulfide must be lower than -0.366 V (*93*).

Acknowledgments We thank Devi K. Ekanayake, Dr. Babak Andi, and Dr. William E. Karsten for the helpful advice on experimental protocols. We are grateful to Prof. Kenneth M. Nicholas for providing access to his lab facilities, and Masa Matsumoto for technical assistance.

Chapter 3

Crystal Structures of Apo-Enzyme and NADH-Bound C205S Saccharopine Dehydrogenase from *Saccharomyces cerevisiae*

"Reproduced with automatic permission of [Kostyantyn D. Bobyk, Leonard M. Thomas, Babak Andi, Paul F. Cook, and Ann H. West] manuscript in preparation"

C3.1 Introduction

Saccharopine dehydrogenase (SDH) [N^6-(glutaryl-2)-L-lysine:NAD-oxidoreductase (L-lysine-forming) (EC 1.5.1.7)] from *Saccharomyces cerevisiae* catalyzes the reversible NAD-dependent oxidative deamination of saccharopine to generate L-lysine (Lys) and α-ketoglutarate (α-Kg) (*10, 14*). The kinetic mechanism of SDH is steady state random, albeit with binding of NAD or NADH (reverse reaction direction) dinucleotides to free enzyme followed by ordered binding of Sacc or a random addition of α-Kg and Lys (reverse reaction direction) (*60*). A general acid-base proton shuttle chemical mechanism has been proposed for the SDH that makes use of two bases, B_1 and B_2, which execute all the chemistry in the catalyzed reaction. Based on the pH-rate and pK_i profiles, ionizable D, E, K, and H side chains in the active site of SDH have been proposed as candidates for the role of B_1 and B_2 (*64*).

The *S. cerevisiae* SDH is a monomer of 373 amino acids, with a calculated molecular weight of 41,464 Da and one binding site for reactants per molecule of enzyme (*51-54*). The crystal structure of the WT Apoenzyme has been solved (PDB ID: 2Q99) with the disulfide bond between the C205 and

C249 residues observed in the domain II Rossmann fold, a typical dinucleotide-binding motif (*72*). Based on the facts that two cysteines forming the disulfide are conserved in all fungal SDH sequences and that there were no observed structure perturbations or any conformational strain associated with the disulfide, it was suggested the disulfide may be physiologically relevant (*52*). An attempt has been made to crystallize the WT SDH with the substrates bound. The study produced structures with AMP, OxGly, and Sulfate ligands bound in the active site of the enzyme, PDB IDs 2QRK, 2QRL, and 2QRJ, respectively (*51*). However, the crystallizations with the natural substrates did not materialize. Interestingly, the disulfide bonds between C205 and C249 were observed in the OxGly-, and Sulfate-bound structures with the similar interatomic distances between the sulfur atoms to that of the Apoenzyme structure. At the same time the cysteines 205 and 249 were in the reduced dithiol form in the AMP-bound structure (*51*). Taken together, these data suggest the absence of a C205-C249 disulfide might somehow facilitate the binding of the dinucleotide(s) or their analogs.

The C205S site directed mutant enzyme was prepared and kinetically characterized in a study concurrent to this investigation. C205S enzyme is more stable and has higher activity than the WT. This change was attributed to the disulfide stabilizing an inactive conformation of the WT enzyme and an equilibrium existing between the dithiol and the disulfide forms in the WT enzyme (see Chapter 2). In case with the C205S, the enzyme is completely in the active dithiol form.

In this investigation the improved stability and higher activity of the C205S mutant made it possible to obtain the NADH-bound crystals of the enzyme. The crystallographic characterization of the enzyme in the Apo and NADH-bound forms yielded structural data which helped determine the role of a disulfide between the C205 and C249. Additionally, a structural basis for the ordered kinetic mechanism and the roles for the active site amino acid residues in the overall reaction mechanism of SDH have been proposed.

SDH is a potential target of the antifungal drug design (*10, 14, 71*). Having a structure with the natural dinucleotide substrate bound in the active site would be of a great assistance to the structure-based rational drug design efforts.

C3.2 Materials and Methods

***Chemicals*.** Chloramphenicol, phenylmethylsulfonyl fluoride (PMSF), ethylenediaminetetraacetic acid (EDTA), and lysozyme were obtained from Sigma-Aldrich. β-NADH, imidazole, ampicillin (Amp), Luria-Bertani (LB) broth, and LB agar were purchased from USB. Hepes was from Research Organics. Sodium dodecyl sulfate (SDS), bis *N*,*N*'-methylene-bis-acrylamide, and Coomassie Brilliant Blue G-250 were from Bio-Rad. Sodium chloride, potassium chloride, and nickel sulfate were from Mallinckrodt Baker. The nickel-nitrilotriacetic acid (Ni-NTA) agarose resin, isopropyl-β-D-1-thiogalactopyranoside (IPTG), polyethylene glycol monomethyl ether (PEG-MME) 2000, and the QuikChange site-directed mutagenesis kit were purchased from Qiagen, Gold Biotechnology, Hampton Research, and Stratagene,

respectively. All other chemicals and reagents were obtained from commercial sources, were reagent grade, and were used without further purification.

***Site-Directed Mutagenesis*.** A single site-directed mutant of SDH, C205S, was prepared using the QuikChange site-directed mutagenesis kit. A pET-16b derivative plasmid pSDHHX1 containing the *LYS1* gene from *Saccharomyces cerevisiae* inserted into the *Nde*I/*Bam*HI restriction sites was used as a template (*60*). Whole gene sequencing was performed at the Sequencing Core facility of the Oklahoma Medical Research Foundation. To confirm the mutation, the resulting sequence was compared to that of the wild type using ClustalW and/or BLAST. To make the C205S mutant enzyme, the forward and reverse primers were 5'-GGT GCG CTA GGA AGA **TCT** GGT TCC GGT GCC-3' and 5'-GGC ACC GGA ACC **AGA** TCT TCC TAG CGC ACC-3', respectively. The mutated codons are shown in bold letters.

Enzyme Expression and Purification. The C205S mutant enzyme was expressed in BL21 (DE3)-RIL *Escherichia coli* cells and purified following the procedure reported previously (*60*) with some modifications. Briefly, induction of protein expression at 37°C was carried out by addition of 0.2 mM IPTG, once cell growth exhibited an OD_{600} nm of 0.3−0.4 and the cell growth was then continued at 37°C for an additional 3-4 h before harvesting. Cells were harvested by centrifugation, resuspended in 100 mM Hepes pH 7.0, 100 mM NaCl, 5 mM imidazole, 1 mM PMSF, 100 µg/ml lysozyme, and 0.5 mM EDTA, and incubated overnight at -20°C. Next day, the cells were thawed and sonicated on ice for twelve minutes with 10 seconds/50 seconds on/off cycle,

using a MISONIX Sonicator XL. After centrifugation to remove the cell debris, the supernatant was applied to a Ni−NTA affinity column, and the chromatogram was developed by a step imidazole gradient from 30 to 300 mM in the sonication buffer. The concentration of NaCl was increased to 300 mM in all elution buffers, and the 150 -300 mM imidazole elution buffers did not contain 1 mM PMSF. Fractions of 150-300 mM imidazole were pooled together and the purity of the SDH was assessed using Coomassie Blue stained SDS gels; the purity of the enzymes was >95%. Enzyme was dialyzed against 100 mM Hepes pH 7.0, 300 mM NaCl and stored at 4°C.

Protein Crystallization and Soaks. The homemade screening kits with PEG-MME 2000 of various percentages (w/v) vs. pH and salt additives were used to explore a range of conditions, starting with those described in (*51*), using the hanging-drop vapor diffusion method (*94*). Crystallization trials were performed by mixing 2 μL of the C205S enzyme solution (5−27 mg/mL in 100 mM Hepes, pH 7.0) with the same volume of reservoir (precipitant) solution equilibrated over 0.5 mL of reservoir solution at 4 and 25 ℃.

The soaks with varied NADH concentrations were set up at 4 ℃. Diffraction quality crystals of C205S Apo were transferred into the replicas of their reservoir solutions (mother liquor) with higher final PEG percentages (original percentage (w/v) plus 2%), containing NADH, and incubated for varied time. The stock NADH of 100 mM was prepared freshly for each new experiment in 10 mM Tris pH 8.0 to minimize the degradation of NADH. The soaking drop was prepared through mixing 1.5 μL of the appropriately

concentrated stock of the mother liquor and 0.5 µL of NADH stock solution. To cryoprotect crystals for data collection, they were transferred successively into 5%, 10%, and then, 15% glycerol in mother liquor before flash-freezing in liquid nitrogen.

Data Collection and Processing. Cryoprotected with the method described above apoenzyme crystals were flash-frozen and kept cool in a stream of nitrogen gas at a temperature of 100 K (Oxford Cryosystems Series 700 cryosystem). X-ray diffraction data were collected using Cu Kα radiation (λ = 1.5418 Å) produced from a Rigaku/MSC RU-H3R rotating anode X-ray generator with Osmic Blue confocal optics, operated at 50 kV/100 mA, and R-Axis IV^{++} image plate detectors. The crystal to detector distance was set at 140 mm for the Apo structure and 160 mm for the NADH soaked structure. Data were collected with a 0.5° oscillation angle and 10 minutes exposure time per image. For initial evaluation all data were processed with the d*TREK data processing package version 9.6D (*95*) with later re-processing of the promising data sets by MOSFLM version 7.0.5 (*96*) and SCALA (*97*) as found in the CCP4 program suite version 6.1.3 (*98*).

Molecular Replacement, Model Building, Structure Refinement, and Validation. The structures were solved by molecular replacement using the maximum-likelihood techniques implemented in the program Phaser version 2.1.4 (*99*). The starting models used where the wild type SDH molecule (*52*), PDB ID 2Q99, for the Apo C205S mutant and the SDH bound with AMP (*51*), PDB ID 2QRK, for the NADH soak of the C205S mutant. The structures were

manually rebuilt using COOT version 0.6 (*100*) followed by 20 cycles of refinement buy REFMAC version 5.5.0091 (*101*). Solvent molecules were added automatically using COOT and then checked manually for proper placement. The quality of the structure factor data and stereochemical properties were checked with SFCHECK (*102*) and the MolProbity server (*103*).

***Molecular Graphics*.** The structures of the Apoenzyme C205S and NADH-bound C205S were solved in collaboration with Dr. Thomas L. M., Macromolecular Crystallography Laboratory manager, Department of Chemistry and Biochemistry, University of Oklahoma. All figures of three dimensional structures in this chapter were prepared using PyMol versions 0.95 and/or 0.99 (*104*), or the Coot version 0.6 (*100*) and GIMP version 2.6 programs, GIMP: a GNU Image Manipulation Program http://www.gimp.org/ (2001-2009) GIMP Development Team.

C3.3 Results

Protein Crystallization and Soaks. Diffraction-quality C205S apo-enzyme crystals were obtained using homemade screening kits. Depending on the concentration of the enzyme in the drop, crystals appeared as square plates in ≥7 days with average dimensions of 0.22 × 0.22 × 0.05 mm. Optimized conditions that resulted in diffraction-quality crystals were 100 mM Tris (pH 7.0), 30% (w/v) PEG-MME 2000 at 4 ℃, with a final enzyme concentration of ≥2.5 mg/mL in the drop. These crystals were used for data collection and structure determination, as well as for the soaks with NADH.

Optimized conditions for the soaks were 100 mM Tris (pH 7.0), 32% (w/v) PEG-MME 2000 at 4 ℃ with a final concentrati on of NADH of 25 mM in the soaking drop. Soaks of up to 4 hours resulted in low occupancy of NADH in the dinucleotide-binding site. Occupancy improved in overnight soaks, but disorder increased. As a result, electron density for only the nicotinamide diphosphate (NDP) portion of NADH was detected; density for the adenosine portion of the NADH molecule is largely missing from the NADH-bound C205S structure reported here, Figure C3-1. This is likely due to its high mobility.

Data Collection and Processing. Processing of the datasets showed the space groups of $P2_12_12_1$ for both Apo- and NADH-bound structures with a = 64.95 Å, b = 75.23 Å, and c = 75.31 Å for the Apo structure and a = 64.95 Å, b = 75.26 Å, and c = 75.56 Å for the NADH-bound structure. A summary of the data collection statistics for both datasets is shown in the Table C3-1.

Molecular Replacement, Model Building, Structure Refinement, and Validation. Molecular replacement for the Apo C205S mutant enzyme was successful starting with the model of Apo WT SDH, PDB ID 2Q99 (*52*), while for the NADH-bound C205S mutant enzyme, the AMP-bound WT SDH model, PDB ID 2QRK (*51*), gave better results. The summary of the refinement statistics for both structures is shown in the Table C3-2.

Characterization of the Apo C205S. The overall structure of the Apo C205S mutant enzyme is very similar to that of WT SDH (*52*). In the alignment of the C205S and WT Apo-structures, a gross examination indicated there was minor movement observed in the loops of the C205S enzyme, Figure C3-2A. As

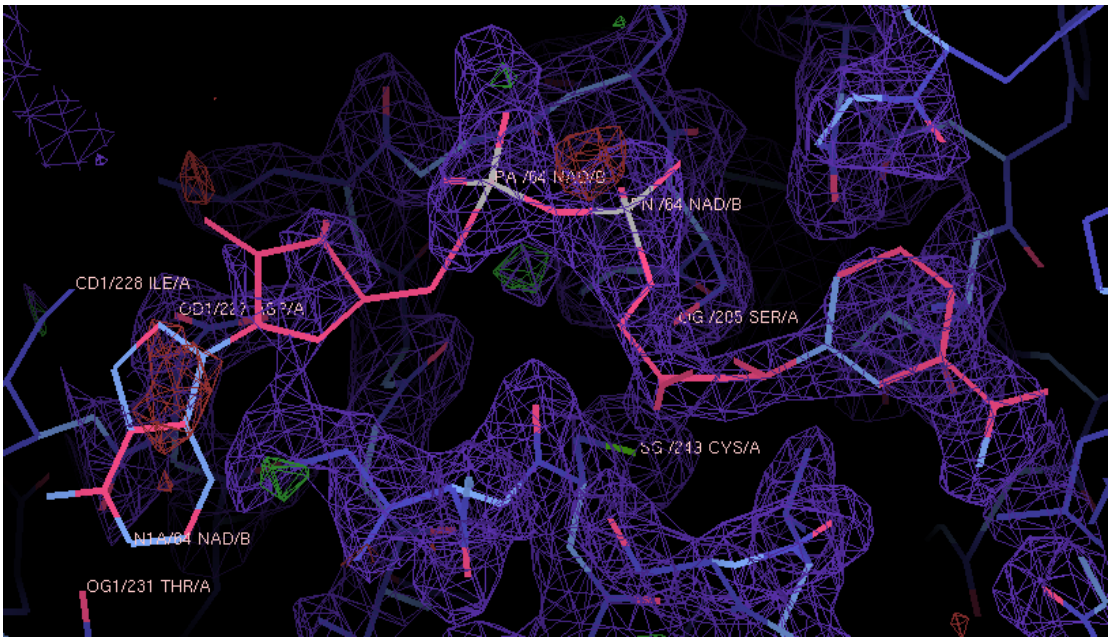

Figure C3-1. A close-up view of the NADH bound in the dinucleotide binding site of C205S enzyme. Electron density is observed for the NMN^+ moiety of the NADH, but is missing for the AMP moiety. This figure was generated using the Coot and GIMP programs (*100*).

Table C3-1: Summary of Data Collection Statistics[a]		
Parameter	Apo-C205S crystal	NADH-bound C205S Crystal
Space group	$P2_12_12_1$	$P2_12_12_1$
a (Å)	64.95	64.95
b (Å)	75.23	75.26
c (Å)	75.31	75.56
Matthews coeff ($Å^3$/Da)	2.24	2.24
Solvent content (%)	45.05	45.17
Resolution (Å)	2.01	2.1
No. of observations	98649	88250
No. of unique reflns	23142	21929
Completeness (%)	97.1 (81.8)	98.0 (94.1)
Mean $I/\sigma(I)$	15.8 (2.6)	13.3 (3.7)
R_{merge}[b] (%)	0.052 (0.285)	0.067 (0.360)

[a] Values in parentheses correspond to the highest resolution shell.

[b] $R_{merge} = \Sigma(I_j - \bar{I}_j) / \Sigma(\bar{I}_j)$, where I_j is the intensity measurement for a given reflection and $\bar{I}_j$ is the average intensity for multiple measurements of this reflection.

Table C3-2: Summary of the Refinement Statistics for the C205S Structures		
Parameter	Apo-C205S structure	NADH-bound 205S Structure
Resolution range (Å)	41.17-2.01	49.25-2.10
No. of protein atoms	2921	2915
No. of solvent molecules	143 H_2O	154 H_2O
No. of ligand molecules	0	1 NADH
av B factor (all) ($Å^2$)	25.5	21.4
av B factor (main) ($Å^2$)	24.3	20.1
av B factor (side) ($Å^2$)	26.6	22.2
R_{cryst} (R_{free} [a]) (%)	19.72 (27.35)	18.37 (24.44)
rms deviation bond length (Å) bond angle (deg)	 0.022 1.754	 0.023 1.903
Ramachandran plot (% residues in) favored regions allowed regions outlier regions disallowed regions	 97.0 3.0 0.0 0.0	 95.93 3.79 0.27 0.0

[a] R_{free} was calculated using 5% of the diffraction data.

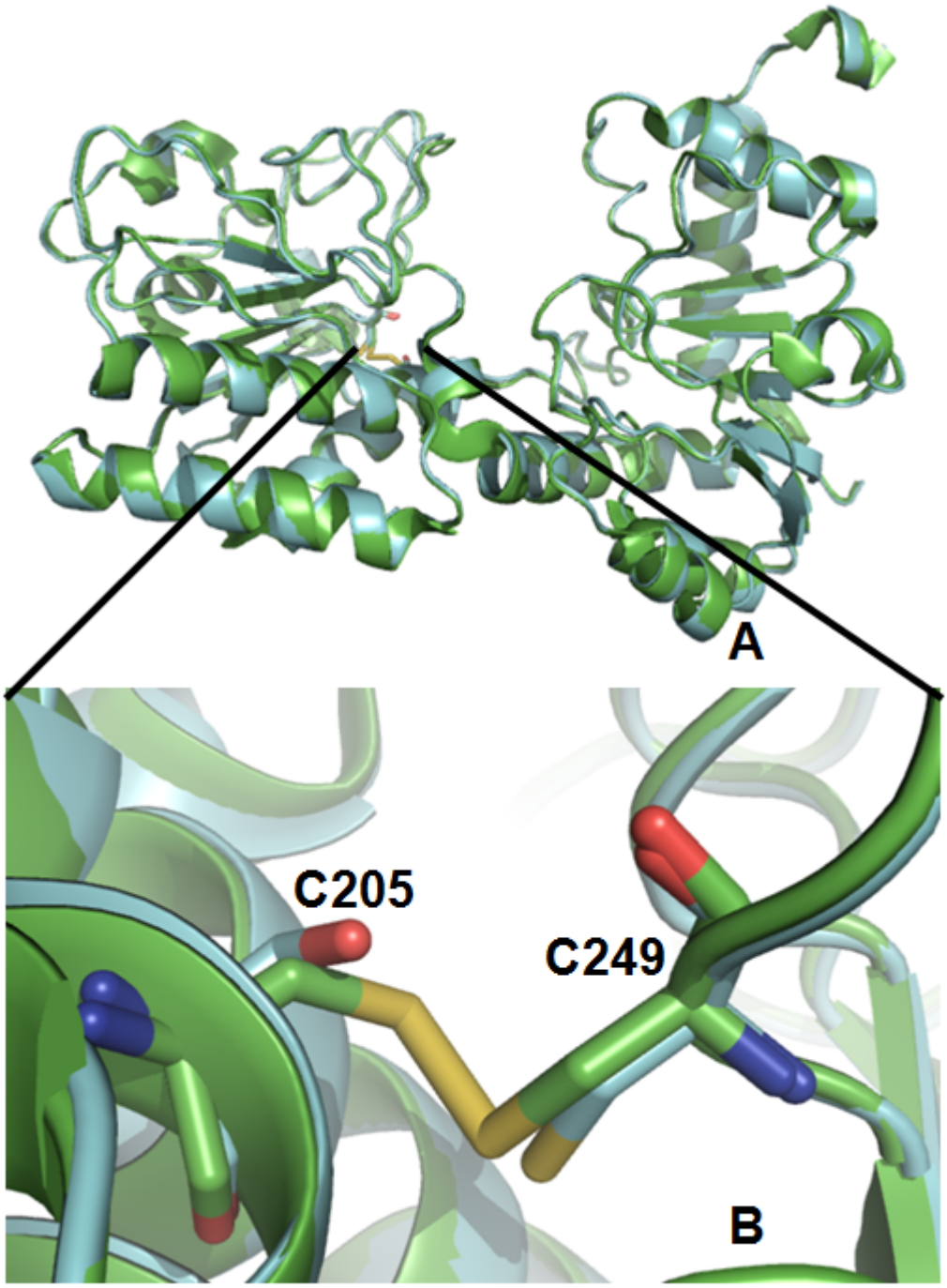

Figure C3-2. Superposition of the Apo WT and C205S SDH structures. WT structure is shown in green while the C205S structure is cyan. (**A)** Overall view; small movement in the loops are observed; (**B)** The disulfide bond is absent in the C205S structure. The figure was generated using PyMOL program.

expected, the disulfide bond is absent in the C205S structure, Figure C3-2B. Upon closer examination of the aligned Apo C205S and WT structures, movement of a number of amino acid residues was observed. Of a particular interest is two areas shown in Figure C3-3.

The first area is near the dinucletide-binding site. When the disulfide bond is absent, the location of the residues next to the cysteines 205 and 249 in the polypeptide chain is changed, Figure C3-3A. Previously, the phosphoryl group of bound AMP was observed to interact through the hydrogen bonds directly with the main chain nitrogen atoms of C205 and R204 and indirectly through a water molecule with the oxygen atom of C249, while I250 contributed to a hydrophobic interaction with the adenine of the AMP (*51*). The potential implications of the observed movement in the side chain of R204 are discussed in greater detail in the results and discussion sections for NADH-bound structure.

The second area of interest is in the substrate binding site, close to the place where the chemistry of the catalyzed reaction takes place. Residues K77 and H96 have been previously proposed to be candidates for the role of the catalytic B_2, in the chemical mechanism of SDH (*64*). The movement of K13 and K77 is observed relative to other ionizable residues nearby, Figure C3-3B. The distance from the nitrogen atom of the ε-amino group of K13 to the carbon atom of the carboxylate group of E16 in the WT Apo structure is 6.10Å, while the distance between the same atoms in the C205S structure is 6.95Å (not shown on the figure). Location of K13 side chain farther away from E16 in the

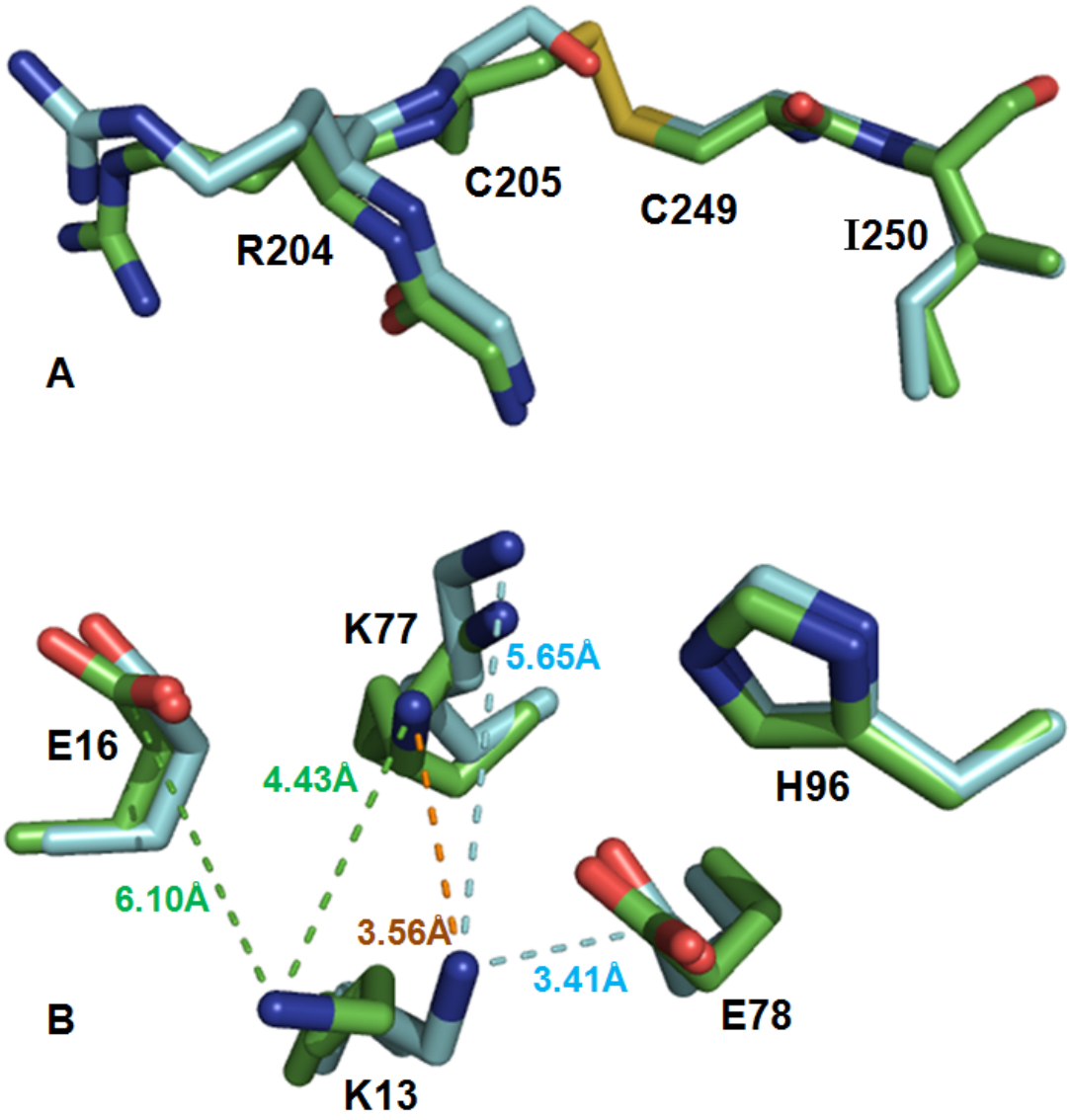

Figure C3-3. Amino acid movements in the C205S Apo structure. WT structure is shown in green while the C205S structure is in cyan. (**A)** Movement of R204 and I250 residues, previously proposed to participate in binding of the AMP moiety of the dinucleotide (*51*); (**B)** Movement of K13 and K77 relative to E16 and E78, the distances between atoms are indicated in green and cyan for WT and C205S Apo structures, respectively. The distance between K13 in the C205S structure to K77 in the WT structure is shown in orange. K77 in the WT structure may be found in two positions. Main chain atoms of the residues and some of the distances are omitted for clarity. This figure was generated using PyMOL program.

C205S structure is compensated by its closer approach to E78. The distance between K13 and E78 is 3.41Å in the C205S structure while the distance between the same atoms in the WT structure is 5.55Å (not shown). The distance between the nitrogen atoms of the K13 and K77 ε-amino groups in the WT structure is 4.43Å, while the distance between the same atoms in the C205S structure is 5.65Å. Interestingly, the “would be” distance between the K13 in the C205S structure and K77 if it had not moved is 3.56Å. A repulsion between K13 and K77 is implied.

***Characterization of the NADH-bound structure of the C205S enzyme*.** In the NADH-bound C205S enzyme structure, NADH is observed close to the location of the C205 and C249. The two phosphoryl groups of NADH, one from the AMP moiety and one from the NMN moiety come into close proximity to the location of where the disulfide bond would be in the WT SDH, Figures C3-1 and C3-4.

Alignments of the C205S mutant enzyme structure with the previously published ligand-bound structures of the WT SDH (*51*) yielded useful results. Positions of the R18, R204, R130, and R131 side chains in the active site of SDH in the AMP- and OxGly-bound WT SDH structures are shown in the Figure C3-5A. Amino acid residues F135 and A134 are located between the R204 and the R18/R131 residues. The guanidium head groups of the R side chains would be positively charged, and the observed distances between guanidium head groups suggest a network of the long-range repulsive electrostatic interactions between the arginines in the active site. Upon binding of the dinucleotide,

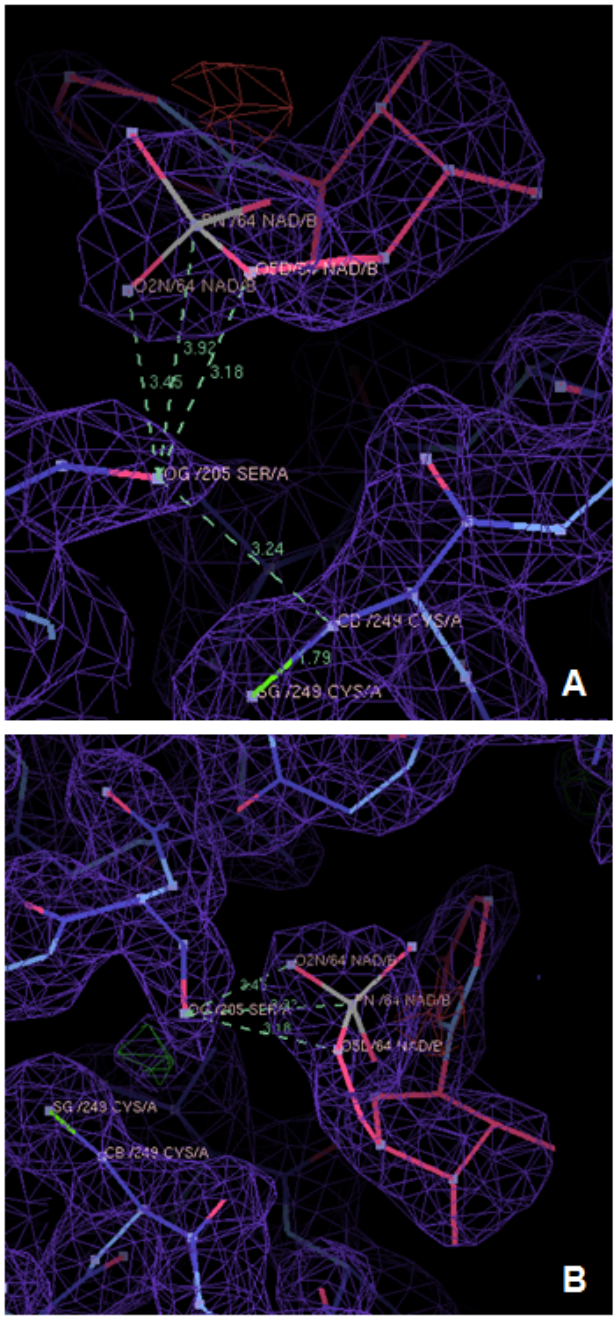

Figure C3-4. A close-up view of the NMN moiety of NADH in the dinucleotide binding site. The NMN moiety of NADH is shown in pink and is perpendicular to the plane of the paper. (**A)** The NMN moiety is above the S205/C249 area. The distances in Å between atoms of the phosphoryl group and the O atom of the S205 are shown in green dotted lines. The distance of 3.24Å – 1.79Å = 1.45Å is below the -S-S- distance (2.04Å) in the WT (*52*). (**B)** A side view of the NMN moiety near the S205/C249 area. A disulfide bond might block/prevent dinucleotide binding. This figure was generated using Coot and GIMP programs (*100*).

specifically the NMN^+ portion of it, positions of the R204, R130, and R131 side chains change, Figure C3-5B, but, the position of the R18 and R131 side chains remain the same, as seen from the superposition of the NADH-bound C205S and OxGly-bound WT structures, Figure C3-5C.

Previously the location of the NMN^+ moiety of the dinucleotide was estimated based on the modeled position in the semiempirical model (*51*). With the NADH-bound structure of C205S available the location of NMN moiety is confirmed. Examination of the NADH-bound structure reveals that the nicotinamide ring of NAD(H) is positioned in the NMN binding pocket with a network of hydrogen bonds, Figure C3-6A. Three cationic acids, K77, H96, and H320 are found within the long-range electrostatic interaction distance to the N^1 atom of the nicotinamide ring of NADH, where most of the + charge is located in NAD. D319 and H320 (yellow) are located close to the amide group of the nicotinamide ring of NAD(H) in the NMN-binding pocket of SDH domain II, while K77 and H96 (purple) are juxtaposed to the nicotinamide ring of NAD(H) and are located across the solvent-filled cleft in domain I. Interestingly, H320 is also within hydrogen bond distance to D319. The distance between N^1 atom of the H320 imidazole group and the closest oxygen atom of the D319 β-COO^- group is 2.60Å. Both residues, H320 and D319 are located in highly hydrophobic environment, Figure C3-6A. Movement of D319 and H320 is observed when apo-enzyme, AMP-, and NADH-bound structures are compared, Figures C3-6B, C.

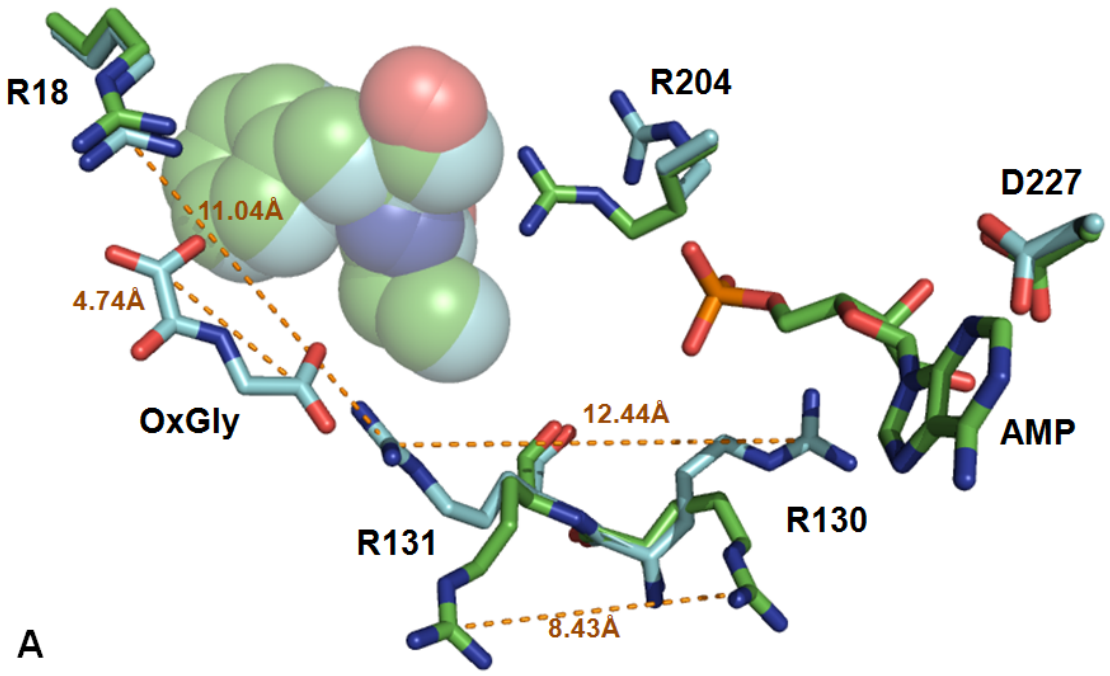

Figure C3-5A: Location of the R side chains in the active site of SDH in AMP- and OxGly-bound WT structures. The WT AMP-bound structure (green) was superimposed on the WT OxGly-bound structure (cyan). The distances are shown in orange (Å) between the carbon atoms of the guanidium head groups of the R side chains. Amino acids F135 and A134 are shown in a space filling model, shielding the guanidium head groups of R204 from R18, R131, and the OxGly binding pocket. D227 is within hydrogen-bonding distance to the ribose of AMP and is shown for reference. Some of the main chain atoms are hidden for clarity, including the C205, G200, C249, and G203 side chains proposed to interact with AMP (*51*). This figure was generated using PyMOL program and PDB IDs: 2QRK and 2QRL.

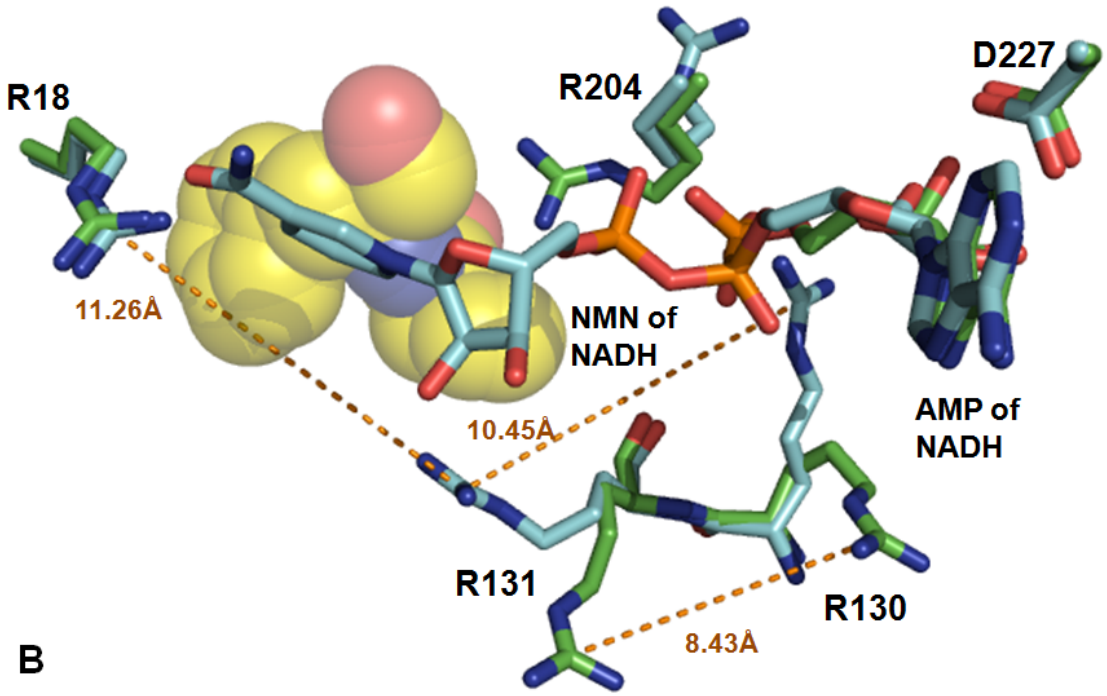

Figure C3-5B: Movement of R side chains upon dinucleotide binding. The WT AMP-bound structure (green) superimposed on the NADH-bound C205S structure (cyan). The presence of the NMN phosphoryl group affects the locations of R204 and R130. Also, movement of R204 affects the location of R130, which, in turn, positions R131 for binding. The distances are shown in orange (Å) between the carbon atoms of guanidium head groups for comparison with Figure C3-5A. Amino acids F135 and A134 are shown in space filling model, shielding the guanidium head groups of R204 from R18, R131, and the OxGly binding pocket. Some of the main chain atoms are hidden for clarity. This figure was generated using PyMOL program and PDB ID: 2QRK.

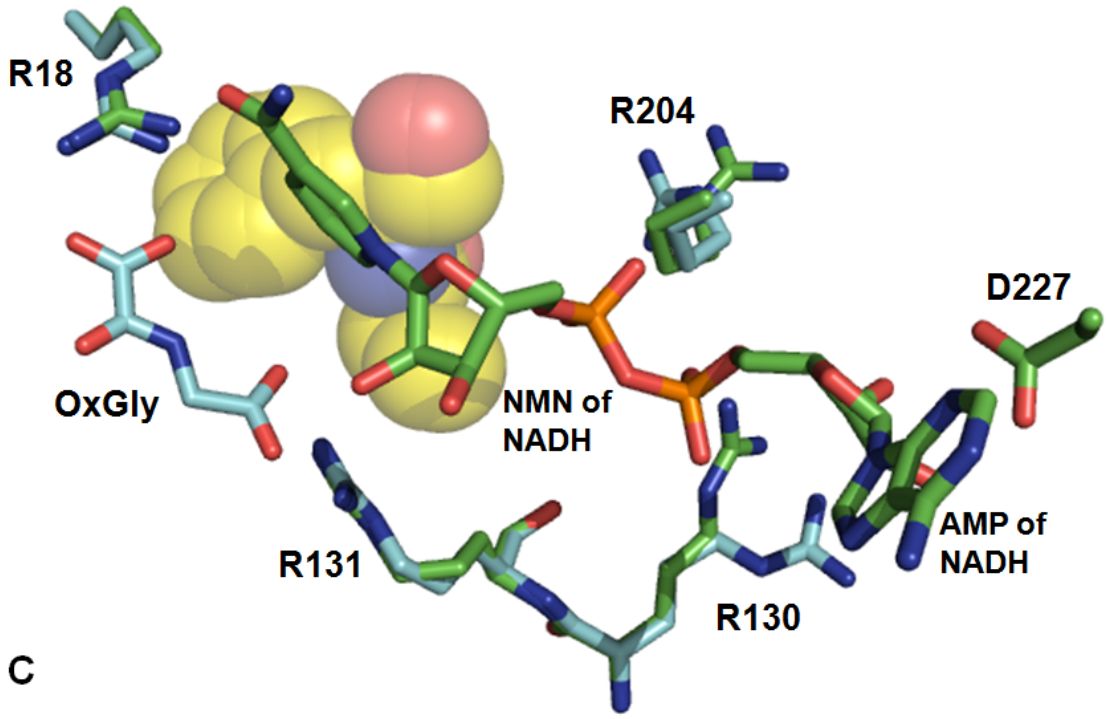

Figure C3-5C: Structural basis for the ordered mechanism of SDH. The NADH-bound C205S structure (green) was superimposed on the WT OxGly-bound structure (cyan) for comparison with Figures C3-5A and C3-5B. Amino acid side chains R18 and R131 are in a suitable location for binding of the substrate in both structures. This figure was generated using PyMOL program and PDB ID: 2QRL. The remainder of the figure is as above, Figures C3-5A,B.

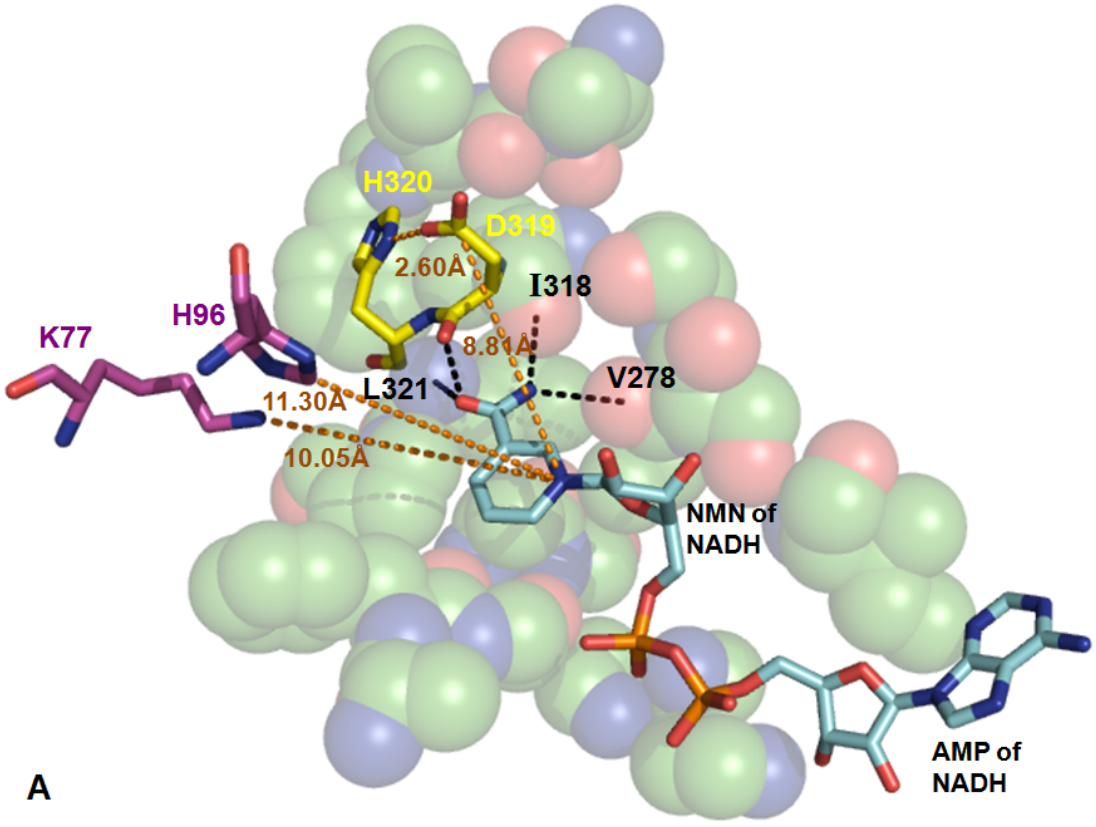

Figure C3-6A: NMN-binding pocket as seen in the NADH-bound structure of C205S SDH. Hydrophobic residues are shown in green space filling model with oxygen and nitrogen atoms in red and blue, respectively. Distances from the N^1 atom of the nicotinamide ring of NADH to the D319 β-COO^- (8.81Å), the K77 ε-NH_3^+ (10.05Å), C2 of H96 (11.30Å), as well as the distance H320 and the closest oxygen atom of the D319 β-COO^- (2.60Å) are shown with dotted orange lines. D319 and H320 (yellow) are located close to the amide group of the nicotinamide ring in the NMN-binding pocket of SDH domain II, while K77 and H96 (purple) are close to the nicotinamide ring of NAD(H) and are located across the solvent-filled cleft in domain I. Hydrogen bond distances are shown, with dotted black lines, between the amide N of NAD(H) to the main chain carbonyl of I318 (2.87Å) and V278 (3.32Å), and between the O atom of the amide group and main chain N atom of L321 (2.79Å).

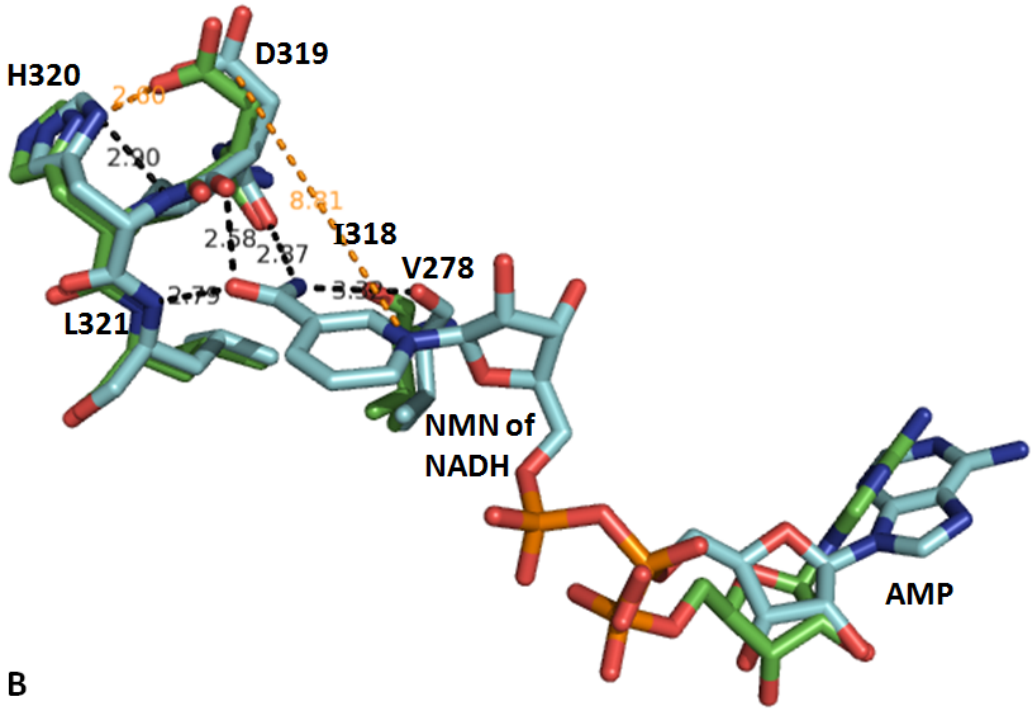

Figure C3-6B: Movement of H320-D319 dyad upon binding NMN of NADH as seen in the superposition of the AMP-bound structure (green), PDB ID: 2QRK (*51*), and the NADH-bound structure (cyan). Potential electrostatic interactions (orange) and hydrogen bonds (black) are between atoms in the NADH-bound structure, same as in Figure C3-6A.

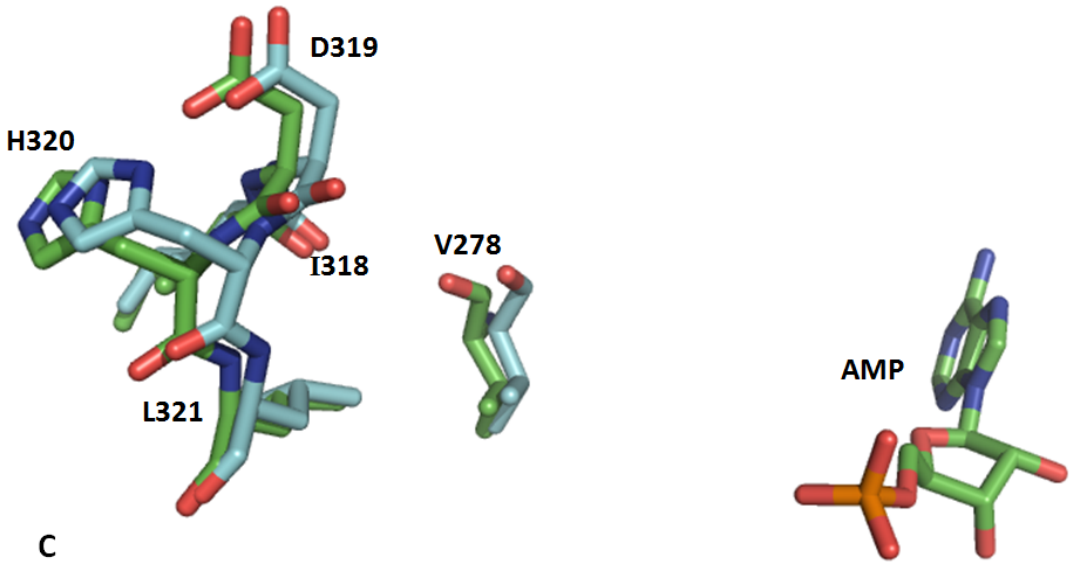

Figure C3-6C: Movement of H320-D319 dyad upon AMP binding as seen in the superposition of the AMP-bound structure (green), PDB ID: 2QRK, and WT SDH apo-enzyme structure (cyan), PDB ID: 2Q99.

The characteristic movement of K13 and K77 relative to each other and to the rest of ionizable residues nearby was observed in the superposition of the Apo C205S and WT structures, Figure C3-3B. The same characteristic movement is observed but at a larger scale in the superposition of the NADH-bound and AMP-bound structures, Figure C3-7. Data suggest a repulsion between K13 and K77 and interrelatedness between the movement of ionizable K13, K77, H96, E78 and E16 side chains.

C3.4 Discussion

In the current study crystal structures of the SDH C205S mutant enzyme in the Apo form and with the NADH bound in the active site were solved. Crystallization of WT SDH with natural substrates bound has been attempted previously but were unsuccessful (*51*). NADH-bound C205S is the first SDH structure with the natural substrate to date.

The C205S mutant enzyme cannot form a disulfide bond, and structural data confirm this, Figure C3-2. Examination of the C205S apoenzyme structure confirms that the dinucleotide binds in close proximity to where the disulfide bond would be in the WT enzyme, Figures C3-1, C3-4. Structural data suggest the disulfide bond hinders binding of the dinucleotide. This is in agreement with kinetic data, Chapter 2.

On the basis of modeled interactions with Sacc (*52*), and observed interactions with the α-Kg substrate analog OxGly (*51*), R18 and R131 were proposed to facilitate binding of the Sacc and α-Kg through interaction with the

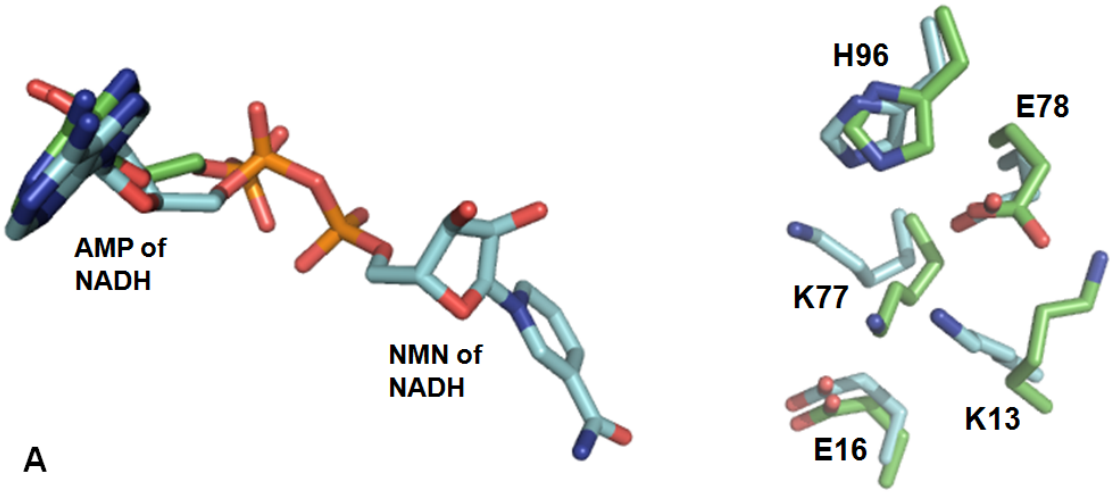

Figure C3-7A: Movement of K13 affects the position of K77 and H96. Superposition of the AMP-bound structure (green), PDB ID: 2QRK, and C205S NADH-bound structure (cyan).

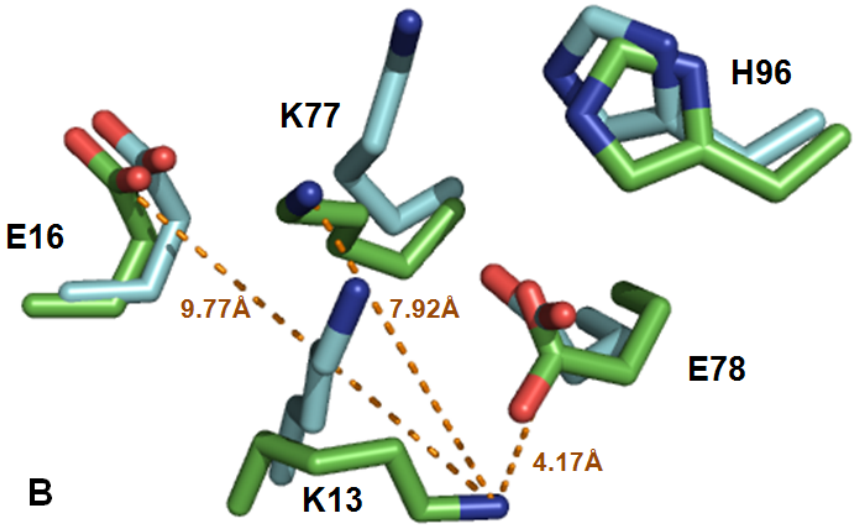

Figure C3-7B: Distances between K13 vs. K77, E16, and E78 in the AMP-bound structure. Superposition of the AMP-bound structure (green), PDB ID: 2QRK, and C205S NADH-bound structure (cyan). E78 is blocking K13 from interacting with H96.

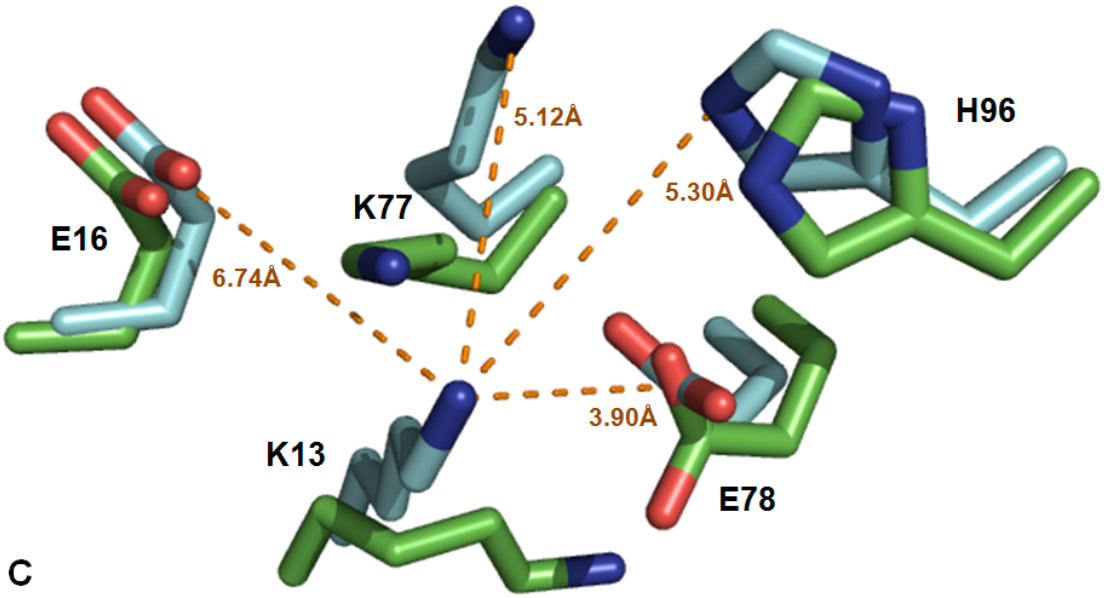

Figure C3-7C: Distances between K13 vs. K77, E16, E78, and H96 in the NADH-bound structure. Superposition of the AMP-bound structure (green), PDB ID: 2QRK, and C205S NADH-bound structure (cyan).

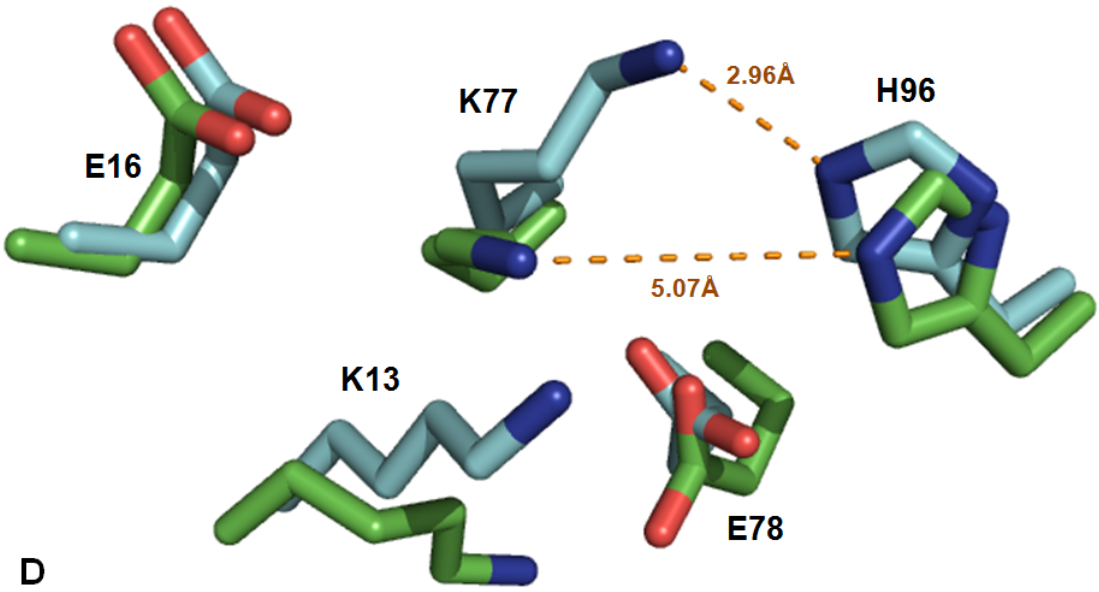

Figure C3-7D: Distances between K77 and H96 in the AMP- and NADH-bound structures. Superposition of the AMP-bound structure (green), PDB ID: 2QRK, and C205S NADH-bound structure (cyan).

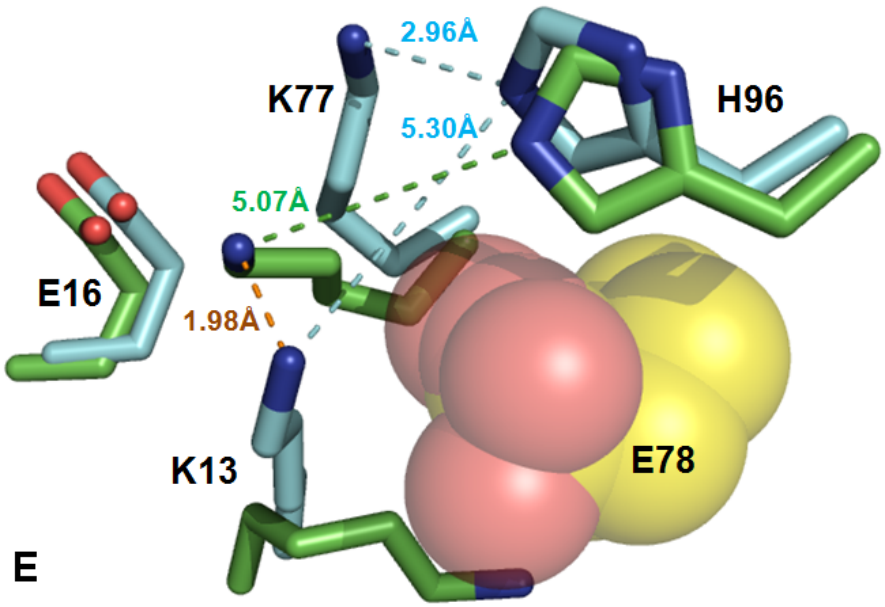

Figure C3-7E: E78 is blocking K13 from interacting with H96 in the AMP-bound structure. Superposition of the AMP-bound structure (green), PDB ID: 2QRK, and C205S NADH-bound structure (cyan). E78 is shown in yellow space filling model. The distances between K13 and K77 vs. H96 in the NADH-bound structure are shown in cyan while the distance between K77 vs. H96 in the AMP-bound structure is shown in green. The "would be" distance between K13 in the NADH-bound structure vs. K77 in the AMP-bound structure is shown in orange.

substrate carboxylates. Superposition of the structure with AMP bound on that with NADH bound, shows movement of the R204, R130, and R131 side chains upon binding of the NMN moiety of NADH, while the R18 side chain remains in the same position, in the absence or presence of the dinucleotide, Figure C3-5B. Movement of the arginine side chains is likely driven by a re-arrangement of the local electrostatic environment caused by the interplay between the negative charges from the phosphoryl oxygens of NAD(H) and positive charges on the guanidium head groups of the arginines. When the crystal structure of C205S with NADH bound was superimposed on either of the Apo structures (WT or C205S), no difference in the location of side chains of R18 and R131 was observed, and only minor changes in the location of the guanidium head groups of R204 and R130 were observed (data not shown). This observation in combination with observations made from the alignments in Figure C3-5, suggest a role for the dinucleotide in rearrangement of location of R side chains. It is tempting to suggest a sequence of events: the location of R204 changes upon dinucleotide binding which in turn re-orients the position of R130, and R130 re-aligns R131 into its position required for binding. In effect, a binding site for α-Kg or Sacc is created between R131 and R18. This description suggests an analogy with a “baseball glove”. i.e. repositioning R130 and R131 is necessary to “catch” α-Kg or Sacc, “the ball”. The kinetic mechanism of SDH is ordered with dinucleotides binding to free enzyme in both reaction directions followed by substrates (*60*). Data observed here provide a structural basis for the ordered mechanism, Figure C3-5C.

Additional interpretation of the pH-rate profiles may be made here. A group with a pK_a of 9.5 (9.6 in the C205S), is observed in the V_2/K_{NADH} pH-rate profile, Chapter 2. The group was not detected in the V_2 pH-rate profile and thus it must be protonated for optimal binding of NADH. Since NADH is the first substrate to bind, and the pK_a of the pyrophosphate moiety of NADH is about 1-2, the group with a pK_a of 9.6 was proposed to be cationic, Arg or Lys, interacting with the negatively charged phosphoryl oxygens of NAD(H) via an ionic interaction (*64*). On the basis of the pH dependence of the K_i for AMP two groups on the enzyme were shown to be important for AMP binding. One group had to be unprotonated and one protonated for optimal binding (*71*). It was observed in the AMP-bound SDH, AMP directly interacts with the main chain N atoms of R204 and C205, and indirectly, through water molecules, with the main chain O atoms of G200 and C249, while the ribose moiety interacts with D227 and the main chain N atom of G203. On the basis of these observations it was proposed that the unprotonated group required for AMP binding is D227, but the nature of the protonated group remained elusive (*51*).

As seen in the structure of C205S with NADH bound, there are no Lys residues in close proximity to the phosphoryl oxygens of NAD(H), but R204, in domain II, is in close proximity, and there is a pair of arginines, R130 and R131 from domain I, in the vicinity of the phosphoryl oxygens of NAD(H), Figure C3-5. The group on the enzyme with a pK_a of 9.6 may be either R204 or R130.

The pH dependence of V_1/K_{NAD} is the on-rate constant for binding of NAD. A group with a pK_a of 7.4 which has to be unprotonated for optimal

binding of NAD is seen in the WT V_1/K_{NAD} pH profile, Figure C2-2B, but is not observed in the WT V_2/K_{NADH} pH profile, Figure C2-3B. It was proposed this group is likely a cationic acid (Lys, His) in the vicinity of the positively charged nicotinamide ring of NAD, and K77 was suggested a candidate (*64*). The pK_a of this binding group is perturbed from 7.4 in WT to 7.1 in C205S as seen on the V_1/K_{NAD} pH profile, Figure C2-2E, and this group is still not seen on the C205S V_2/K_{NADH} pH profile, Figure C2-3F. The protonation state of this NAD-binding group does not affect the binding of NADH. The NADH-bound C205S SDH structure may provide clues to the identity of this group.

The distance from the N^1 atom of the nicotinamide ring of NADH to the D319 β-COO^- group is shorter (8.81Å), than the distance to the K77 ε-NH_3^+ (10.05Å), or to C2 of H96 (11.30Å). Also, K77 and H96 are located in domain I of SDH across the solvent-filled cavity from the NMN-binding pocket of the dinucleotide binding domain of SDH. Electrostatic interactions are expected to be weakened by the polar environment. For these reasons K77 and H96 seem unlikely as candidates for the role of the NAD binding group, while H320 and D319 are located in a hydrophobic pocket. The pK_a of the NAD binding group is 7.4. The pK_a of an imidaloze group is ~6.0 in an aqueous environment, and would be expected to increase in a hydrophobic environment and/or in the presence of a negative charge nearby. Both conditions are met for H320. Thus, the group on the enzyme with a pK_a of 7.4 may be H320.

Residues K77 and H96 have been previously proposed to be candidates for the role of the catalytic base (B_2) with a pK_a of 7.2 in the chemical

mechanism of SDH (*64*). Movement of K13 and K77 is observed relative to other ionizable residues nearby in the superimposed structures of the WT and C205S apoenzymes, Figure C3-3B. Similar, but more pronounced movement is observed in the superimposed structures with the AMP and NADH bound to the dinucleotide binding site of the enzyme, Figure C3-7. The presence of the NMN moiety of NADH generates a distinctly different conformation of the enzyme, with the side chains of K13, K77, H96, E16, and E78 in different locations, Figure C3-7A. The side chains of K13 and K77 exhibit the most movement, Figure C3-7B, C. The distance from the nitrogen atom of the ε-amino group of K13 to the carbon atom of the carboxylate group of E16, ε-amino group of K77 and the carbon atom of the carboxylate group of E78 in the AMP-bound structure is 9.77Å, 7.92Å, and 4.17Å, respectively, Figure C3-7B. The ε-amino group of K13 is blocked from interacting with the imidazole group of H96 by E78, Figure C3-7B,E. In the NADH-bound structure, the distance between K13 and K77 is decreased (5.12 Å) but the expected repulsion between the positively charged amino groups is compensated by the decrease in the distances to E16 (6.74 Å) and E78 (3.90 Å) and the resulting attraction between the positively charged amino group to the negatively charged carboxylate groups. Also, the distance from K13 to the N^3 atom of the H96 imidazole group is 5.30 Å , Figure C3-7C,E. Interestingly, the distance between the K13 in the C205S structure and K77 if it had not moved is 1.98Å, Figure C3-7E. A repulsion between two lysines and a histidine as well as an attraction between lysines and a histidine vs. glutamates is implied. In effect, a network of

electrostatic interactions exists between K13, K77, H96, E16, and E78 and the changes in the charge distribution upon binding of the NMN moiety of the dinucleotide cause K77 and H96 to change their position. Additionally, the location of K77, close to the K13 and H96 pair, is likely going to decrease the pK_a of this candidate catalytic group, while the pK_a of H96 may increase as a result of its location close to E78.

Thus, a role for the network of electrostatic interactions between K13, K77, H96, E16, and E78 is proposed in positioning K77 and H96 for reaction and modulating the pK_as of these catalytic side chains close to neutrality, with K13 playing an essential part.

Chapter 4

Overall Discussion and Summary

As observed in the Apo- and ligand-bound SDH crystal structures and a semi-empirical model of the E•NAD•Sacc ternary complex of SDH, there are more than a dozen ionizable groups in the active site of SDH: K77, H96, K13, K99, H320, E78, E122, E16, D281, D319, R18, R131, R130, R204, and D227 (*51, 52*), Figures C1-7, 8. On the basis of the C205S pH-rate profiles, two of these likely participate in binding of dinucleotides, NAD (7.1), and NADH (9.5); two are likely catalytic (B_1 and B_2) and are involved in binding of Sacc (5.7 and 6.5) and Lys (7.0 and 8.1); and two groups contribute to the binding of α-Kg, a change in kinetic mechanism at the pH extremes (e.g. high pH), and a conformational change (5.7 and 7.4). Data support the multiple sequence alignments of *S. cerevisiae* SDH with homolog sequences from other fungal organisms that show several highly conserved ionizable amino acid residues (*52*).

Here, on the basis of the pH-rate studies of the C205S mutant enzyme and comparison to those of the WT, Chapter 2, an attempt has been made to synthesize the currently available information on the pK_as and the proposed function of the ionizable side chains in the active site of the SDH, Table C4-1. To assist the reader, the pK_a values of the groups are color-coded with the same side chain shown in the same color. The group from the V_1/K_{NAD} pH-rate

Table C4-1: Proposed roles for the side chains of C205S mutant enzyme vs. WT

pH-rate profile	pK_a of the side chain	proposed role of the side chain	pK_a of the side chain	proposed role of the side chain
	_____ WT[a] _____		_____C205S_____	
V_1	**7.3** ± 0.2[b]	cat.[c] (**:B_2**)	**7.5-7.7**[d]	conf.
V_1/K_{NAD}	**7.4** ± 0.2	bind. NAD & cat. (**:B_2**)	**7.1** ± 0.2	bind. NAD
V_1/K_{Sacc}	**6.2** ± 0.3	bind. Sacc & cat. (**:B_1**)	**5.7** ± 0.3	bind. Sacc & cat. (**:B_1**)
	7.2 ± 0.2	bind. Sacc & cat. (**:B_2**)	**6.5** ± 0.2	bind. Sacc & cat. (**:B_2**)
V_2	**5.8** ± 0.2	conf.	-[e]	
	8.4 ± 0.5	mech.	**7.5** ± 0.1	conf. & mech.
V_2/K_{NADH}	9.6 ± 0.2	bind. NADH	9.5 ± 0.1	bind. NADH
$V_2/K_{\alpha\text{-Kg}}$	-		**5.7** ± 0.2	bind. α-Kg, mech. conf.
	8.9 ± 0.1	bind. α-Kg & mech.	**7.4** ± 0.3	bind. α-Kg & mech.
V_2/K_{Lys}	**7.2** ± 0.5[f]	bind. Lys & cat.	**7.0** ± 0.1	bind. Lys & cat. (**:B_1**)
		two groups (**:B_1** &**:B_2**)	**8.1** ± 0.1	bind. Lys & cat. (**:B_2**)

[a]From Xu et al. (*64*). [b]Values are ± SE. [c]cat., catalysis; bind., binding; conf., conformational change; mech., kinetic mechanism change. [d]Value estimated from a curve drawn by hand. [e]The group was not observed. [f]Average value.

profile which contributes to binding of NAD (7.1) is shown in blue, while the group for NADH binding (9.5) is in black font. The two catalytic bases are in green (B_1), red (B_2) and yellow in the forward and reverse reaction directions, respectively. Two groups contributing to binding of α-Kg, a change in kinetic mechanism at the pH extremes (e.g. high pH), and a conformational change are shown in cyan (5.7) and blue (7.4). The blue group (7.4) from the $V_2/K_{\alpha\text{-Kg}}$ pH-rate profile is the same as a group with pK_a of 7.5 from the V_2 pH-rate profile, a group with a pK_a of 7.1 from V_1/K_{NAD} pH-rate profile, and a group with a pK_a of 7.5-7.7 from the V_1 pH-rate profile. The same color codes were used to label the groups observed for WT. A group (5.8) is seen in the WT V_2 pH-rate profile that is likely the same side chain seen in the $V_2/K_{\alpha\text{-Kg}}$ pH-rate profile (5.7) with both groups shown in cyan.

Kinetic studies with C205S mutant enzyme helped to distinguish between the catalytic and binding groups and clarify the mechanism of SDH. In the C205S mutant enzyme, the disulfide cannot form, and this makes the enzyme catalytically more efficient at low pH compared to WT. The C205S mutant enzyme is less sensitive to the protonation state of the group with a pK_a about 7.1, which affects (1) activity of the enzyme and (2) binding of NAD (disulfide bond in the WT may prevent binding of the dinucleotide at low pH). A pH dependent conformational change before NAD binds is reflected in the V_1 and V/K_{NAD} pH-rate profiles and is corroborated by isotope effects data.

Crystallographic studies of the C205S mutant enzyme provided some useful structural information. In agreement with kinetic data, Chapter 2, the

structural data suggested that disulfide between the C205 and C249 in the wild type enzyme might prevent the dinucleotide binding. Also, NADH-bound C205S structure has been superimposed with all other available ligand-bound structures of SDH. Observations were made that resulted in hypotheses concerning aspects of the SDH mechanism. The movement of arginine 204, 130, and 131 side chains upon dinucleotide binding and the resulting position of arginine 131 in a location optimal for substrate binding has been proposed as a structural basis for the ordered kinetic mechanism. A group on the enzyme with a pK_a of 7.4 that contributes to NAD binding has been hypothesized to be H320. Also, a role for the network of electrostatic interactions between K13, K77, H96, E16, and E78 has been proposed in positioning K77 and H96 for reaction and modulating the pK_as of these catalytic side chains close to neutrality, with K13 playing an essential part. To test these hypotheses site-directed mutagenesis will have to be utilized followed by the complete kinetic characterization of the mutants under investigation. For example, R204, R130, R131, F135, H320, K13, and E16 are good candidates for future studies probing the mechanism of SDH.

REFERENCES

1. Vogel, H. J. (1959) On biochemical evolution: a dichotomy in microbial lysine synthesis, *Federation Proc 18*, 345.

2. Vogel, H. J. (1960) Two modes of lysine synthesis among lower fungi: evolutionary significance, *Biochim Biophys Acta 41*, 172-173.

3. Bhattacharjee, J. K. (1985) alpha-Aminoadipate pathway for the biosynthesis of lysine in lower eukaryotes, *Crit Rev Microbiol 12*, 131-151.

4. Bryan, J. K. (1980) Synthesis of the aspartate family and branched-chain amino acids, In *The biochemistry of plants* (Miflin, B. J., Ed.), pp 402–440, Academic Press, New York.

5. Lejohn, H. B. (1971) Enzyme regulation, lysine pathways, and cell structures as indicators of major lines of evolution in fungi, *Nature (London) 231*, 164-168.

6. Rothstein M., S., E.M. (1963) Lysine biosynthesis in algae, *Arch Biochem Biophys 101*, 373.

7. Vogel, H. J. (1959) On Biochemical Evolution: Lysine Formation in Higher Plants, *Proc Natl Acad Sci U S A 45*, 1717-1721.

8. Vogel, H. J. (1959) Lysine biosynthesis in Chlorella and Euglena: phylogenetic significance, *Biochim. Biophys. Acta 34*, 282–283.

9. Vogel, H. J. (1961) Lysine synthesis and phylogeny of lower fungi: some chytrids versus Hyphochytrium, *Nature 189*, 1026-1027.

10. Zabriskie, T. M., and Jackson, M. D. (2000) Lysine biosynthesis and metabolism in fungi, *Nat. Prod. Rep. 17*, 85-97.

11. Berges, D. A., DeWolf, W. E., Jr., Dunn, G. L., Grappel, S. F., Newman, D. J., Taggart, J. J., and Gilvarg, C. (1986) Peptides of 2-aminopimelic acid: antibacterial agents that inhibit diaminopimelic acid biosynthesis, *J Med Chem 29*, 89-95.

12. Cox, R. J. (1996) The DAP pathway to lysine as a target for antimicrobial agents, *Nat Prod Rep 13*, 29-43.

13. Scapin, G., and Blanchard, J. S. (1998) Enzymology of bacterial lysine biosynthesis, *Adv Enzymol Relat Areas Mol Biol 72*, 279-324.

14. Xu, H., Andi, B., Qian, J., West, A. H., and Cook, P. F. (2006) The alpha-aminoadipate pathway for lysine biosynthesis in fungi, *Cell Biochem Biophys 46*, 43-64.

15. Palmer, D. R., Balogh, H., Ma, G., Zhou, X., Marko, M., and Kaminskyj, S. G. (2004) Synthesis and antifungal properties of compounds which target the alpha-aminoadipate pathway, *Pharmazie 59*, 93-98.

16. Yamamoto, T., and Eguchi, T. (2008) Thiahomoisocitrate: a highly potent inhibitor of homoisocitrate dehydrogenase involved in the alpha-aminoadipate pathway, *Bioorg Med Chem 16*, 3372-3376.

17. Urrestarazu, L. A., Borell, C. W., and Bhattacharjee, J. K. (1985) General and specific controls of lysine biosynthesis in Saccharomyces cerevisiae, *Curr Genet 9*, 341-344.

18. Matsuda, M., and Ogur, M. (1969) Separation and specificity of the yeast glutamate-alpha-ketoadipate transaminase, *J Biol Chem 244*, 3352-3358.

19. Matsuda, M., and Ogur, M. (1969) Enzymatic and physiological properties of the yeast glutamate-alpha-ketoadipate transaminase, *J Biol Chem 244*, 5153-5158.

20. Li, J. J. (2003) *Name Reactions: A Collection of Detailed Reaction Mechanisms*, 2nd ed., Springer-Verlag, Berlin, New York.

21. Andi, B., West, A. H., and Cook, P. F. (2004) Kinetic mechanism of histidine-tagged homocitrate synthase from Saccharomyces cerevisiae, *Biochemistry 43*, 11790-11795.

22. Andi, B., West, A. H., and Cook, P. F. (2005) Regulatory mechanism of histidine-tagged homocitrate synthase from Saccharomyces cerevisiae. I. Kinetic studies, *J Biol Chem 280*, 31624-31632.

23. Tracy, J. W., and Kohlhaw, G. B. (1975) Reversible, coenzyme-A-mediated inactivation of biosynthetic condensing enzymes in yeast: a possible regulatory mechanism, *Proc Natl Acad Sci U S A 72*, 1802-1806.

24. Qian, J., Khandogin, J., West, A. H., and Cook, P. F. (2008) Evidence for a catalytic dyad in the active site of homocitrate synthase from Saccharomyces cerevisiae, *Biochemistry 47*, 6851-6858.

25. Qian, J., West, A. H., and Cook, P. F. (2006) Acid-base chemical mechanism of homocitrate synthase from Saccharomyces cerevisiae, *Biochemistry 45*, 12136-12143.

26. Betterton, H., Fjellstedt, T., Matsuda, M., Ogur, M., and Tate, R. (1968) Localization of the homocitrate pathway, *Biochim Biophys Acta 170*, 459-461.

27. Beinert, H., Kennedy, M. C., and Stout, C. D. (1996) Aconitase as Ironminus signSulfur Protein, Enzyme, and Iron-Regulatory Protein, *Chem Rev 96*, 2335-2374.

28. Lin, Y., Alguindigue, S. S., Volkman, J., Nicholas, K. M., West, A. H., and Cook, P. F. (2007) Complete kinetic mechanism of homoisocitrate dehydrogenase from Saccharomyces cerevisiae, *Biochemistry 46*, 890-898.

29. Lin, Y., Volkman, J., Nicholas, K. M., Yamamoto, T., Eguchi, T., Nimmo, S. L., West, A. H., and Cook, P. F. (2008) Chemical mechanism of homoisocitrate dehydrogenase from Saccharomyces cerevisiae, *Biochemistry 47*, 4169-4180.

30. Karsten, W. E., and Cook, P. F. (2006) An isothermal titration calorimetry study of the binding of substrates and ligands to the tartrate dehydrogenase from Pseudomonas putida reveals half-of-the-sites reactivity, *Biochemistry 45*, 9000-9006.

31. Lin, Y., West, A. H., and Cook, P. F. (2008) Potassium is an activator of homoisocitrate dehydrogenase from Saccharomyces cerevisiae, *Biochemistry 47*, 10809-10815.

32. Tipton, P. A. (2000) Tartrate dehydrogenase, an enzyme with multiple catalytic activities, *Protein Pept Lett 7 (5)*, 323-332.

33. Lin, Y., West, A. H., and Cook, P. F. (2009) Site-directed mutagenesis as a probe of the acid-base catalytic mechanism of homoisocitrate dehydrogenase from Saccharomyces cerevisiae, *Biochemistry 48*, 7305-7312.

34. Kiick, D. M., and Cook, P. F. (1983) pH studies toward the elucidation of the auxiliary catalyst for pig heart aspartate aminotransferase, *Biochemistry 22*, 375-382.

35. Velick, S. F., and Vavra, J. (1962) A kinetic and equilibrium analysis of the glutamic oxaloacetate transaminase mechanism, *J Biol Chem 237*, 2109-2122.

36. Sagisaka, S., and Shimura, K. (1962) Studies in lysine biosynthesis. IV. Mechanism of activation and reduction of alpha-aminoadipic acid, *J Biochem 52*, 155-161.

37. Sinha, A. K., and Bhattacharjee, J. K. (1971) Lysine biosynthesis in *Saccharomyces*, conversion of α-aminoadipate into α-aminoadipic δ-semialdehyde, *Biochem J 125*, 743-749.

38. Larson, R. L., Sandine, W. D., and Broquist, H. P. (1963) Enzymatic reduction of α-aminoadipic acid: relation to lysine biosynthesis *J Biol Chem 238*, 275-282.

39. Ehmann, D. E., Gehring, A. M., and Walsh, C. T. (1999) Lysine biosynthesis in *Saccharomyces cerevisiae*: mechanism of α-aminoadipate reductase (*LYS2*)

involves posttranslational phosphopantetheinylation by *LYS5* *Biochemistry 38*, 6171-6177.

40. Brunhuber, N. M., and Blanchard, J. S. (1994) The biochemistry and enzymology of amino acid dehydrogenases, *Crit Rev Biochem Mol Biol 29*, 415-467.

41. Stillman, T. J., Baker, P. J., Britton, K. L., and Rice, D. W. (1993) Conformational flexibility in glutamate dehydrogenase. Role of water in substrate recognition and catalysis, *J Mol Biol 234*, 1131-1139.

42. Baker, P. J., Sawa, Y., Shibata, H., Sedelnikova, S. E., and Rice, D. W. (1998) Analysis of the structure and substrate binding of Phormidium lapideum alanine dehydrogenase, *Nat Struct Biol 5*, 561-567.

43. Baker, P. J., Turnbull, A. P., Sedelnikova, S. E., Stillman, T. J., and Rice, D. W. (1995) A role for quaternary structure in the substrate specificity of leucine dehydrogenase, *Structure 3*, 693-705.

44. Vanhooke, J. L., Thoden, J. B., Brunhuber, N. M., Blanchard, J. S., and Holden, H. M. (1999) Phenylalanine dehydrogenase from *Rhodococcus sp*. M4: high-resolution X-ray analyses of inhibitory ternary complexes reveal key features in the oxidative deamination mechanism *Biochemistry 38*, 2326-2339.

45. Scapin, G., Reddy, S. G., and Blanchard, J. S. (1996) Three-dimensional structure of meso-diaminopimelic acid dehydrogenase from Corynebacterium glutamicum, *Biochemistry 35*, 13540-13551.

46. Nishida, H., and Nishiyama, M. (2000) What is characteristic of fungal lysine synthesis through the alpha-aminoadipate pathway?, *J Mol Evol 51*, 299-302.

47. Broquist, H. P. (1971) Lysine biosynthesis (yeast), *Methods Enzymol 17*, 112-129.

48. Jones, E. W., and Fink, G. R. (1982) Regulation of amino acid and nucleotide synthesis in yeast, In *Molecular Biology of the Yeast Saccharomyces, Metabolism and Gene Regulation* (Strathern, J. N., Jones, E. W., and Broach, J. R., Eds.), pp 181-299, Cold Spring Harbor Laboratory, Cold Spring Harbor, NY.

49. Vashishtha, A. K., West, A. H., and Cook, P. F. (2008) Overall kinetic mechanism of saccharopine dehydrogenase (L-glutamate forming) from Saccharomyces cerevisiae, *Biochemistry 47*, 5417-5423.

50. Vashishtha, A. K., West, A. H., and Cook, P. F. (2009) Chemical mechanism of saccharopine reductase from Saccharomyces cerevisiae, *Biochemistry 48*, 5899-5907.

51. Andi, B., Xu, H., Cook, P. F., and West, A. H. (2007) Crystal structures of ligand-bound saccharopine dehydrogenase from Saccharomyces cerevisiae, *Biochemistry 46*, 12512-12521.

52. Burk, D. L., Hwang, J., Kwok, E., Marrone, L., Goodfellow, V., Dmitrienko, G. I., and Berghuis, A. M. (2007) Structural studies of the final enzyme in the alpha-aminoadipate pathway-saccharopine dehydrogenase from Saccharomyces cerevisiae, *J. Mol. Biol. 373*, 745-754.

53. Ogawa, H., and Fujioka, M. (1978) Purification and characterization of saccharopine dehydrogenase from baker's yeast, *J. Biol. Chem. 253*, 3666-3670.

54. Ogawa, H., Okamoto, M., and Fujioka, M. (1979) Chemical modification of the active site sulfhydryl group of saccharopine dehydrogenase (L-lysine-forming), *J. Biol. Chem. 254*, 7030-7035.

55. Saccharomyces Genome Database, Department of Genetics, School of Medicine, Stanford University, Stanford, CA, http://www.yeastgenome.org/

56. Fujioka, M., and Nakatani, Y. (1970) A kinetic study of saccharopine dehydrogenase reaction, *Eur J Biochem 16*, 180-186.

57. Fujioka, M., and Nakatani, Y. (1972) Saccharopine dehydrogenase. Interaction with substrate analogues, *Eur J Biochem 25*, 301-307.

58. Sugimoto, K., and Fujioka, M. (1978) The reaction of pyruvate with saccharopine dehydrogenase, *Eur J Biochem 90*, 301-307.

59. Fujioka, M., and Nakatani, Y. (1974) Saccharopine dehydrogenase. A kinetic study of coenzyme binding, *J Biol Chem 249*, 6886-6891.

60. Xu, H., West, A. H., and Cook, P. F. (2006) Overall kinetic mechanism of saccharopine dehydrogenase from Saccharomyces cerevisiae, *Biochemistry 45*, 12156-12166.

61. Fujioka, M., Takata, Y., Ogawa, H., and Okamoto, M. (1980) The inactivation of saccharopine dehydrogenase (L-lysine-forming) by diethyl pyrocarbonate, *J Biol Chem 255*, 937-942.

62. Ogawa, H., and Fujioka, M. (1980) The reaction of pyridoxal 5'-phosphate with an essential lysine residue of saccharopine dehydrogenase (L-lysine-forming), *J Biol Chem 255*, 7420-7425.

63. Fujioka, M., and Takata, Y. (1981) Role of arginine residue in saccharopine dehydrogenase (L-lysine forming) from baker's yeast, *Biochemistry 20*, 468-472.

64. Xu, H., Alguindigue, S. S., West, A. H., and Cook, P. F. (2007) A proposed proton shuttle mechanism for saccharopine dehydrogenase from Saccharomyces cerevisiae, *Biochemistry 46*, 871-882.

65. Fujioka, M. (1984) Chemical mechanism of saccharopine dehydrogenase (NAD+, L-lysine-forming) as deduced from initial rate pH studies, *Arch. Biochem. Biophys. 230*, 553-559.

66. Fujioka, M., and Takata, Y. (1979) Stereospecificity of hydrogen transfer in the saccharopine dehydrogenase reaction, *Biochim. Biophys. Acta. 570*, 210-212.

67. Baker, R. H., Jr. (1962) Studies on the mechanism of enzyme-catalyzed oxidation reduction reactions. III. A characterization of the mechanism of the liver alcohol dehydrogenase reaction, *Biochemistry 1*, 41-47.

68. Mahler, H. R., Baker, R. H., Jr., and Shiner, V. J., Jr. (1962) Studies on the mechanism of enzyme-catalyzed oxidation reduction reactions. IV. A proposed mechanism for the over-all reaction catalyzed by liver alcohol dehydrogenase, *Biochemistry 1*, 47-52.

69. Cook, P. F., and Cleland, W. W. (1981) pH variation of isotope effects in enzyme-catalyzed reactions. 2. Isotope-dependent step not pH dependent. Kinetic mechanism of alcohol dehydrogenase, *Biochemistry 20*, 1805-1816.

70. Hermes, J. D., Roeske, C. A., O'Leary, M. H., and Cleland, W. W. (1982) Use of multiple isotope effects to determine enzyme mechanisms and intrinsic isotope effects. Malic enzyme and glucose-6-phosphate dehydrogenase, *Biochemistry 21*, 5106-5114.

71. Xu, H., West, A. H., and Cook, P. F. (2007) Determinants of substrate specificity for saccharopine dehydrogenase from Saccharomyces cerevisiae, *Biochemistry 46*, 7625-7636.

72. Rossman, M. G., Liljas, A., Branden, C., Banaszak, L.J. (1975) Evolutionary and structural relationships among dehydrogenases In *The enzymes* (Boyer, P. D., Ed.), pp 51-102, Academic Press, New York

73. Bellamacina, C. R. (1996) The nicotinamide dinucleotide binding motif: a comparison of nucleotide binding proteins, *FASEB J 10*, 1257-1269.

74. Jang, M. S., Kang, N. Y., Kim, K. S., Kim, C. H., Lee, J. H., and Lee, Y. C. (2007) Mutational analysis of NADH-binding residues in triphenylmethane reductase from Citrobacter sp. strain KCTC 18061P, *FEMS Microbiol Lett 271*, 78-82.

75. Voet, D., and Voet, J. G. (1995) *Biochemistry*, 2nd ed., John Wiley & Sons, Inc., New York, Chichester, Brisbane, Toronto, Singapore.

76. Bhattacharjee, J. K. (1992) Evolution of α-aminoadipate pathway for the synthesis of lysine in fungi, In *Evolution of metabolic function* (Mortlock, R. P., Ed.), pp 47-80, CRC Press, Boca Raton, FL.

77. Bhattacharjee, J. K., and Strassman, M. (1967) Accumulation of tricarboxylic acids related to lysine biosynthesis in a yeast mutant, *J Biol Chem 242*, 2542-2546.

78. Gaillardin, C. M., Ribet, A. M., and Heslot, H. (1982) Wild-type and mutant forms of homoisocitric dehydrogenase in the yeast Saccharomycopsis lipolytica, *Eur J Biochem 128*, 489-494.

79. Ye, Z. H., and Bhattacharjee, J. K. (1988) Lysine biosynthesis pathway and biochemical blocks of lysine auxotrophs of Schizosaccharomyces pombe, *J Bacteriol 170*, 5968-5970.

80. Glass, J., and Bhattacharjee, J. K. (1971) Biosynthesis of lysine in Rhodotorula: accumulation of homocitric, homoaconitic, and homoisocitric acids in a leaky mutant, *Genetics 67*, 365-376.

81. Kunze, G., Bode, R., Schmidt, H., Samsonova, I. A., and Birnbaum, D. (1987) Identification of a lys2 mutant of Candida maltosa by means of transformation, *Curr Genet 11*, 385-391.

82. Jaklitsch, W. M., and Kubicek, C. P. (1990) Homocitrate synthase from Penicillium chrysogenum. Localization, purification of the cytosolic isoenzyme, and sensitivity to lysine, *Biochem J 269*, 247-253.

83. Garrad, R. C., and Bhattacharjee, J. K. (1992) Lysine biosynthesis in selected pathogenic fungi: characterization of lysine auxotrophs and the cloned LYS1 gene of Candida albicans, *J. Bacteriol. 174*, 7379-7384.

84. Lorand, T., and Kocsis, B. (2007) Recent advances in antifungal agents, *Mini. Rev. Med. Chem. 7*, 900-911.

85. Viola, R. E., Cook, P. F., and Cleland, W. W. (1979) Stereoselective preparation of deuterated reduced nicotinamide adenine nucleotides and substrates by enzymatic synthesis, *Anal. Biochem. 96*, 334-340.

86. Northrop, D. B. (1977) Determining the absolute magnitude of hydrogen isotope effects., In *Isotope effects on enzyme-catalyzed reactions* (Cleland, W. W., O'Leary, M. H., and Northrop, D. B., Eds.), pp 122-152, University Park Press, Baltimore MD.

87. Cook, P. F., and Cleland, W. W. (1981) Mechanistic deductions from isotope effects in multireactant enzyme mechanisms, *Biochemistry 20*, 1790-1796.

88. Schowen, K. B., and Schowen, R. L. (1982) Solvent isotope effects of enzyme systems, *Methods. Enzymol. 87*, 551-606.

89. Cook, P. F., and Cleland, W. W. (2007) *Enzyme kinetics and mechanism*, Garland Science, London ; New York.

90. Marquardt, D. W. (1963) An algorithm for least square estimation of nonlinear parameters, *J. Soc. Ind. Appl. Math. 11*, 431-441.

91. Cleland, W. W. (1963) Computer programmes for processing enzyme kinetic data, *Nature 198*, 463-465.

92. Cleland, W. W. (1979) Statistical analysis of enzyme kinetic data, *Methods. Enzymol. 63*, 103-138.

93. Cleland, W. W. (1964) Dithiothreitol, a New Protective Reagent for SH Groups, *Biochemistry 3*, 480-482.

94. McPherson, A. (1999) Crystallization of biological macromolecules, pp 159-214, Cold Spring Harbor Laboratory Press, Cold Spring Harbor, NY.

95. Pflugrath, J. W. (1999) The finer things in X-ray diffraction data collection, *Acta Crystallogr D Biol Crystallogr 55*, 1718-1725.

96. Leslie, A. G. W. (1992) Recent changes to the MOSFLM package for processing film and image plate data, In Joint CCP4 + ESF-EAMCB Newsletter on Protein Crystallography, No. 26.

97. Evans, P. R. (2005) Scaling and assessment of data quality, *Acta Cryst D62*, 72-82.

98. Collaborative Computational Project Number 4. (1994) The CCP4 Suite: Programs for Protein Crystallography, *Acta Cryst D50*, 760-763.

99. McCoy, A. J., Grosse-Kunstleve, R. W., Adams, P. D., Winn, M. D., Storoni, L. C., and Read, R. J. (2007) Phaser crystallographic software, *J Appl Crystallogr 40*, 658-674.

100. Emsley, P., Lohkamp, B., Scott, W. G., and Cowtan, K. (2010) Features and development of Coot, *Acta Crystallogr D Biol Crystallogr 66*, 486-501.

101. Murshudov, G. N., Vagin, A. A., and Dodson, E. J. (1997) Refinement of macromolecular structures by the maximum-likelihood method, *Acta Crystallogr D Biol Crystallogr 53*, 240-255.

102. Vaguine, A. A., Richelle, J., and Wodak, S. J. (1999) SFCHECK: a unified set of procedures for evaluating the quality of macromolecular structure-factor data

and their agreement with the atomic model, *Acta Crystallogr D Biol Crystallogr 55*, 191-205.

103. Davis, I. W., Leaver-Fay, A., Chen, V. B., Block, J. N., Kapral, G. J., Wang, X., Murray, L. W., Arendall, W. B., 3rd, Snoeyink, J., Richardson, J. S., and Richardson, D. C. (2007) MolProbity: all-atom contacts and structure validation for proteins and nucleic acids, *Nucleic Acids Res 35*, W375-383.

104. DeLano, W. L. (2004) The PyMOL molecular graphics system, DeLano Scientific, San Carlos, CA, www.pymol.org.

Appendix

A1. List of Abbreviations

AAA	α-aminoadipate pathway
AAS	L-α-aminoadipate-δ-semialdehyde
AMP	adenosine monophosphate
Apo	apoenzyme, with no ligands bound
Ches	2-(*N*-cyclohexylamino) ethanesulfonic acid
E	enzyme
Hepes	*N*-(2-hydroxyethyl) piperazine-*N*'-(2-ethanesulfonic acid)
Lys	L-lysine
Mes	2-(*N*-morpholino)ethanesulfonic acid
MgHIc	chelate complex of magnesium and homoisocitrate
NAD	β-nicotinamide adenine dinucleotide (the + charge is omitted for convenience)
NADD	reduced β-nicotinamide adenine dinucleotide with deuterium in the 4-R position
NADH	reduced β-nicotinamide adenine dinucleotide
NADP	nicotinamide adenine dinucleotide phosphate
NADPH	reduced nicotinamide adenine dinucleotide phosphate
NDP	nicotinamide diphosphate
Ni-NTA	nickel-nitrilotriacetic acid

NMN	nicotinamide mononucleotide (the + charge is omitted for convenience)
OAA	oxaloacetate
OxGly	oxalylglycine
Sacc	L-saccharopine
SDH	saccharopine dehydrogenase
SE	standard error
SKIE	solvent deuterium kinetic isotope effect
Taps	3-[*N*-tris(hydroxymethyl) methylamino]-propanesulfonic acid
WT	wild type
α-Kg	α-ketoglutarate

A2. List of Schemes

A3. Kinetic studies of K77M and H96Q mutant enzymes

A3.1 Initial velocity studies at pH 7.0

Initial velocities were measured in the direction of Sacc formation for K77M and H96Q single site-directed mutant enzymes using a Beckman DU 640 UV-visible spectrophotometer following the procedure described in the Materials and Methods section of chapter 2. Kinetic parameters are summarized in Table A3-1, and compared to those obtained for WT (*60*). Replacing K77 with M resulted in close to a 100-fold decrease in $V_2/\mathbf{E_t}$ and 20-, >430-, and 130-fold decrease in $V_2/K_{NADH}\mathbf{E_t}$, $V_2/K_{\alpha\text{-}Kg}\mathbf{E_t}$, $V_2/K_{Lys}\mathbf{E_t}$, respectively. There was no change in K_{Lys} and a 3-fold increase and a 6-fold decrease in $K_{\alpha\text{-}Kg}$ and K_{NADH}, respectively. Replacing H96 with Q resulted in a 4-fold decrease in $V_2/\mathbf{E_t}$ and 35-, 540-, 420-fold decrease in $V_2/K_{NADH}\mathbf{E_t}$, $V_2/K_{\alpha\text{-}Kg}\mathbf{E_t}$, $V_2/K_{Lys}\mathbf{E_t}$, respectively. Increases in Michaelis constants were observed for all three reactants, with 76-, 87-, and 6-fold increases in K_{Lys}, $K_{\alpha\text{-}Kg}$, and K_{NADH}, respectively.

There was a larger change observed in the first order rate constant for the K77 mutant enzyme compared to the H96 mutant enzyme, while for the H96 mutant enzyme the larger changes were observed in the second order rate constants compared to the K77 mutant enzyme. Data are consistent with K77 acting as base 1 and H96 as base 2 in the chemical mechanism of SDH, Scheme C1-5.

The data are consistent with K77 acting as :B1 and H96 acting as :B2

SDH kinetic Parameters	V_2/E_t (s^{-1})	$V_2/K_{NADH}\ E_t$ ($M^{-1}s^{-1}$)	$V_2/K_{\alpha\text{-}KG}\ E_t$ ($M^{-1}s^{-1}$)	$V_2/K_{Lys}\ E_t$ ($M^{-1}s^{-1}$)	K_{NADH} (mM)	$K_{\alpha\text{-}KG}$ (mM)	K_{Lys} (mM)
wt[a]	20	1.6×10^6	2.8×10^5	2.5×10^4	0.019	0.11	1.1
H96Q[b]	5	4.6×10^4	521	59	0.11	9.6	83.8
Fold Δ H96Q vs wt	4	35	537	424	6	87	76
K77M[b]	0.23	8.2×10^4	650	194	0.003	0.35	1.2
Fold Δ K77M vs wt	87	20	431	129	6	3	no Δ

[a] Xu et al., Biochemistry 2006; 45 : 12156-12166
[b] Standard errors are ≤ 10%

Table A3-1: Initial Velocity Data for K77M and H96Q Mutant Enzymes at pH 7.0 in the Direction of Saccharopine Formation

A3.2 Isotope effects

Primary substrate deuterium, solvent deuterium, and multiple solvent deuterium/substrate deuterium kinetic isotope effects were measured for the double K77M/C205S and H96Q/C205S mutant enzymes following the procedure described in the Materials and Methods section of chapter 2. The data are summarized in Table A3-2, and compared to those obtained for C205S mutant enzyme, chapter 2.

Primary substrate deuterium kinetic isotope effects of 5.38 and 2.2 on $^{D}(V_2/K_{Lys})$ and $^{D}(V_2)$ were observed for the K77M/C205S and H96Q/C205S mutant enzymes, respectively, compared to a value of 1.31 in the C205S enzyme at pH 9.0. A primary substrate deuterium kinetic isotope effect reflects the hydride transfer, step A, in the Scheme C1-5. Data suggest that while H96 may contribute to the hydride transfer step, the K77 is the main catalytic base that abstracts a proton from the secondary amine of Sacc at the hydride transfer step.

Solvent isotope effects of 4.9 and 2.8 on $^{D}(V_2/K_{Lys})$ and $^{D}(V_2)$ were observed for H96Q/C205S and K77M/C205S mutant enzymes, respectively, compared to a value of 2.62 for the C205S enzyme at pH 7.3. Data suggest H96 contributes to imine hydrolysis, activating water.

On the basis of the data obtained for primary substrate deuterium and solvent kinetic deuterium isotope effects, K77 does not contribute to proton transfer steps other than the proton transfer concerted with the hydride transfer. This is corroborated by the measured multiple isotope effects, where NADD

was fixed and H_2O/D_2O were varied. The multiple isotope effects $^{D_2O}(V_2/K_{Lys})$ and $^{D_2O}(V_2)$ of 2.06 (slightly increased) was observed for K77M/C205S compared to the multiple isotope effect of 1.83 for the C205S enzyme, and it reflects the solvent isotope effect on the hydride transfer step in both cases.

Proton transfer steps during imine hydrolysis are catalized by H96, and it also contributes to proton transfer in the hydride transfer step. This is corroborated by the multiple isotope effects $^{D_2O}(V_2/K_{Lys})$ and $^{D_2O}(V_2)$ of 3.59 (increased more than in case with K77) compared to 1.83 for the C205S enzyme.

Overall, isotope effect data suggest K77 is base 1 and H96 is base 2 in the chemical mechanism of SDH, Scheme C1-5.

Summary of the Kinetic Isotope Effects for C205S, K77M/C205S, and H96Q/C205S Mutant Enzymes

Enzyme	$^{D}(V_2/K_{Lys})$	$^{D}(V_2)$	$^{D2O}(V_2/K_{Lys})$	$^{D2O}(V_2)$	$^{D2O}(V_2/K_{Lys})_D$	$^{D2O}(V_2)_D$
	PKIE[b]		SKIE		MKIE	
C205S[a]						
pH 5.4	1.9± 0.3[c]	1.9± 0.3	2.2±0.8[d]	1[e]	3.9± 0.4	3.9± 0.4
pH 7.3	2.2±0.1	2.2±0.1	**2.6± 0.4**	**2.6± 0.4**	1.8± 0.1	1.8± 0.1
pH 9.0	**1.3± 0.2**	**1.3± 0.2**	1.5±0.1	1.5±0.1	1.5± 0.1	1.5± 0.1
K77M/C205S[a]						
pH 5.4	ND[f]	ND	ND	ND	ND	ND
pH 7.3	ND	ND	2.8 ± 0.2	2.8 ± 0.2	2.1± 0.2	2.1± 0.2
pH 9.0	**5.4 ± 0.2**	**5.4 ± 0.2**	ND	ND	ND	ND
H96Q/C205S[a]						
pH 5.4	ND	ND	ND	ND	ND	ND
pH 7.3	ND	ND	**4.9 ± 0.3**	**4.9 ± 0.3**	3.6± 0.3	3.6± 0.3
pH 9.0	2.2 ± 0.1	2.2 ±0.1	ND	ND	ND	ND

[a]Data obtained from the fit to an equation, where $V=V/K$. [b]PKIE, primary substrate deuterium kinetic isotope effect; SKIE, solvent deuterium kinetic isotope effect; MKIE, multiple solvent deuterium/substrate deuterium kinetic isotope effect. [c]Values are ± SE. [d]Data obtained from the fit to an equation, where isotope effect on V is missing. [e]Estimated value (not well defined). [f]ND, no data available.

Table A3-2: Isotope Effects Data for K77M/C205S and H96Q/C205S Mutant Enzymes

THE END